CONDITION ASSESSMENT OF REINFORCED CONCRETE BRIDGE DECKS AS CONDUCTIVE MEDIA USING GPR

by

Adam J. Sketchley

Submitted in partial fulfilment of the requirements
for the degree of Master of Applied Science

at

Dalhousie University
Halifax, Nova Scotia
June 2014

Table of Contents

List of Tables

List of Figures

Abstract

Bridge and overpass infrastructure are crucial parts of transportation networks that must be adequately maintained to ensure minimal repair costs and traffic disruption. The majority of the bridges and overpasses in North America are constructed with a concrete deck, with many of these decks acting as the wearing surface. It is well known that these types of steel reinforced concrete structures are susceptible to corrosion damage, especially when in environments rich in chlorides. In order to identify areas at risk of chloride-induced corrosion, this research aims to correlate chloride content in bridge decks with material properties determined using ground penetrating radar.

It has generally been accepted that areas of a concrete deck showing high levels of signal attenuation indicate high chloride levels. While low signal loss conditions are often assumed in modeling wave propagation through concrete, this research aims to improve the detection of chloride laden areas using a conductive media approach. By assuming a constant moisture content throughout the structure and measuring the relative attenuation in each scan, the conductivity of the deck is determined.

To determine the validity of this method, the conductive model was employed for the evaluation of five bridge decks surveyed in previous research. By accounting for both power fluctuations and geometric spreading, signal attenuation was isolated and conductive properties were determined. Conductive results were then compared to half-cell and chain drag reference tests from each of the five bridge decks investigated. The areas with the highest conductivity levels were strongly correlated with both half-cell and chain drag results, confirming that the conductive model is capable of identifying concrete in need of repair.

Finally, determined conductivities were compared to chloride contents measured from cores taken from each deck at the time of testing. Conductivity was shown to increase linearly with chloride content, confirming the ability of ground penetrating radar to detect chlorides. This relationship can be used to map chloride content across a bridge deck and estimate the time to corrosion, greatly increasing the efficiency of bridge deck inspection.

List of Abbreviations and Symbols Used

AAR	Alkali Aggregate Reactivity
ASTM	American Society for Testing and Materials
FHWA	Federal Highway Administration
GSSI	Geophysical Survey Systems Incorporated
GPR	Ground Penetrating Radar
HPC	High Performance Concrete
NDEVC	Nondestructive Evaluation Validation Center

A	Horizontal resolution of antenna	(m)
A(t)	Amplitude as a function of time	(AU)
A_0	Initial amplitude	(AU)
Amp_{AU}	Signal amplitude in Radan's amplitude units	(AU)
Amp_{dB}	Signal amplitude in decibels	(dB)
B	Spreading loss coefficient	(-)
c	Speed of light in a vacuum	(m/s)
C	Chloride concentration	(kg/m^3)
C_i	Initial chloride content in location of interest	(kg/m^3)
C_s	Chloride content at concrete surface	(kg/m^3)
d	Electromagnetic wave propagation distance	(m)
D	Diffusion coefficient	(m^2/s)
D_{REF}	Diffusion coefficient at reference time	(m^2/s)
E	Energy of electromagnetic signal	(J)
E_i	Energy of incident electromagnetic signal	(J)
E_r	Energy of reflected electromagnetic signal	(J)
E_t	Energy of transmitted electromagnetic signal	(J)
erfc	Complimentary error function	(-)
f	Frequency of electromagnetic signal	(Hz)
F	Chloride flux	($kg/m^2 \cdot s$)
m	Age parameter for diffusion	(-)

$\mathbf{t}$	Time	(s)
$\mathbf{t_{REF}}$	Reference time	(s)
$\mathbf{v}$	Propagation velocity	(m/s)
$\mathbf{v_{REF}}$	Reference propagation velocity	(m/s)
$\mathbf{x}$	Linear position	(m)
$\boldsymbol{\alpha}$	Attenuation coefficient	(Np/m)
$\mathbf{\Delta dB}$	Decibel loss	(dB)
$\mathbf{\Delta dB_{ATTEN}}$	Decibel loss due to attenuation	(dB)
$\mathbf{\Delta dB_{SPREAD}}$	Decibel loss due to spreading	(dB)
$\boldsymbol{\varepsilon}$	Dielectric permittivity	(F/m)
$\boldsymbol{\varepsilon_0}$	Permittivity of free space	(F/m)
$\boldsymbol{\varepsilon_r}$	Relative permittivity	(-)
$\boldsymbol{\lambda}$	Wavelength of electromagnetic signal	(m)
$\boldsymbol{\mu}$	Magnetic permeability	(H/m)
$\boldsymbol{\mu_0}$	Permeability of free space	(H/m)
$\boldsymbol{\mu_r}$	Relative permeability	(-)
$\boldsymbol{\sigma}$	Electric conductivity	(S/m)
$\boldsymbol{\sigma_0}$	Initial conductivity of concrete	(S/m)
$\boldsymbol{\sigma_E}$	Conductivity from external factors	(S/m)
$\boldsymbol{\omega}$	Angular frequency	(rad/s)

Acknowledgements

I would like to acknowledge the funding and support of NSERC and NSTIR in the completion of this research. I would also like to thank Dr. Chris Barnes and Dr. John Newhook for their support and guidance throughout this thesis and for the data and equipment I was provided with. I would also like to acknowledge Eileen McEwen who collected the radar, half-cell, and chain drag data and created diffusion models for each deck in this study. Finally, I would like to acknowledge Tye Minion for his collaboration in the laboratory portion of this research.

Chapter 1: Introduction

Concrete bridge decks are a valuable part of public infrastructure all over the world. Maintaining this infrastructure is crucial to sustaining the transportation networks that are an essential part of the global economy. Proper maintenance includes inspections of each bridge, preventative measures, and appropriate structural repairs. Implementation of a bridge management system dramatically increases the efficiency of this process and reduces long term costs. The best way to implement this system is with frequent inspections and timely repairs. If a bridge is repaired when there is not significant deterioration, the result is the replacement of sound concrete, unnecessary disruption of traffic, and the mobilization of equipment in order to do very little work. If repairs are too late, parts of the deck that could have been protected or rehabilitated must undergo more extensive repair or replacement. In either situation the unnecessary costs can skyrocket, potentially crippling agencies in charge of a large network of bridge decks.

It is estimated that repairs are best scheduled when 10-12% of a given concrete deck is damaged (Fitch et al. 1995, Williamson et al. 2007). In order to conduct repairs at this ideal point, inspections must accurately determine deterioration levels of bridge decks and be carried out frequently enough to predict the rate of damage to the deck. Proper preventative maintenance and inspection will lengthen the lifespan of each deck and will significantly reduce total lifetime costs.

By recording the results of frequent inspections for a given bridge deck, it may even be possible to estimate when repairs should take place. Making these predictions would give management agencies an idea of the magnitude of future costs and when to expect them. It would also allow efficient repairs to be scheduled for large networks of bridges as there is only a finite amount of repair funding each year. This would allow more realistic financial planning of bridge maintenance and reduce unexpected costs, especially when managing a large network of bridges.

Since much of the current infrastructure is invested in concrete construction, the deterioration rate of these decks should be modeled in a bridge management system by carrying out appropriate inspections. Testing procedures specific to concrete decks must

be implemented and an understanding of the common causes of damage to these decks must be achieved. Concrete is a variable material as each mix design has its own proportions and types of aggregate, cement, water, and admixtures. Each unique combination has its own advantages and disadvantages, so there are no clear guidelines as to how fast deterioration may progress in a given deck.

The main cause of damage to concrete bridge decks is corrosion of reinforcement. During the corrosion process, reinforcing bars can expand up to six times their initial volume, causing significant stresses at the steel-concrete interface (Bertolini et al. 2004). As the corrosion progresses it damages the concrete, beginning with small cracks and eventually causing delamination and spalling of sections of the deck. Sufficient corrosion can result in the loss of structural capacity of both the reinforcing steel and the concrete itself. Due to the severity of this damage, it is important to be able to detect areas of corrosion early on in its progression and plan repairs accordingly. Chlorides have been shown to significantly accelerate the onset of reinforcement corrosion by assisting in the breakdown of the protective passive film formed during curing (Ahmad 2003). This is of special concern for concrete bridge decks due to the use of deicing salts during winter months as well as any salt water spray if the deck is in a marine environment. These chlorides penetrate the deck, diffusing through the concrete to the steel reinforcement.

Current bridge deck inspection methods determine evidence of existing deterioration but cannot often identify the risk of damage or the rate of deterioration. The traditional inspection methods for concrete decks are visual inspection, chain drag, and half-cell potential. Other methods to assess the condition of concrete bridge decks include impact-echo, resistivity measurement, ultrasonic methods, and ground penetrating radar.

The use of Ground Penetrating Radar (GPR) as a tool to determine the condition of bare concrete bridge decks is the focus of this thesis. Bare concrete bridge decks are those decks that use the concrete as the wearing surface for passing traffic instead of adding a paving layer. GPR surveys determine areas of deterioration by transmitting electromagnetic pulses into the concrete deck. These pulses reflect off of any significant change in materials, most notably the steel reinforcement within the concrete deck, and return to the radar antenna. The amplitude and travel time of each returning pulse is then recorded and processed. The

strength of the returning signal is reduced by both spreading and attenuation losses as it passes through the concrete (Leucci 2008). Spreading losses are a function of wave propagation distance while attenuation is due to the conductive properties of the material the wave is passing through. Chloride concentration in concrete has been shown to cause the attenuation of GPR signals by increasing the conductivity (Hugenschmidt and Loser 2008). By mapping out areas that show significant conductivity and therefore attenuation, chloride content and therefore corrosion risk can be estimated.

Current concrete evaluation methods using GPR take a non-conductive approach to analysis. Employing a conductive model will allow for a more complete representation of the physical process involved in electromagnetic wave propagation through concrete, determining signal attenuation with greater accuracy. Ideally, this method will result in conductivity thresholds that can be applied to in-service concrete bridge decks scanned with GPR that will identify corrosion risk due to chlorides. Tracking the conductivity values over time and incorporating them into a diffusion model could afford management agencies the ability to monitor and even predict chloride penetration into concrete bridge decks.

In order to prove this model to be valid as a condition assessment tool, the following capabilities must be demonstrated:

- Determination of a conductivity profile for an investigated deck.
- Strong correlation between increased conductivities identified by the model and deterioration identified by reference half-cell and chain drag testing.
- Credible relationship between calculated conductivities and measured chloride contents.

Chapter 2: Literature Review

This chapter will contain background information relevant to the subjects explored over the course of this research. The purpose of this literature review is to outline both the concepts and the previous research involved in assessing the condition of reinforced concrete bridge decks with GPR. A review of the current bridge and overpass infrastructure will highlight the challenges management agencies will face and the importance of thorough inspections. A review of the concepts behind chloride induced corrosion and nondestructive testing of concrete decks will also be presented, along with an outline of the relevant research.

2.1 Current State of Infrastructure

As of 2007, bridges and overpasses accounted for 8% of total public infrastructure in Canada, amounting to $23.9 billion (Gagnon et al 2008). Gagnon's report showed that the average age of these structures had increased from 21.3 years to 24.5 years since 1985 due to a lack of investment in construction. A significant portion of this ageing, 0.8 years, had occurred since 2001 as the investment in these assets rose an average of only 0.4% per year. During this same period, the average inflation rate in Canada was 2.2% per year (Bank of Canada 2014). Compared to a mean service life of 43.3 years, the study noted that bridges and overpasses had passed 57% of their useful life with provincial highs of 66% in Nova Scotia and 72% in Quebec.

As the age of these structures is increasing, it is more important than ever to inspect and repair them effectively. Prolonging bridge maintenance will only increase the total cost of these bridge decks over their lifetimes and could potentially shorten lifetimes by allowing deterioration to continue longer than necessary. The current philosophy of saving maintenance money for a later date will end up costing much more, especially if several bridges get to a point of critical deterioration over a short time span, which would incur a substantial replacement cost.

In the United States, the Federal Highway Administration (FHWA) National Bridge Inventory lists 607 380 bridges as of 2012 with 11% structurally deficient and an additional

14% functionally obsolete (FHWA 2014). The estimated cost to rehabilitate these structures based on the national average cost was $35.2 billion in 2012 (FHWA 2013a). Of these structures, the FHWA lists 69% as having a concrete deck (FHWA 2013b) and 34% of all decks as having a concrete wearing surface (FHWA 2013c).

The state of these bridges in both countries illustrates the need for thorough and efficient inspection techniques. Inspections must focus on the deterioration mechanisms and strive to detect the signs of these mechanisms before the damage is done. The large number of concrete bridge decks present in the infrastructure is evidence of the need for concrete specific techniques. By identifying areas of concrete bridge decks that have a high risk of deterioration, the cost of maintaining the decks will decrease while their expected lifespans will improve. It has been determined that significantly increasing the accuracy of condition assessments could decrease the total cost of repair contracts by 2-8% (Cowell 1988). These savings over the number of repairs for each bridge in a network would provide substantial cost savings to managing agencies.

2.2 Chloride Induced Corrosion

A major cause of deterioration to concrete bridge decks is corrosion of the reinforcement. As the reinforcement corrodes, the corrosion product increases the volume of the reinforcing bar while reducing the structurally effective area of steel (Bertolini et al. 2004). The process of corrosion is essentially the metal reverting back to its original mineral and ore components. In fact, the same energy required to make metal iron from iron ore is released during corrosion (Roberge 2008). Corrosion is an electrochemical process that consists of two half reactions, an anodic reaction and a cathodic reaction. In order for it to take place, corrosion requires enough water and oxygen to be in the concrete pore structure to permit the transfer of electrons between anodic and cathodic cells. The chemical environment surrounding steel reinforcement determines when corrosion will begin as well as how far and at what rate it will progress.

2.2.1 Corrosion Electrochemical Process

The corrosion of steel reinforcement is an electrochemical process as it is a chemical reaction involving the transfer of electrons. For this reaction to occur, a cell must form to allow electron transfer from one half to the other. The two halves of the cell are the anodic region where electrons are released in oxidation and the cathodic process that absorbs the electrons in the reduction of oxygen or hydrogen. To complete the cell, electrons must be able to pass through both the reinforcement and the concrete to promote all the necessary reactions. While the reinforcement will naturally transfer electrons, concrete needs to have sufficient ions in solution to act as an electrolyte and allow the transfer. Under normal circumstances the anodic half reaction is as described in Equation 2.1 and the cathodic half reaction is described as in Equation 2.2 or 2.3 depending on the availability of oxygen (Ahmad 2003).

$$Fe \rightarrow Fe^{2+} + 2e^{-} \quad \textbf{[2.1]}$$

$$O_2 + 2H_2O + 4e^{-} \rightarrow 4(OH)^{-} \quad \textbf{[2.2]}$$

$$2H^{+} + 2e^{-} \rightarrow H_2 \quad \textbf{[2.3]}$$

As the anode releases electrons, ionic iron dissolves into ferrous oxide and can further oxidize into ferric oxide as shown in Equations 2.4 and 2.5 respectively. These iron oxides accumulate as a corrosion product while the solid iron decreases, causing the loss of effective steel area. This accumulation of corrosion product is what causes the volumetric expansion that results in a buildup of stress in the surrounding concrete. The process also increases the acidity of the pore solution by releasing hydrogen ions into solution.

The cathodic reaction involves either the reduction of hydrogen ions or the splitting of water. In either case, the balance between H^+ and OH^- is shifting and the concrete pore solution is becoming more basic, effectively protecting the steel at the cathode as low pH environments experience much more aggressive corrosion.

$$Fe^+ + 2H_2O \rightarrow Fe(OH)_2 + 2H^+ \quad \textbf{[2.4]}$$

$$4Fe(OH)_2 + 2H_2O + O_2 \rightarrow 4Fe(OH)_3 \quad \textbf{[2.5]}$$

During the early stages of concrete hydration, the pore solution is a highly alkaline environment. While in this alkaline stage, a thin passive oxide film is formed at the interface between the concrete and the reinforcement. This passive film prevents the reinforcement from forming a corrosion cell and it is only once this passive layer breaks down that corrosion begins to occur (Montemor et al. 2003). In order to maintain this protective film, the environment surrounding the reinforcement must maintain its alkalinity. The common catalysts for the depassivation of reinforcing steel are carbonation and chloride contamination. Carbonation occurs when sufficient carbon dioxide from the atmosphere lowers the pH to about 9 and the passive protection layer destabilizes (Bertolini et al. 2004). The carbonation reaction is as seen in Equation 2.6 and reacts with the calcium hydroxide present during the hydration of concrete.

Chloride concentration in concrete can cause depassivation locally in the reinforcement that also leads to the initiation of corrosion. The abundance of chlorides from deicing salts and marine environments makes this process of additional concern for concrete bridge decks. While these can both cause corrosion, chloride generally initiates corrosion in modern structures much earlier than carbonation (Broomfield 2006). Poor concrete or construction practices as well as shallow reinforcement could cause carbonation to initiate

corrosion first, but this is seldom the case. Chloride induced corrosion is also typically more aggressive and more damaging than corrosion due to carbonation (Berke 2006).

$$CO_2 + Ca(OH)_2 \rightarrow CaCO_3 + H_2O \qquad \textbf{[2.6]}$$

Corrosion can take place as one or both of two electrochemical processes in a concrete bridge deck. The first process is macrocell corrosion where chemical reactions take place between two separate bars. This occurs when the anodic areas of one bar increase and the anodic areas of the other bar decrease while the opposite can be said for the cathodic areas of the bars as seen in Figure 2.1. This process requires the two bars to be in different environments, such as a top mat of reinforcement encased in concrete laden with chloride ions in solution and a bottom mat in clean concrete (Hansson et al. 2006). The second process is microcell corrosion which is much more common in practice. This process occurs between anodic and cathodic areas of the same reinforcing bar as seen in Figure 2.2. These two reactions can occur independently or both can be present in the same bridge deck, but the corrosion rate for microcells is significantly higher (Hansson et al. 2006).

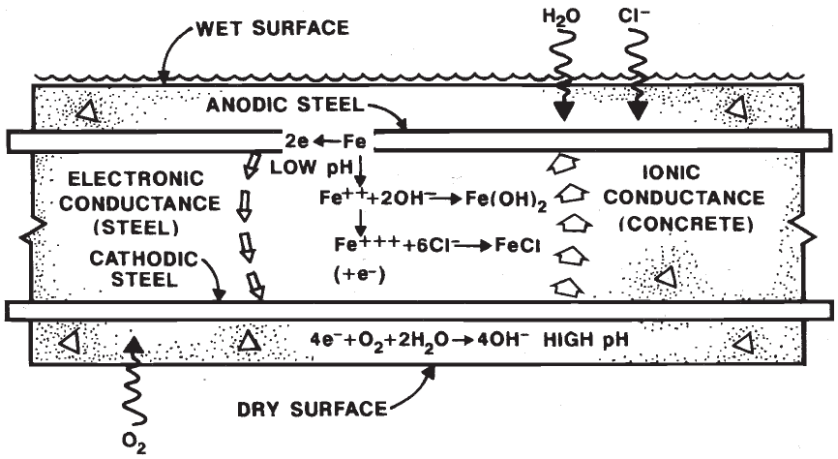

Figure 2.1: Macrocell corrosion process (Berke 2006)

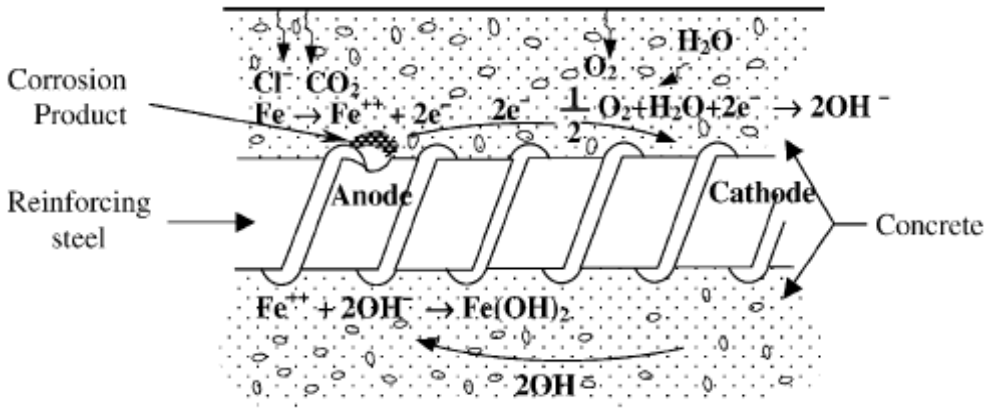

Figure 2.2: Microcell corrosion process (Ahmad 2003)

2.2.2 Effect of Chloride Contamination

When chlorides in a concrete structure reach a threshold level, the reinforcement depassivates and the corrosion process can begin. This threshold level is a function of the concrete composition and its environment (Poulsen and Mejlbro 2006, Glass and Buenfeld 1997). As the passive layer breaks down, the reinforcement becomes anodic and forms a corrosion cell with areas of reinforcing that are still cathodic. Threshold levels are variable based on the composition of the concrete used in different decks and there is no universally accepted method for determining this threshold for a given deck (Frederiksen 2009). There is little variability in the range of thresholds, which can be estimated but not specifically defined (Glass and Buenfeld 1997). This variability makes it difficult to determine when corrosion will begin in a given deck due to chloride contamination.

Corrosion can be either uniform over a section of reinforcement composed of multiple bars or localized to a relatively small anodic region of one bar. When the localized area of corrosion is small and the corrosion is aggressive, it is referred to as pitting due to the hollowing of the steel section in the anodic region of the bar. As the pit develops in the bar, chlorides as well as ionized hydrogen and iron enter into solution and create a highly aggressive environment with a pH that can drop below 5 (Poulsen and Mejlbro 2006). This pitting can be of added concern due to the relatively rapid loss of effective steel area and buildup of corrosion product. When pitting progresses sufficiently, it can completely

destroy the structural capacity of the bar and could lead to structural failure if allowed to progress unfettered on a number of reinforcing bars simultaneously.

Chlorides that have already infiltrated concrete can be either free or bound. Free chlorides are chloride ions that are within the pore solution of the concrete and free to migrate through the deck. Bound chlorides are chemically bound to the hydration products of the cement and are fairly stable (Ahmad 2003). In chloride testing, either water or acid is used to separate the chloride from the concrete to be measured. Water soluble chloride content is the measure of only the free chloride content while acid soluble chloride content is the sum of free and bound chlorides. It is generally accepted that free chlorides are what contribute to the corrosion of reinforcement, so naturally water soluble chlorides are often measured to determine corrosion risk. Free chlorides cause depassivation instead of bound chlorides due to the fact that bound chlorides are already interacting with the cement, so they will have little or no effect on the passivity of the steel. Also, bound chlorides will not diffuse through the concrete like free chlorides as they are held in place by their chemical bonds.

Once it has initiated, the rate of corrosion can vary from micrometers to millimeters per year based on the humidity and chloride content of the concrete surrounding the reinforcement (Bertolini et al. 2004). Increases in humidity, temperature, and chloride content increase the corrosion rate drastically. The effect of humidity on the corrosion rate is highly dependent on the mix design of the concrete and the chloride content in the region. It has been shown that increases in conductivity increase the corrosion current in cement as electrons will flow through the concrete more freely (Alonso et al. 1988, Glass et al. 1991). Chloride has been shown to increase conductivity, so naturally higher levels of chlorides would increase the corrosion current around the reinforcement in addition to aiding in the depassivation of the steel. This is shown to an extreme in the pitting corrosion described earlier where the chlorides within the pit create a highly acidic solution that results in an aggressive corrosion environment.

2.2.3 Chloride Transport Mechanism

Concrete bridge decks are routinely exposed to chlorides over the course of their service lives. Chloride exposure is often due to sea spray or the use of deicing salts during the winter months. This exposure results in a surface concentration of chlorides over a given concrete deck that can vary substantially due to traffic effects as well as ponding and cracking of the deck. Over time, chlorides from the surface infiltrate through pore spaces, cracks, and voids through a diffusion process described by Fick's first and second laws. The first law, as seen in Equation 2.7, relates the flux of chlorides (F) to the diffusion coefficient (D) and the change in chloride concentration (C) with depth. Fick's second law relates the change in the flux with depth to the change in chloride concentration with time as seen in Equation 2.8. These equations can be combined for one-dimensional problems such as the vertical diffusion of chloride in concrete to fully describe the physical process as seen in Equation 2.9. Naturally, regions with higher sustained surface concentrations over time will experience more aggressive infiltration than regions exposed to less chlorides due to the steepness of the concentration gradient at the surface.

$$\mathrm{F} = -\mathrm{D}\frac{\partial C}{\partial x} \qquad \textbf{[2.7]}$$

$$\frac{\partial C}{\partial t} = -\frac{\partial F}{\partial x} \qquad \textbf{[2.8]}$$

$$\frac{\partial C}{\partial t} = \frac{\partial}{\partial x}\left(\mathrm{D}\frac{\partial C}{\partial x}\right) \qquad \textbf{[2.9]}$$

where:

C – chloride concentration (kg/m3)
D – diffusion coefficient (m2/s)
F – chloride flux (kg/m2·s)
t – time (s)
x – distance from surface of concrete (m)

To add complexity to this situation, the diffusion coefficient in a concrete deck is time dependent as the curing and the degree of hydration of the concrete deck affects the pore structure significantly (Poulsen and Mejlbro 2006). Different concrete mixtures have different diffusion coefficients based on the pore structure and chemical properties of the concrete. The diffusion coefficient decreases over time as shown in Equation 2.10. The exponent m is the age parameter and is dependent on the mixture properties of the concrete, representing the rate of decay of the coefficient (Song et al. 2009). This equation bases the calculated diffusion coefficient on a reference diffusion value determined at a reference time. It has been shown that the time effects are substantial and that admixtures also have significant effect on the coefficient (Thomas and Bamforth 1999).

$$D(t) = D_{ref}\left(\frac{t_{ref}}{t}\right)^{m} \quad \textbf{[2.10]}$$

where:

D_{ref} – diffusion coefficient at reference time (m^2/s)
m – age parameter for diffusion
t_{ref} – reference time (s)

In order to use Fick's laws to calculate chloride profiles, numerical models must be constructed. One model that has been fairly popular relates current chloride content to boundary conditions and uses the complimentary error function as seen in Equation 2.11

(Crank 1975). The boundary conditions in this equation are C_s, the chloride concentration at the surface, and C_i, the chloride concentration at the point of interest at time zero. A more robust method that can accept changing surface chloride contents as well as changes in the diffusion coefficient both over time and as the result of repaired sections of a bridge deck is required for complete determination of chloride profiles. The method that has been gaining traction is a finite difference approach based on the Crank-Nicholson model (Song et al. 2009, Pérez et al. 2000). All this method requires is some knowledge of the diffusive properties and initial chloride concentrations of the concrete in order to determine a chloride profile.

$$C(x,t) = C_i + (C_s - C_i)\text{erfc}\left[\frac{x}{2\sqrt{tD}}\right] \quad \textbf{[2.11]}$$

where:

C_i – chloride concentration at point of interest at time zero (kg/m^3)
C_s – chloride concentration at the surface (kg/m^3)
erfc – complimentary error function

Since the diffusion of chloride is the transfer of ions through the pore structure of the concrete, the size and connectedness of the pores greatly influence the diffusivity. There are several test methods to determine the pore structure; each with varying degrees of effectiveness (Hearn et al. 2006). The pore structure can vary significantly due to the chemical makeup of the concrete and the age of the structure, significantly effecting the diffusivity.

2.3 Nondestructive Testing of Concrete Bridge Decks

Several nondestructive testing techniques have been applied to concrete bridge decks to determine condition. Ideally these tests should be fast, requiring minimal traffic disruption

and labour, while avoiding damage to the structure of the deck. A drawback to these methods is that they are identifying deterioration after it has begun instead of identifying its causes. To improve nondestructive testing procedures, an effort should be made to accurately identify areas at risk of deterioration by investigating the specific deterioration mechanisms to determine when maintenance or repairs should be scheduled.

2.3.1 Visual Inspection

Many concrete structures are primarily inspected visually. An inspector looks at various aspects of the bridge structure in order to find evidence of damage. These inspections can vary significantly in rigour from a close examination of minor defects to a brief look for serious decay. An in-depth study of the reliability of this method was carried out for the Federal Highway Administration by Moore et al. (2001). This study analyzed the responses and performance of several practicing bridge inspectors to determine the variability of inspection results. In all, 49 inspectors from 25 different states participated in the study. The inspectors were asked to perform 10 inspection tasks, including both routine and in depth inspections, on seven test bridges in Virginia and Pennsylvania. Inspection results were compared to very thorough inspections conducted on the same bridges by the Nondestructive Evaluation Validation Center (NDEVC). The inspectors were asked to evaluate the bridge on a scale of 0-9 with 9 being excellent condition and 0 being beyond repair as illustrated in the Bridge Inspector's Training Manual (FHWA 1995).

The study concluded that the results of visual inspection were highly variable with 4-6 different rating values being applied to each primary structural element. They also noted that the inspectors would often neglect important information during inspections. For instance, less than 25 percent of inspectors correctly identified the support conditions while inspecting a bridge. There was also a fair bit of variability when it came to what exactly was inspected and what areas of concern were recorded.

The high variability of the results of visual inspections is troublesome and would prove to be costly if repairs were not done early enough or if they were conducted before there was sufficient damage to warrant them. While it is convenient to be able to inspect bridges without specialized equipment or significant traffic disruption, more care should be taken

in the accuracy of condition assessments of the structures when determining repair quantities. Visual inspections only identify areas that are already sufficiently damaged to the point of being visible to inspectors. However, the versatility of this method should not be overlooked as there are not standard tests for every component of a bridge. The inspections should however be accompanied by frequent tests of higher accuracy for an overall assessment of the condition of a given bridge. Bridge decks especially are not easily visually inspected as traffic would have to be diverted and deterioration would have to progress significantly to be visible to inspectors.

2.3.2 Chain Drag

Chain drag surveys are conducted by inspectors sounding the bare bridge deck with a chain or rock hammer, sometimes as part of an in depth visual inspection. Areas of delamination are outlined based on a change in pitch of the chain or hammer contacting the deck, which are indicative of reinforcement that has sufficiently corroded to cause a separation with the concrete cover (ASTM 2012). Additional areas are outlined due to visual anomalies like poor concrete or construction practices as would be identified in a visual inspection alone. This method is limited to the determination of areas that are already severely damaged to the point of delamination.

The FHWA survey also compared the results of chain drag surveys among the sample of inspectors in what was identified as task J in the study (Moore et al. 2001). The results were compared to the NDEVC results in which an extremely in-depth sounding survey, taking approximately two man days was conducted on the same bridge. Participants were put into 22 teams and performed a chain drag survey on the bridge deck. Only 5 of the teams provided delamination estimates that fell within 5% of the deck area determined by the NDEVC. Each survey was plotted against the reference results and many of the inspectors were significantly off. All of the participants' maps were superpositioned and the areas where at least 5 teams independently identified delaminations were well correlated with the NDEVC results.

Cores were taken and compared to both NDEVC results and those from the inspectors' surveys. The cores confirmed the NDEVC results and refuted some areas the participants

claimed were delaminated. The NDEVC determined that 19% of the surveyed deck was delaminated while responses from the survey participants showed deck percentages from 2-35% and averaged 13% delamination.

The large variability shown in this study shows that results are extremely dependent on the individual inspector and the degree of scrutiny during testing. Also, the test is very nonspecific in that it only identifies areas that are delaminated to some degree and cannot identify the cause or rate of delamination. Further, chain drag surveys cannot assess the risk of future delamination to sections of the deck.

2.3.3 Half-Cell

Half-cell potential tests measure the difference in electric potential between embedded steel reinforcement and a reference copper/copper sulfate electrode. To enhance the connection, the reference electrode is connected to the concrete surface with a moist sponge. This provides a liquid bridge with low electrical resistance to create electrical continuity with the bridge deck. The reference electrode is connected to a voltmeter, as is an electrode connected to an exposed part of the reinforcing mat. It must be determined that the reinforcing mat is electrically continuous by checking for continuity between diagonally opposite ends of the reinforcing in a bridge deck before testing can commence. This assures that the readings are accurately measuring the correct locations.

The concrete deck itself is pre-wetted unless the voltmeter shows no variation above 0.02V over 5 minutes when placed on the concrete surface. Variations will usually exceed this threshold, so pre-wetting is often a requirement. The reference electrode is then wetted and placed on the surface of the concrete deck at several points in a grid as seen in Figure 2.3. The difference in electric potential at each point is recorded and compared to threshold values found in the testing standard (ASTM 2009). A threshold of -0.35V is listed in the standard as indicative of corrosion with a certainty greater than 90%. Regions showing a more negative potential difference than this are typically plotted as having active corrosion and regions with a potential difference of -0.20V or lower are noted as well. Areas with a potential difference more positive than -0.20V are listed in the standard as having a greater than 90% chance of having no active corrosion.

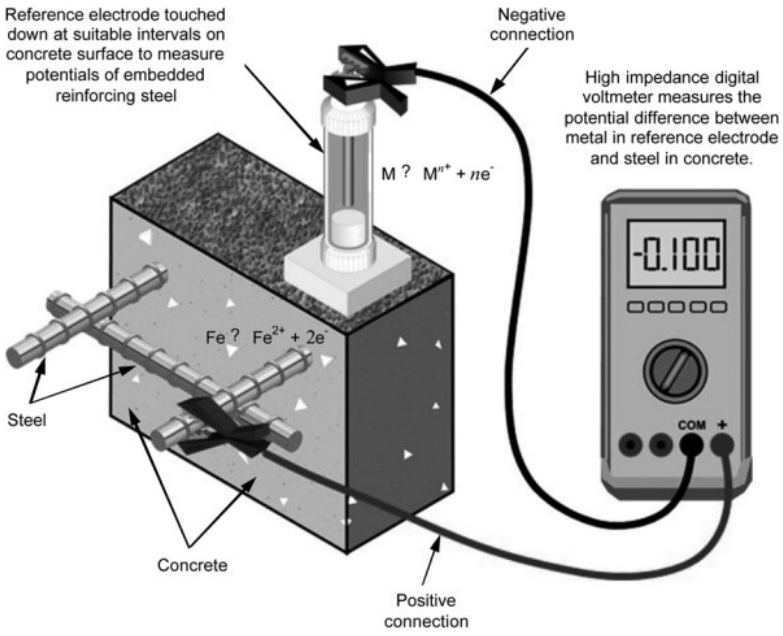

Figure 2.3: Standard half-cell potential test (ASTM 2009)

Half-cell has proven useful as a tool to measure the current state of corrosion for concrete bridge decks. It should be noted that while half-cell surveys can delineate areas that are likely undergoing active corrosion, it is not indicative of the rate of corrosion or the degree of corrosion damage. Half-cell is also unable to predict time to corrosion of points on a deck or the corrosion risk associated with the deck.

As with other methods, half-cell potential readings can be variable. It has been shown that the length of time between pre-wetting and testing has a significant effect on potential values and that the weather over the previous days can also change readings due to moisture within the concrete deck (Poursaee and Hansson 2009). In some cases where the reinforcement is sufficiently detached from the concrete due to delamination, there is no electrical connectivity and corrosion becomes undetectable by the half-cell (Barnes and Trottier 2004). Significant changes in cover depth affect results as well due to the fact that large cover depths cause passive and corroding steel to have similar recorded potentials (Elsener and Bohni 1990). It has also been determined that the reference electrode potential can vary due to temperature, direct sunlight, and contamination (Ansuini and Dimond

1994). The standard itself even says of the test that corrosion potentials are not necessarily indicative of corrosion current and that they may be partially or fully due to the chemistry of the environment surrounding the electrode (ASTM 2009).

2.3.4 Ground Penetrating Radar

Radar has been used to some degree since the early 1900s, but has been gaining interest as an evaluation tool since the 1970s (Daniels 2004). A GPR antenna is a transmitter and receiver pair that emit and record electromagnetic signals. These signals are transmitted as a pulse and reflect back when there is a change in propagation velocity of materials. As the change in velocity increases, the strength of the reflected signal increases. If the waves sent from the transmitter are assumed to be planar and to propagate normal to the interface of two materials, they are reflected as seen in Figure 2.4 where v_1 and v_2 are the propagation velocities of the waves within the two materials. The energy (E) of each wave is described by Equations 2.12 and 2.13.

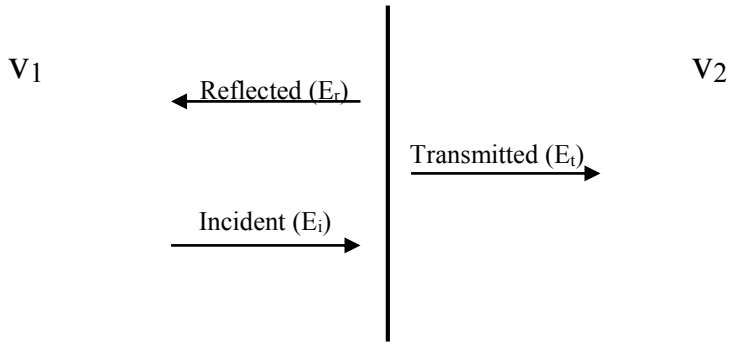

Figure 2.4: Planar reflection

$$E_t = \frac{2}{1 + \frac{v_1}{v_2}} E_i \qquad \textbf{[2.12]}$$

$$E_t = E_i + E_r \quad \textbf{[2.13]}$$

where:

E_i – energy of incident wave (J)
E_r – energy of reflected wave (J)
E_t – energy of transmitted wave (J)
v_1 – velocity in material 1 (m/s)
v_2 – velocity in material 2 (m/s)

For condition assessment of bare concrete bridge decks by GPR, the emitted signal pulse encounters two such boundaries. The first is between the air and the concrete surface, while the second is between the concrete and reinforcement. Two types of antennas are generally used in condition assessment. The first type is a horn antenna which is referred to as an air coupled antenna due to the fact that it is elevated 200-500mm from the ground during scanning. These antennas provide the benefit of being able to scan bridge decks at or near traffic speeds when mounted to a vehicle.

The second type of antenna is a dipole ground coupled antenna that consists of a transmitter and receiver pair that is dragged along the surface of the deck, although there is still a gap between the antenna and the ground of approximately 5-10mm. These antennas require traffic disruption during scanning, but provide higher resolution images of the scanned area. One drawback to ground coupled antennas is that reflections at or near the surface being inspected are within the near field of the antenna which greatly complicates the interaction the electromagnetic signal has with the material being investigated (Jol 2009). Due to this added complexity, very little tangible information about the concrete properties at the surface can be determined from the strength of signals reflected at the surface with ground couple investigation.

A diagram of the signal travel path for a ground coupled antenna is found in Figure 2.5 and includes the direct signal that passes from transmitter to receiver. As seen in the above equations, the strength of the returning signal reflected from the surface is based on the propagation velocity of the pulse in the material being scanned as its velocity in air is

constant. This velocity is a function of the material properties the signal is passing through and how they interact with the electromagnetic wave. As the antenna passes over a reinforcing bar, its reflection shows up as a parabola on the GPR display. This is due to the fact that the travel path is shortest directly above the reinforcement and longer approaching and leaving the bar as shown in Figure 2.6 where the antenna is travelling from left to right.

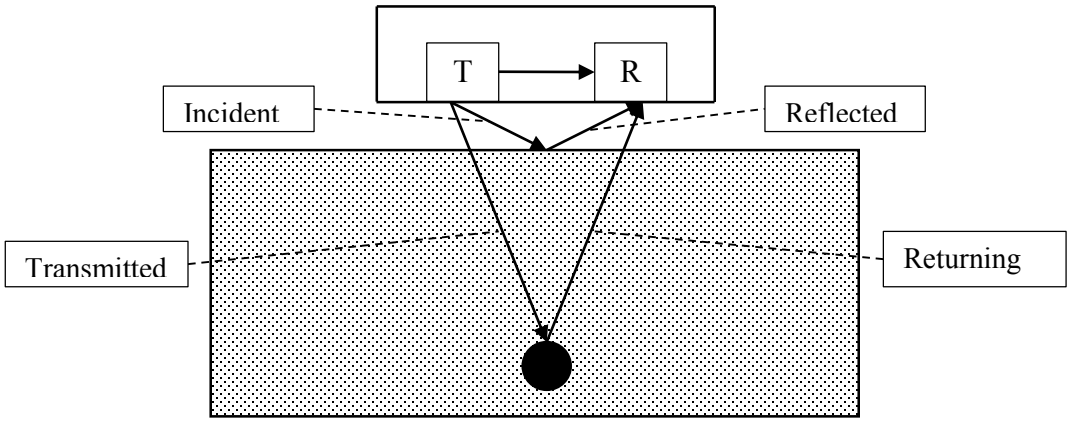

Figure 2.5: Wave paths for ground coupled antenna

The strength of the signals reflected from the reinforcement are indicative of the condition of the concrete surrounding the reinforcing bar in question. These signals naturally decay due to spreading losses as they propagate through space, but further attenuation of signals is due to the conductive properties of the concrete itself. Areas of the deck that are chloride laden show attenuation, while clean areas of the deck show up much brighter as indicated in Figure 2.7. This figure shows the longitudinal distance travelled by the GPR antenna on the horizontal axis versus the two way travel time of the returning signal on the vertical axis. Positive signal peaks are displayed as white while negative peaks are black. As signals get weaker, they show up greyer whether or not they are positive or negative as a solid grey would represent zero amplitude. A larger image of the reinforcement reflections is shown in Figure 2.8 with tracings of the reflection parabolas. Signal processing techniques can be applied to GPR data once it has been collected in order to remove unwanted portions of the signal or simply to make returning signals more visible. Once any processing is complete,

reinforcement locations can be selected and their signal information is compiled and analyzed.

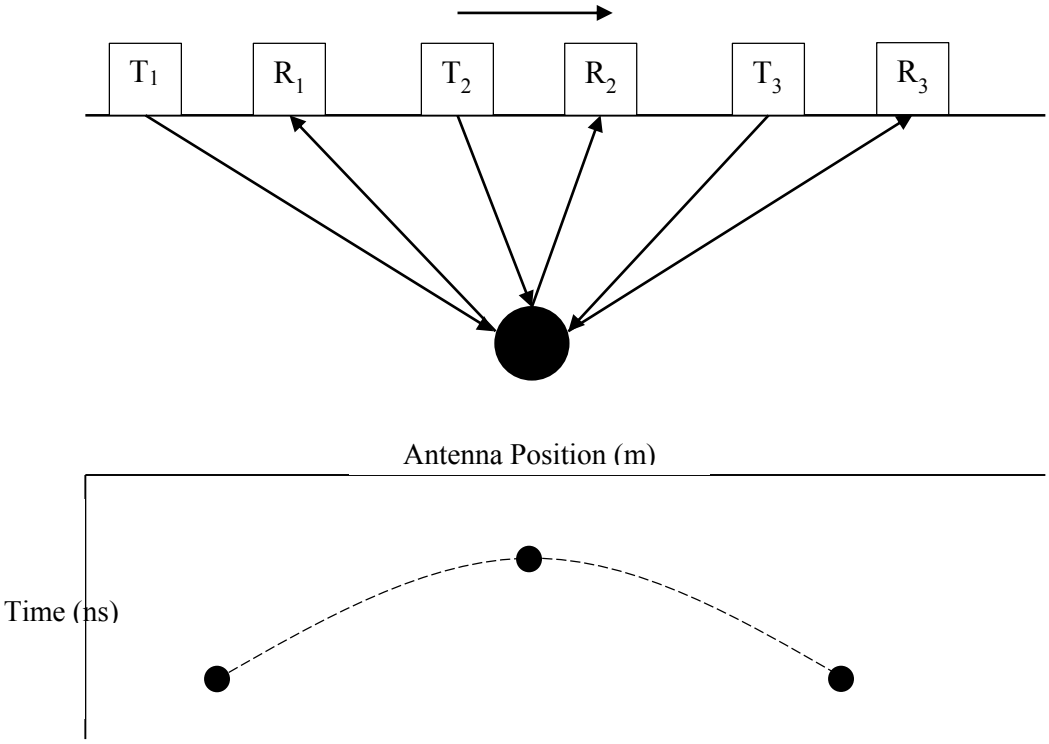

Figure 2.6: Reflection time due to antenna position

The material properties that govern the propagation velocity and signal attenuation are dielectric permittivity (ε), electric conductivity (σ), and magnetic permeability (μ). Dielectric permittivity describes how the atomic structure of the material reacts to the presence of an electric field and the ability of the atoms to become polarized by the field. Electric conductivity describes the ability of a charge to move freely through the material. Magnetic permeability describes atomic response to magnetic fields and is of little concern to GPR signals. These properties are all linked and can be fully described by Maxwell's equations (Jol 2009).

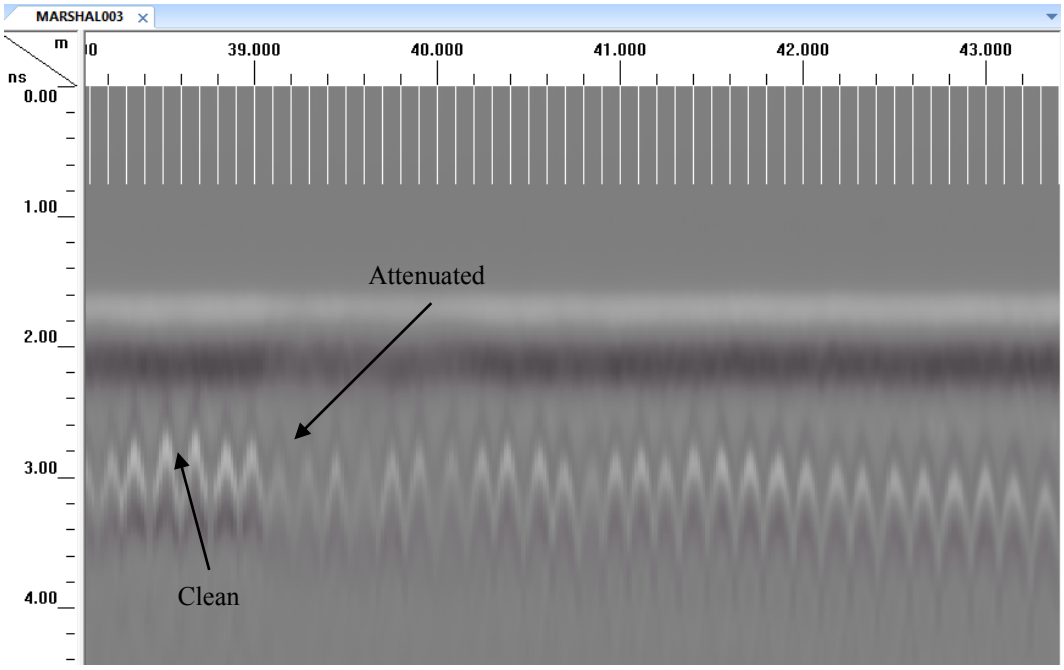

Figure 2.7: Typical reinforcement reflections

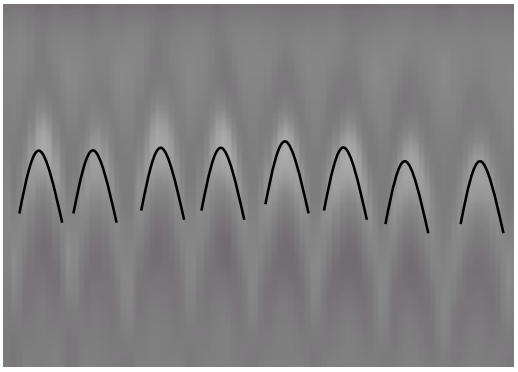

Figure 2.8: Close up of reinforcement reflections

Permeability and permittivity both have base values in free space and define the speed of light (c) in a vacuum. The permittivity of free space (ε_0) is approximately 8.854 x 10^{-12} F/m while the permeability of free space (μ_0) is 4π x 10^{-7} H/m. As they have base values, their relative values (ε_r and μ_r) are often quoted for materials. These relative values are the permittivity or permeability of the material divided by the base value of the property as seen in Equations 2.14 - 2.15. The relationship between permittivity, permeability, and the

speed of light in a vacuum is shown in Equation 2.16. For GPR analysis, μ_r has a value of 1 and any changes are known to be negligible.

$$\varepsilon = \varepsilon_r \varepsilon_0 \quad \textbf{[2.14]}$$

$$\mu = \mu_r \mu_0 \quad \textbf{[2.15]}$$

$$c = \frac{1}{\sqrt{\varepsilon_0 \mu_0}} \quad \textbf{[2.16]}$$

where:

c – speed of light in a vacuum (m/s)
ε – dielectric permittivity (F/m)
ε_0 – permittivity of free space (F/m)
ε_r – relative permittivity
μ – magnetic permeability (H/m)
μ_0 – permeability of free space (H/m)
μ_r – relative permeability

Permittivity has been shown to best relate to moisture content while it is not significantly affected by chloride content (Kalogeropoulos 2012). Chlorides and moisture content both affect the conductivity of concrete which is known to be the driving force of attenuation. This relationship with conductivity is the reason that attenuation is assumed to be indicative of poor concrete as increased chloride levels are often a sign of an environment that is conducive to the onset of corrosion.

Several methods of condition assessment of concrete bridge decks with GPR have been used over the years. Early studies were able to identify deteriorated concrete by noting

significant perturbations in individual scans (Cantor and Kneeter 1978). Scans were recorded on magnetic tape and accentuated peaks were manually identified which represented delaminations and significant cracking. These peaks were accentuated due to internal reflections that created constructive interference. In an effort to expedite the process of identifying these pronounced reflections, groups of 10 or so signals were superimposed over top of each other (Cantor and Kneeter 1982). Good concrete would have scans that overlapped nicely while deteriorated regions would exhibit spikes in the data. These methods were incredibly labour intensive and could only detect delaminations or substantial cracking.

Similar methods were used on both paved and unpaved concrete bridge decks with varying degrees of accuracy (Clemeña 1983, Manning and Holt 1983). Problems arose with the radar incorrectly identifying sound concrete as deteriorated in both of these studies, bringing into question the validity of radar for concrete assessment. Other research was also being done on the use of radar that was more cognizant of the properties of concrete during radar surveys by accounting for permittivity when analyzing surface reflections, although it was incorrectly assumed that all concrete had the same permittivity (Alongi et al. 1982). The effect of changes in the dimensions of voids was analyzed in this same study with the intent of better identifying internal reflections.

An investigation of the characteristic reflections of several defects in concrete decks developed mathematical methods of determining the type of defect present as well as the asphalt thickness on paved concrete decks (Carter et al. 1986). In order to identify these defects, a bare concrete deck with evidence of delamination was paved 3 years before GPR investigation was conducted. Before paving, debonding of the asphalt from the concrete was induced by applying a non-stick coating to areas of the deck and scaling was simulated by applying a coarse sand to the deck. Asphalt thickness measurements were deemed accurate by coring if the asphalt thickness was greater than 50mm. Detection of defects such as delamination and scaling were determined to be accurate while detection of asphalt debonding was determined to be unreliable. This study did not discuss how accurate scaling detection would be in practice relative to the simulated condition in this testing. In order to make the identification process more efficient, an automated process was developed using

ray based methods similar to Figure 2.5. The signal path is drawn out and detailed calculations are made for each reflection that takes place. This study determined that GPR was useful in condition assessments, but acknowledged the fact that the combination of deteriorations was difficult for the radar to properly detect. Determination of the type of deterioration may in fact prove to be more difficult in a less controlled environment and with significant deterioration of asphalt.

Further research led to the development of a methodology that was able to determine deck deterioration to within 4% of chain drag and visual inspections by area (Maser 1989). This research contained numerical analysis of radar signals as well as field and lab data. Contrary to the above study, this work determined that GPR could not detect delaminations unless they were at least 3mm wide and filled with moisture. Unless both of these criteria were met, it was determined that there would not be significant change in the waveform of a GPR signal to identify between sound concrete and delaminated concrete. It was also determined that increasing chloride content caused increasing attenuation of radar signals during testing. This was determined by comparing radar signals to chloride contents measured in the field.

One unpaved and twelve paved bridge decks were analyzed with a combination of GPR, infrared thermography, and visual inspection of the underside of the deck. Repair quantities were determined by overlapping the test methods and were within 4% by area of the actual area in need of repair determined destructively. A case study on how inspection accuracy affects cost during this research concluded that improvements in the accuracy of condition assessment could reduce life cycle costs by up to 20% while reducing the average deterioration level of the group of decks by 20-65%. Due to the apparent necessity of combining GPR with other test methods, it was determined that the radar alone was not sufficient to conduct condition assessment of concrete bridge decks. However, it was also stated that the assessment method showed great potential for future use if some advancements were made.

A second phase of the above research was conducted on an additional 15 paved decks to confirm and verify the previous results (Maser 1990). This second phase came to the conclusion that the first method was inadequate due to questionable results of the infrared

thermography that affected the accuracy of the condition assessment as a whole. A new GPR method was devised that, when combined with visual inspection of the underside of the deck, had an average of 2.8% error by area versus an average error of 6.8% by inspection engineers as determined by destructive results.

The American Society for Testing and Materials developed ASTM D6087 for evaluating decks both with and without asphalt which was originally introduced in 1997, but has since been updated (ASTM 2008b). This standard consists of two techniques that are applicable to both air and ground coupled antennas. The method accounts for asphalt overlay by more or less ignoring it and isolating reflections from the concrete surface. However, voids between the asphalt and concrete layers could be empty or filled with water and would substantially alter the signal at this interface. This phenomenon is left unmentioned in the standard.

The first of these techniques requires reflection from both the top and bottom surfaces of the concrete deck. In order to accomplish this, the bottom surface reflection must be of sufficient strength to analyze. Unfortunately it is seldom the case that this signal is clearly visible, let alone clear enough to determine the deck condition. If it is possible to use this method, delaminations are identified by setting a threshold for the bottom surface reflection in relation to the maximum bottom surface reflection. The problem with this method is that it does not account for differences in spreading losses due to changes in deck thickness. Further, delaminations must be of significant width to adversely affect the signal. The second method is based on the reflections from individual reinforcing bars in the top mat of reinforcement. Reflection amplitudes are measured and compared to a threshold that is not made available in the standard although an approximate range of values is given. Again, any constant threshold would not take into account variations in cover thickness that would significantly affect spreading losses.

The standard acknowledges the fact that there is insufficient data to substantiate the results gathered from this test method. It suggests an average error in predicting delamination quantities of 11.2% of deck area based on a sample of decks in New York, Virginia, and Vermont based on chain drag, coring, and repair quantities. This error is too large to see

this method used on its own to determine deck condition. Repeatability and bias tests had not been completed as of the most recent revision of the standard in 2008.

Further testing in cooperation with the Missouri Department of Transportation investigated 11 unpaved bridge decks with a ground coupled antenna (Cardimona et al. 2000). GPR data was visually examined and attenuated areas were identified. These areas proved to be a good fit to areas identified by half-cell and chain drag tests. It was noted however that it was difficult to determine the type of deterioration present in the deck, contrary to some previous research that claimed to accomplish this by visually analyzing waveforms.

Pre-repair analysis of travertine panels in the Bank of Naples was completed in part with GPR in an effort to detect the presence of voids in the mortar holding the panels, causing instability (Leucci 2003). Due to the small thickness of the panels (3cm) and the mortar (1cm or more), the accuracy of the GPR was put to the test. The through thickness resolution of the antenna is taken as one quarter of the wavelength (λ) which is dependent on the propagation velocity and the antenna frequency as shown in Equation 2.17. Horizontal resolution (A), which is in the plane of the panel surface, is dependent on the wavelength, the relative permittivity, and the distance from the target due to spreading of the signal and is described in Equation 2.18.

$$\lambda = \frac{v}{f} \qquad \textbf{[2.17]}$$

$$A = \frac{\lambda}{4} + \frac{d}{\sqrt{\varepsilon_r + 1}} \qquad \textbf{[2.18]}$$

where:

A – horizontal resolution (m)
d – distance from antenna to target (m)
f – frequency of antenna (Hz)
v – signal velocity (m/s)

λ – wavelength of signal (m)

Research was conducted with a 1 GHz ground coupled antenna in two phases. The first phase being in the laboratory on a recreated panel with known voids and the second phase being a field inspection of the panels in the bank. Due to the panel thicknesses involved, an additional 6cm travertine layer was placed between the antenna and the panel to eliminate the near field effects. Data collected in the laboratory portion of the investigation was used to analyze the panel in the bank and encouraging results were stated, although at the time of publishing in 2003 they had not been confirmed by coring. This study illustrates the difficulties present in identifying small voids in concrete bridge decks with GPR. Any voids in the decks are likely significantly smaller than the voids in the bank, the detection of which proved difficult in fairly ideal conditions.

The Handbook on Nondestructive Testing of Concrete details the issues and benefits associated with short pulse radar methods (Clemeña 2003). In detection of delaminations, the handbook states that GPR is an effective tool and is the only viable nondestructive process to use on paved decks. The handbook does note that GPR occasionally will miss delaminations or detect them when there are in fact none present. This is especially true for small delaminations at the reinforcing level as the reflections are received concurrently with those from the reinforcement and are indistinguishable from each other. A further limitation outlined was the lack of understanding of the effects of structure condition such as moisture content and the presence of defects in the concrete on GPR signals.

Thickness measurements with the GPR were deemed to be accurate based on the literature review in this handbook. The only significant limitation to this measurement is the case of negligible reflection at the interface between two materials. This could happen due to similar dielectric properties in both the material being measured and that underneath which would result in a negligible signal reflection. Another cause of this negligible reflection could be significant signal attenuation before reaching the interface. If the signal decays enough in the layer being measured, the returning signal will not be detectable. A brief mention was given to the use of GPR to determine both the water content of new concrete

and the degree of cement hydration. At the time of publishing of the handbook, little information was available on these methods as the processes were in their infancy.

A study on the validity of GPR for condition assessment of a paved deck was conducted in Missouri by comparing to half-cell and chain drag testing (Kim et al. 2003). During the half-cell test, areas of the deck with a potential difference greater in magnitude than -150mV were identified as deteriorated. The ASTM standard for half-cell measurements (ASTM 2009) states that potentials more positive than -200mV are not experiencing corrosion with 90% certainty and suggests using a threshold of -350mV. Therefore the validity of the half-cell measurements and the comparison to the radar data is questionable. Further, determining deteriorated concrete with the radar was done with a threshold signal level that did not attempt to correct for spreading losses due to differences in cover.

The effects of variations in weather condition were analyzed during this same study (Kim et al. 2003). No significant change in deteriorated areas were noted due to increased humidity and temperature although reflection returned in wet conditions were slightly stronger as would be expected due to an increased permittivity. No significant change in travel times was recorded due to changes in moisture levels. This paper concluded that GPR should not be used to locate delaminations or corrosion within bridge decks but that it could be used to identify areas of high relative permittivity or attenuation as these are sometimes linked to delaminations. No effort was made to link permittivity or attenuation to the condition of the deck directly.

An in depth study of the effectiveness of GPR on paved decks was conducted in Nova Scotia (Barnes and Trottier 2004). This study compared GPR results on 24 bridge decks to half-cell and chain drag quantities. It was concluded that GPR is most effective when a bridge deck is between 10 and 50% deteriorated although it was still not accurate enough to be used alone. Attention was drawn to the fact that it is outside this 10 to 50% deterioration range that visual inspection is most effective due to clear damage or lack thereof. While the potential of GPR to determine chloride ingress or corrosion damage was acknowledged, it was determined that GPR did not perform well in mapping precise locations between 10 and 50% deterioration even though it was the most effective

deterioration range. In this range, the GPR did produce similar repair quantities to chain drag due to false identification of both sound concrete and deteriorated areas balancing out to show no net error. Outside of this range however, GPR failed to provide useful repair quantities. Since the radar did not accurately identify the location of deteriorated concrete, it was concluded that GPR should be used as a second opinion to visual inspection to mitigate discrepancies between estimated and actual repair quantities.

Several previous methods of GPR condition assessment of bridges have been able to determine areas of deterioration comparable to half-cell and chain drag by using signal loss thresholds (Maser 1990, Cardimona et al. 2000) despite the fact that other research had questioned the validity of GPR for condition assessment due to its variability (Kim et al. 2003, Barnes and Trottier 2004). While loss thresholds may be effective for determining bad concrete versus good concrete, they do not give an estimation of the physical properties of the concrete or the risk of deterioration. In these analyses, a good correlation was found between the radar results and reference half-cell and chain drag tests but, without the results of these tests for reference, determining thresholds proved difficult. Omitting the effects of spreading and attenuation may be the cause of the variation that has so often been reported as the downfall of radar.

In an effort to make loss thresholds more indicative of the true concrete condition, methods have been developed to account for spreading losses by correcting for cover depth in an attempt to isolate the degree of attenuation experienced by each electromagnetic pulse (Barnes et al. 2008, Gucunski et al. 2009). Use of the depth correction approach in Barnes' research provided condition assessments within 5% of deck area (with one deck having an error of 12% compared to half-cell due to severe debonding) when compared to chain drag and half-cell testing on both paved and unpaved decks by simply accounting for spreading losses. The depth correction approach used by Gucunski was a part of a condition assessment with a variety of techniques and the specific accuracy of GPR was not discussed, although its usefulness as a condition assessment tool with depth correction was acknowledged.

For simplicity, much of the previous research has assumed concrete to have negligible conductivity, so velocity has been modeled as non-conductive as seen in Equation 2.19.

However, it is well known that GPR signals attenuate in concrete, which is primarily a function of conductivity. In order to include conductivity properly, conductive velocity and attenuation would be as shown in Equations 2.20 and 2.21 respectively. If the conductivity of concrete was in fact zero as has traditionally been assumed, Equation 2.20 would become Equation 2.19 and attenuation would be zero.

$$v = \frac{1}{\sqrt{\varepsilon * \mu}} = \frac{c}{\sqrt{\varepsilon_r}} \quad \textbf{[2.19]}$$

$$v = \frac{1}{\sqrt{\frac{\varepsilon * \mu}{2} * \left\{\sqrt{1 + \left(\frac{\sigma}{\omega * \varepsilon}\right)^2} + 1\right\}}} \quad \textbf{[2.20]}$$

$$\alpha = \omega * \sqrt{\frac{\varepsilon * \mu}{2} * \left\{\sqrt{1 + \left(\frac{\sigma}{\omega * \varepsilon}\right)^2} - 1\right\}} \quad \textbf{[2.21]}$$

where:

c – speed of light in a vacuum (m/s)
v – signal velocity (m/s)
α – attenuation coefficient (Np/m)
ε – dielectric permittivity (F/m)
ε_r – relative permittivity
μ – magnetic permeability (H/m)
σ – electric conductivity (S/m)
ω – angular frequency (rad/s)

Current models that include conductivity are fairly limited. One method isolates the attenuation by factoring out gain and spreading losses in an archaeological investigation

(Leucci 2008) while other authors have used the conductive model for soil investigation (Reppert et al. 2000, Lambot et al. 2004, Huisman et al. 2003). Very few models of concrete as a conductive medium for condition assessment have been published in the literature. One model of radar signals in concrete modeled the concrete as a low pass filter to account for signal attenuation, but did not include the conductive portion of velocity (Shaari et al. 2004).

Another method of modeling GPR signals used a waveform inversion approach to determine depth dependent material properties in a laboratory setting based on a finite-difference, time-difference forward model (Kalogeropoulos 2012). This method acknowledged the conductive properties of chloride laden concrete but used a non-conductive velocity method. Other researches have applied finite-difference time-difference techniques to model the GPR signal and determine concrete properties (Belli et al. 2009, Travassos et al. 2007). Again, these models treat the concrete as non-conductive while accounting for the attenuation of the signal.

Chapter 3: Methodology

To use the conductive properties of concrete to determine bridge deck condition, a conductive model of electromagnetic propagation had to both be created and proven accurate. The creation of the model was based on known electromagnetic equations and will be discussed in detail in Chapter 4. An outline of the process used to evaluate the conductive model can be seen in Figure 3.1. This chapter will describe both this evaluation process and the necessity of this model for the evaluation of reinforced concrete bridge decks.

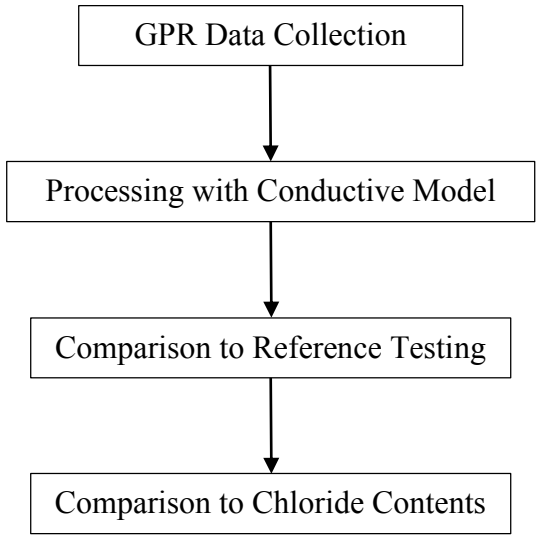

Figure 3.1: Progression of conductive model validation

3.1 Need for Conductive Model

As discussed in Section 2.3.4, the majority of current GPR analysis is performed under the assumption that concrete is a non-conductive medium. Due to this assumption, Equation 2.19 is routinely used to describe the velocity of each antenna pulse. However, it is widely accepted that attenuation of GPR signals is present in the condition assessment of concrete bridge decks. What is routinely neglected is the fact that, with zero conductivity, Equation

2.21 would also go to zero and no attenuation would be present. Since this is not the case, conductivity is clearly a factor. For this reason, Equation 2.20 will be used in this thesis along with Equation 2.21 to describe the propagation of electromagnetic signals through concrete as a conductive medium. This model is hoped to provide a more realistic representation of wave propagation and signal losses, allowing an increase in the accuracy of condition assessment.

Including conductivity in this model greatly increases the difficulty in determining velocity and attenuation due to the fact that both permittivity and conductivity become variable. To simplify calculation, the permittivity of a given deck is assumed constant with conductivity varying throughout. This assumption is valid due to the fact that permittivity is primarily a function of moisture content of the hardened concrete. Since the deck should have experienced the same degree of curing and environmental exposure, permittivity changes throughout the majority of the deck should be negligible.

The only areas of the deck that would be exceptions to this assumption would be areas of substantial cracking, where water would be free to infiltrate and collect. This change in permittivity would only happen in the most deteriorated regions of the deck. These same regions would likely show the highest levels of attenuation due to chloride content and would be identified as such whether or not the permittivity was assumed constant. However, since the permittivity would in fact be increased in these areas, they were avoided during the calibration of model curves, ensuring that the constant permittivity assumption would hold true for the model.

The effects of changing permittivity and conductivity on Equations 2.20 and 2.21 were examined. Plots of their effects can be found in Figures 3.2-3.5. These figures clearly show that permittivity is the driving force of velocity and that conductivity is the driving force of attenuation. However, Figure 3.5 shows that conductivity can actually have a significant effect on velocity, especially at low permittivities. This is evidence that a conductive model of propagation velocity is necessary to accurately model the effects that concrete, and especially chloride laden concrete, has on electromagnetic waves. Correctly modeling the velocity allows depth determination to improve, providing better estimates of spreading and attenuation losses.

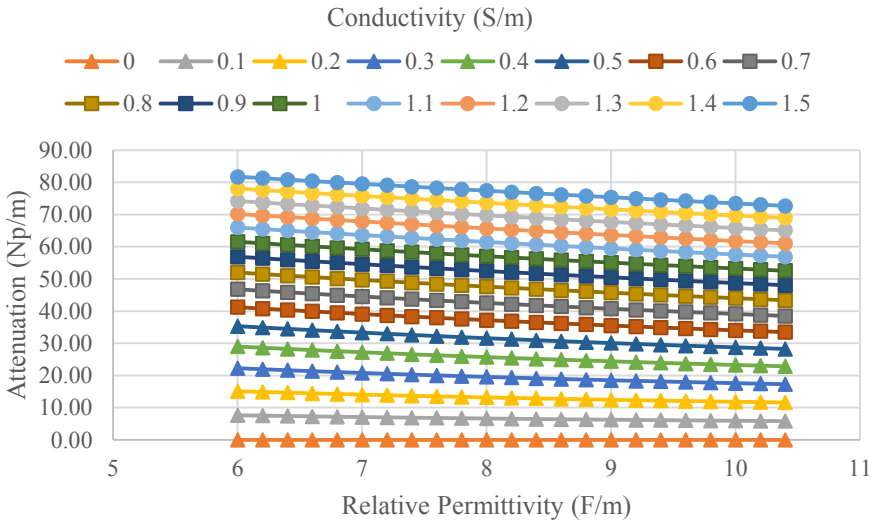

Figure 3.2: Effect of permittivity on attenuation coefficient for different values of conductivity

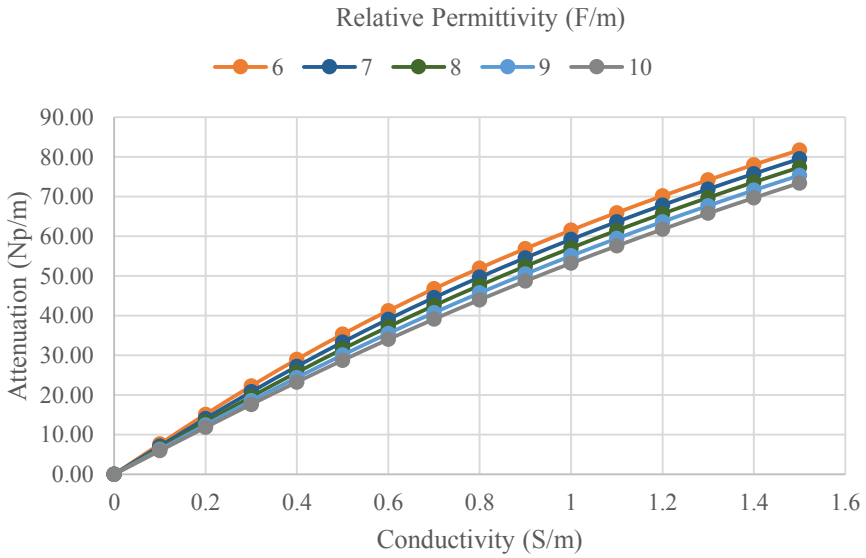

Figure 3.3: Effect of conductivity on attenuation coefficient for different values of permittivity

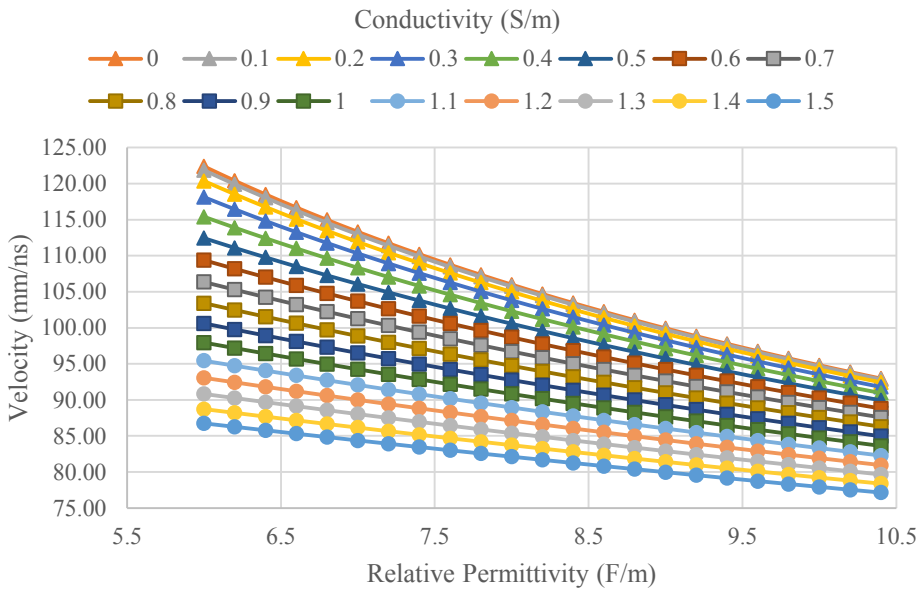

Figure 3.4: Effect of permittivity on velocity for different values of conductivity

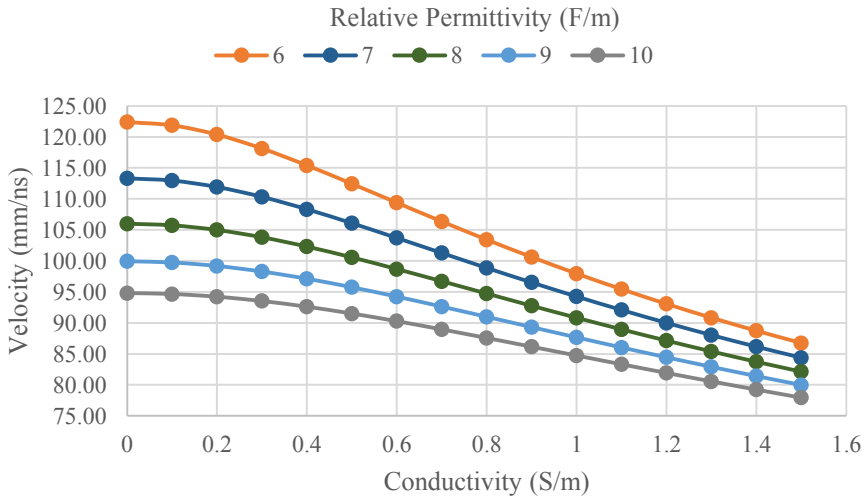

Figure 3.5: Effect of conductivity on velocity for different values of permittivity

3.2 Comparison to Reference Bridges

In order to prove the validity of a conductive model of electromagnetic wave propagation through concrete, previous GPR data from 5 unpaved bridge decks (Redmond 2007) were reanalyzed. Along with GPR surveys, each deck was tested with both the half-cell and chain drag techniques and cores were extracted for visual inspection and establishment of chloride profiles. After analysis of the GPR data with the conductive model, results were compared to the other testing methods to assess the accuracy of the model.

Data collection for all bridges discussed in this thesis was performed with a 1.5 GHz model 5100 ground coupled antenna from Geophysical Survey Systems Incorporated (GSSI). The antenna was used in conjunction with a SIR-20 controller, also from GSSI. Data collection was completed during previous research (Redmond 2007) and was reprocessed from its raw format for use in this thesis. During the scanning of each bridge, survey lines were drawn in the direction of traffic flow beginning 0.25 metres from each curb and then every 0.5 metres after that as seen in Figure 3.6.

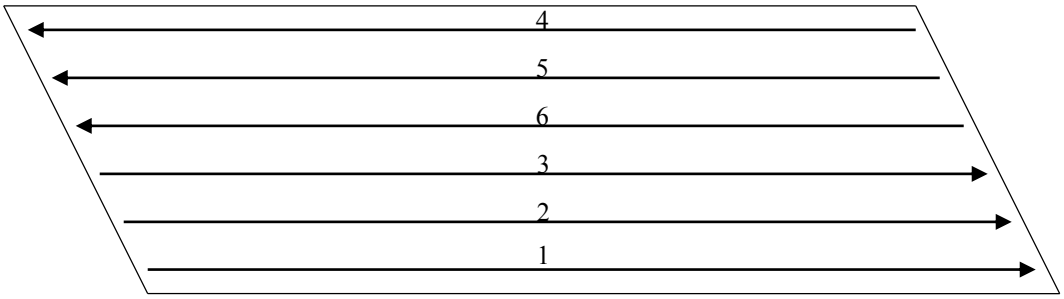

Figure 3.6: Example of scan pattern for GPR survey

Five unpaved concrete decks in Nova Scotia were investigated to demonstrate the capabilities of the conductive model as described in Table 3.1. These structures had varying ages and levels of degradation in order to test the model for a variety of scenarios. Upon completion of data processing, the model was compared to the reference testing and the chloride contents determined from cores in order to establish the effectiveness of the model. In order to be deemed successful in assessing the condition of a concrete deck, the model

would have to closely match both half-cell and chain drag results. Since half-cell identifies the onset of corrosion and chain drag identifies areas where corrosion has progressed to the point of delamination, it would be natural to assume that a conductivity value that would match half-cell results would be lower than a value that would match chain drag results. For this reason, two conductivity values were determined for each bridge for comparison with the reference tests.

Table 3.1: Bridges used in study

	Location	Age (Years)	Span (m)	Area (m^2)	Lanes Scanned
Milford	Bridge on Rt. 2	36	61.5	502	2
Sambro Harbour	Bridge on Rt. 349	27	57.6	317	1
Shubenacadie	Overpass for Exit 10, Hwy 102	38	74.4	658	2
Victoria Harbour	Overpass for Exit 16, Hwy 101	28	43.3	493	2
West River	Overpass on Hwy 104	8	70.8	175	1

To be successful in determining chloride contents with conductivities determined from GPR testing, calculated conductivities should show a consistent relationship with the chloride contents established from the cores extracted from the decks. Ideally this relationship would allow chloride content to be directly calculated from conductivities determined through the model. Results of this comparison, along with those of the conductive model compared to the reference testing, will be discussed in Chapter 5. These comparisons will aid the establishment of a conductivity threshold to identify areas of a concrete deck that have significant corrosion risk.

Chapter 4: Conductive Model and Data Processing

Each of the five bridge decks in this study were scanned, processed, and modeled in the same general fashion. Minimal processing was performed on the data before modeling in order to avoid significantly affecting the results. Processing steps such as filtering the returning signals or adjusting the travel time of the data could affect the amplitudes of the signals reflected from the reinforcing which would alter the properties determined by the model. The overall procedure for each bridge was as shown in Figure 4.1. Each of these steps will be described in this chapter with any adjustments being discussed in full in Chapter 5.

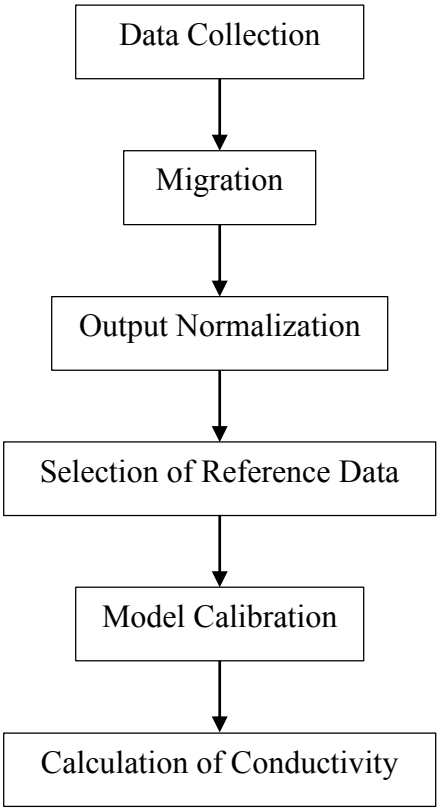

Figure 4.1: Condition assessment progression

4.1 Processing

Once the data was collected, it was processed using Radan 7; the commercial software provided by GSSI. The only processing that was done to each scan in the software was a Kirchhoff migration to collapse reflection parabolas to single points through an averaging process. This process assumes a signal velocity for a given scan and uses it to collapse the parabolas into a single point (Yilmaz 2001). If too high a velocity has been used, inverted parabolic tails can be seen above each rebar reflection. If too low a velocity has been used, parabolic tails are visible below each bar. An example of each of these cases is shown in Figure 4.2. Once the correct velocity has been chosen, these tails are either no longer visible or slightly visible both above and below the reinforcement location. In Radan 7, the velocity is entered by the data analyst. If the parabolas appear incorrect, a different velocity is chosen and the migration is carried out again. One way to ensure a velocity is being used that is close to the true value is to use a process available in Radan 7 to fit a model parabola to the reflections in the raw data. This is done by adjusting the model parabola to fit a reflection parabola in the data that appears to be typical of the rest of the antenna pass. Each antenna pass for each bridge was migrated separately to ensure the correct velocity was chosen for each pass. A narrow range of velocities were used for each of the bridges as seen in Table 4.1.

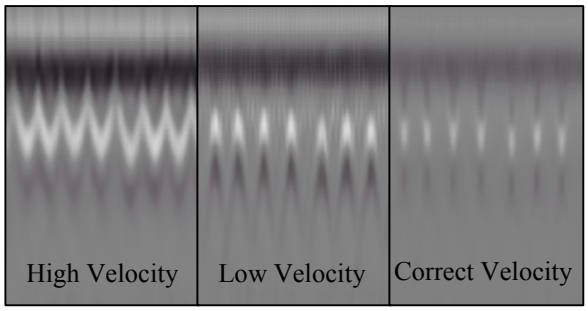

Figure 4.2: Reinforcement reflections after migration

Table 4.1: Propagation velocities for migration of tested bridges (mm/ns)

	Milford	Sambro	Shubenacadie	Victoria	West River
Average	80.8	86.3	86.3	81.9	95.3
Minimum	78	84	84	80	94
Maximum	84	88	88	86	98

The velocities used for migration did not match well with calculated velocities or those determined from core data. This could be due to the assumptions made in the migration process. Migration assumes that the velocity is laterally invariant, that there is no separation between the transmitter and receiver, and that all materials are lossless, among other things (Jol 2009). All of these assumptions are invalid when modeling concrete as a conductive medium and could cause significant errors in the estimation of velocity. Further, velocity will vary significantly laterally; not only due to the chloride content, but as the pulse passes through cement, aggregate, voids, or any changes in moisture content. While it is reassuring that the velocities for each deck are consistent, the overall magnitudes should not be taken as entirely accurate. Migration was still used to process the GPR data in this study as it averages all of the scans for each reinforcing bar, providing a more representative value of signal amplitude. The amplitude values returned may be lower than those before migration due to attenuation that is not accounted for in the migration process, but the decrease should be fairly uniform and is not expected to significantly affect results.

Once migration had been completed for a data file, points were manually picked for the ground couple reflection and for each rebar reflection. Radan then allows these picked points to be exported to a text file which can then be transferred to a Microsoft Excel spreadsheet. The data transferred consists of the longitudinal position of each scan, the amplitude in Radan's amplitude units, and the two way travel time. This information is provided for both layers of reflections that are selected. To compare amplitudes, the value at each point is converted to decibels by comparing each signal to the maximum possible recorded signal amplitude of 2^{15} based on the 16 bit data acquisition system used with the radar as seen in Equation 4.1 (Barnes et al. 2008). Since each radar pass of each bridge was

processed separately, they were pieced together in Microsoft Excel to analyze the bridge as a whole.

$$\mathrm{Amp_{dB}} = 20 * log\left(\frac{\mathrm{Amp_{AU}}}{2^{15}}\right) \quad \textbf{[4.1]}$$

where:

$\mathrm{Amp_{AU}}$ – signal amplitude in Radan's Amplitude Units (AU)
$\mathrm{Amp_{dB}}$ – signal amplitude in decibels (dB)

In order to represent the physical processes that take place during the propagation of an electromagnetic wave through concrete, a conductive model was applied to each set of GPR data. By using the conductive velocity equation in conjunction with attenuation as in Equations 2.20 and 2.21 respectively, determination of conductivities throughout the deck is made possible. This model assumes that the moisture content in the majority of the concrete is constant due to consistent curing throughout the deck and will be explained fully in Section 4.4. Since moisture content is assumed constant, permittivity must be constant as well since it is almost entirely affected by moisture. Furthermore, since conductivity is affected by both moisture and chloride content, a constant moisture content would imply that any change in conductivity would be driven by chlorides or other external forces. The fact that a very narrow range of velocities was used for the migration of each bridge deck in this study gives credence to the assumption that permittivity remains relatively constant throughout the deck as it is the driving factor in the velocity equation. Although the magnitude of these velocities may not be entirely accurate due to the assumptions made during migration, the low degree of variation in each deck should indicate fairly low fluctuations in the true velocity. If the moisture content and therefore signal velocity was changing significantly throughout a bridge deck, it would be apparent in the migration velocities for the deck.

Any variations in velocity in each scan can be attributed to a change in conductivity when constant permittivity is assumed. There are areas in the decks where the velocity chosen is not a perfect match but these are a relatively small percentage of each deck and are indicative of more extensive deterioration. These areas are picked up as having elevated conductivity in the model while permittivity is held constant, so they are not neglected in condition assessment of the deck.

To determine the conductive properties of a given bridge deck, each scan must be isolated and its conductivity solved for. This is accomplished by determining the attenuation and velocity of each signal instead of simply applying loss thresholds. By combining Equations 2.20 and 2.21, signal properties were broken down into values of conductivity and permittivity for points along each deck. If each scan was calculated individually, it would not be possible to determine the two parameters as it would be one equation with two unknowns. This problem is resolved by holding permittivity constant for the deck and iteratively solving for conductivity.

4.2 Theory

The assumption of constant permittivity in this model only applies to concrete that is not seriously damaged. This would only limit use in cases of decks so severely damaged that moisture could freely pass through cracks and delaminations throughout the entire deck. Damage this severe to an entire deck would likely be easily identified either visually or once GPR data had been collected. The areas of the deck that have excessive cracking and void spaces will have excess moisture and an increased permittivity as conductivity increases even further due to additional chlorides being brought into the deck along with the moisture. Given this more detailed assumption, it is understood that any velocity or attenuation changes from one scan to the next are due to increases in conductivity in sound concrete and due to increases in permittivity along with conductivity in cracked concrete with excess moisture. This mechanism can be seen in Figures 4.3 through 4.6 which are taken from the Milford bridge deck. The main points on these figures are the individual reinforcement reflections with changing amplitude and travel time values due to changes in concrete cover and attenuation.

Figure 4.3 shows the amplitude and two-way travel time changes when there is no change to either the conductivity or permittivity parameters. There is a given two-way travel time change as the cover thickness of the concrete deck changes, lengthening the path of the signal. The amplitude changes are due to both spreading losses and attenuation of the signal as it travels through the deck. Since the parameters are constant, the attenuation coefficient and signal velocity are also constant.

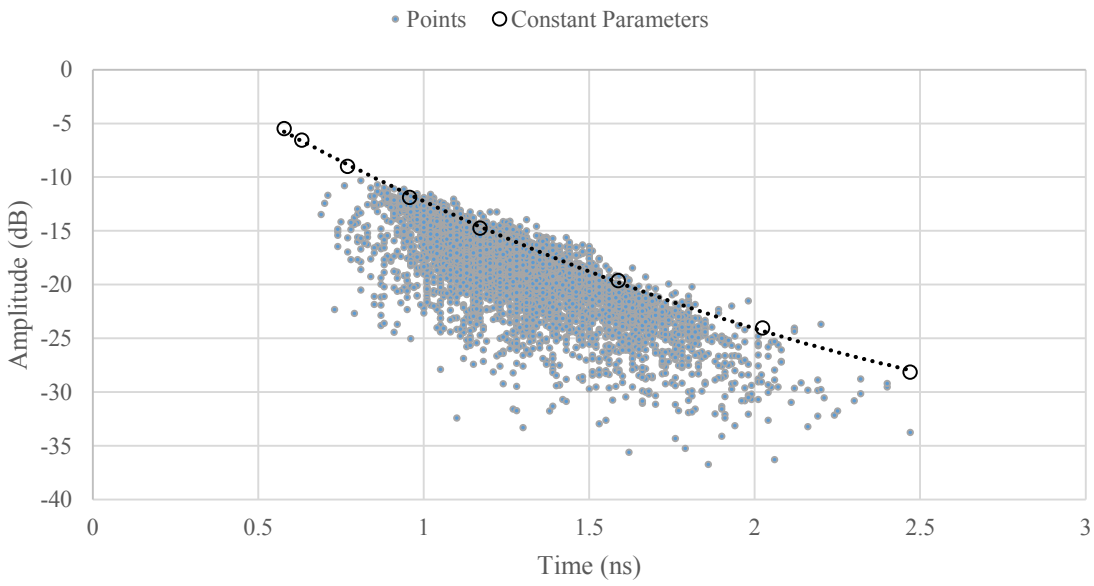

Figure 4.3: Time and amplitude changes with constant permittivity and conductivity

Figure 4.4 shows the changes to amplitude and travel time caused by increases in conductivity. The conductivity increases the attenuation losses in the concrete which decreases the amplitude. Increased conductivity also decreases the signal velocity, increasing the travel time. Any reinforcement reflections that fall on the changing conductivity curve have the same concrete cover thickness as the point where the changing conductivity curve intersects the constant parameters curve. The differences in amplitude and travel time are due to the changes in the velocity and attenuation coefficient that correspond to the changes in conductivity. This would be true at any point on the constant

parameters curve, which means that the changing conductivity curve essentially slides along the constant parameters curve, with the effects of the changing attenuation coefficient and velocity becoming more significant the further the signal has to travel in the concrete. This is shown in Figure 4.5 where the changing conductivity curve is compared to the constant parameters curve at several cover thicknesses, each time increasing conductivity from 0.04 S/m to 0.22 S/m as the amplitudes decrease. If only the conductivity is changing as in this figure, known differences in amplitude and travel time between the constant parameters curve and a given reinforcement reflection due to a conductivity change can be used to determine the conductivity of the concrete cover above each individual bar.

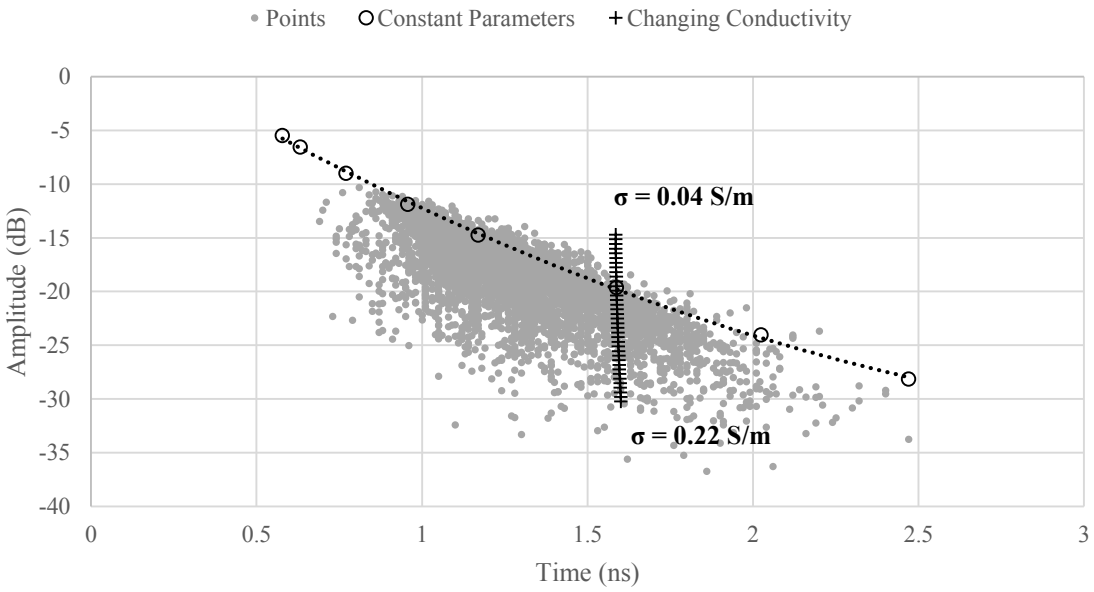

Figure 4.4: Effect of changing conductivity on amplitude and travel time

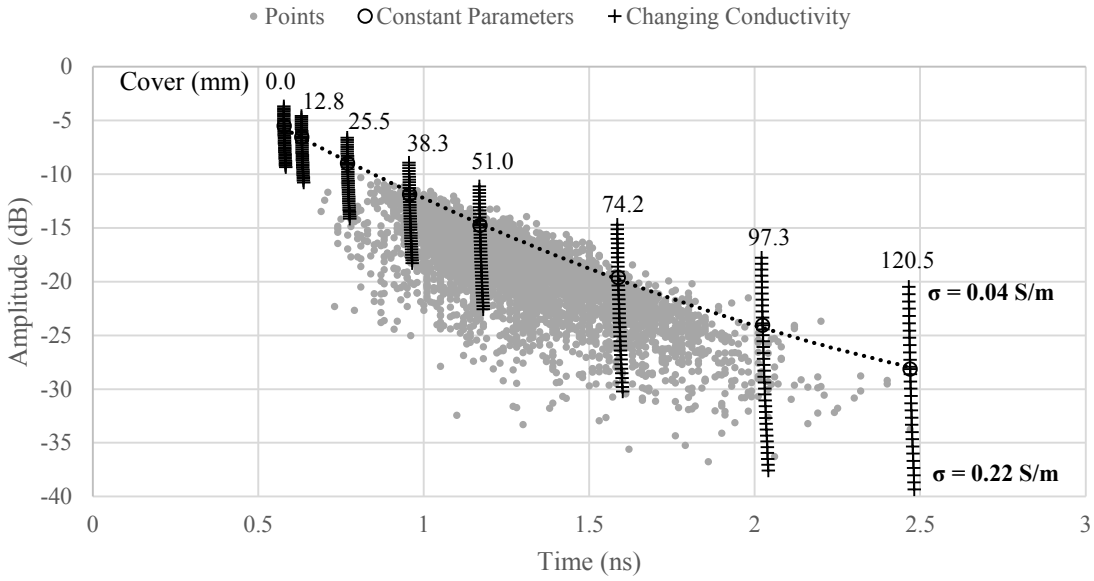

Figure 4.5: Effect of changing conductivity for varying cover thicknesses

Figure 4.6 shows what happens when permittivity increases along with conductivity. This would happen in the severely deteriorated areas of a deck where moisture penetrates large cracks and delaminations. Velocity decreases are more significant with the increase of permittivity along with increasing conductivity. Amplitude changes are slightly less significant than when only conductivity changes as increased permittivity slightly decreases the attenuation coefficient. As was the case when only conductivity was changing, this curve slides along the constant parameters curve and can be related to any reinforcement reflection with the same concrete cover. In this case however, any changes are due to both permittivity and conductivity changing, greatly complicating calculation of the properties. Since both properties could change, it becomes unclear if permittivity, conductivity, or some combination of the two is changing from one reinforcement reflection to the next.

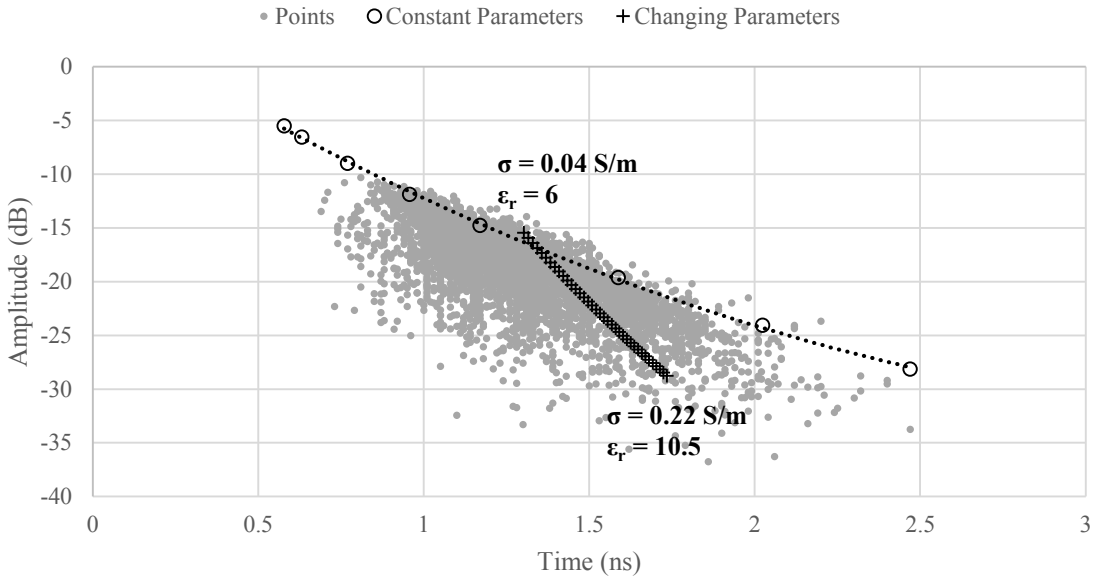

Figure 4.6: Effect of changing permittivity and conductivity on amplitude and travel time

Much of the deck appears to follow the rapid drop in amplitude due to increasing conductivity while the lowest amplitude values also have an increase in travel time due to both permittivity and conductivity increasing, similar to the changing parameters curve in Figure 4.6. How deteriorated the bridge deck is will affect the point at which the moisture effects begin to be seen as they will be in the most deteriorated regions.

During analysis, it is assumed for simplicity that only conductivity is changing. This is due to the complex nature of determining whether changes in conductivity, permittivity, or a mixture of the two are affecting amplitudes and travel times throughout the deck. This assumption should not adversely affect the model as the severely degraded areas with changing permittivity would be found to have the highest conductivity values and would be identified as poor concrete. While model curves were established to analyze the data, the more degraded regions having higher moisture levels were avoided in order to keep the curves representative of the deck as a whole. These deteriorated regions were compared to the model curves in the same manner as other points, but model curves were not plotted through them due to their inherent variability and the fact that it would invalidate the

constant permittivity assumption. Regions this deteriorated would be represented by the sparse points with low amplitude seen below the bulk of the data in Figure 4.6.

4.3 Output Normalization

Ground penetrating radar sends signals that originate from a slightly variable power source, the degree of the variability being based on the quality of the equipment being used. These variations alter the amplitude of the outgoing signal which of course affects the amplitude recorded once the signal is returned. To account for these fluctuations, the ground couple reflections are used as an indicator of original signal strength as any signal losses should be minimal and relatively constant between scans. Ground couple reflections are a combination of the direct signal between the transmitter and receiver and the signal that reflects off of the concrete surface as shown in Figure 2.5. These signals both travel through constant material properties and travel distances during each scan, so returning amplitudes should not vary significantly.

Previous research has been done on the usefulness of the surface reflection for condition assessment of concrete decks (Sbartaï et al. 2006). In this study, they determined that the surface reflection was well correlated with the reinforcement reflection and even cautioned against low quality power supplies due to variations in the signal output. They determined that the surface reflection may be indicative of some concrete properties at the surface relative to those at other locations but the results were not definitive. It does however show that the surface and reinforcement reflections are linked, as would be expected. It also brings to attention the variability that can be experienced in GPR output due to the power supplied to the antenna.

Surface reflections are often difficult to analyze with ground coupled GPR antennas due to the fact that the direct signal and surface reflections interfere with each other and the complex near field effects of the antenna. It is difficult to separate these two waves for analysis purposes as both the initial signal strength and the degree of reflection from the surface can vary. The purpose of this normalization was to limit variations in signal strength due to power fluctuations by forcing the surface reflections to remain constant. The ground couple reflection was used for this purpose because it should not be

significantly affected by the material properties of the concrete as reinforcement reflections would, so any variations in signal strength would be indicative of power fluctuations.

To study the effects of power fluctuations in the equipment used in this research, polystyrene was placed over a steel plate to examine the amplitudes returned by the direct couple signal and by reflections from the plate. Polystyrene was used because it has a permittivity very close to that of air and is non-conductive, so no significant surface reflection or attenuation would occur. The direct couple returning amplitude was analyzed both when the antenna was held in the air and when it was in contact with the polystyrene. The equipment used was a GSSI 5100 1.5GHz antenna with a SIR-20 controller, the same equipment that was used in the field. Data analysis was performed with Radan 7 software in the same fashion as for the bridge decks, with the only exception being that since there were no reinforcing bars, no migration could be performed on the data. The steel surface was cleaned and dried and all polystyrene was brushed clean. Sheets of polystyrene with dimensions of 406 x 508 x 51 mm were added one at a time and scanned. This process was repeated twice and a total of eight polystyrene sheets were used in each trial. One additional scan was recorded in each trial to record the direct couple amplitude while the antenna was held in the air. A range of antenna heights relative to the steel plate were used to ensure that reflections from the plate were not interfering with the direct signal from transmitter to receiver.

After completion of the tests, the amplitude data was collected for each scan. The range of amplitudes for each scan was broken into fifteen amplitude bins and the frequency of returned amplitudes in each of these bins was plotted. These plots showed that the signal amplitude tended to a normal distribution. A normal distribution makes sense for initial signal strength as it is likely to appear random due to the fact that scan rate of the antenna is unlikely to match with the frequency of any power fluctuations. Representative examples of the test data can be seen in Figures 4.7 - 4.9. It should be noted that the two way travel time of direct couple signals varied within 0.02 ns, even while the antenna was held in the air. Since this discrepancy does not make sense from the perspective of a physical signal transmitting through constant material properties, it must be due to the method of picking points within the Radan software varying slightly as it automatically chooses the strongest

amplitude in a given signal that is selected by the user. This process is not perfect, and will have some variation. It should also be noted that from one scan to the next, the initial surface two way travel time can vary significantly. This variation is likely due to the state of the antenna at the instant the scan is begun and is ignored by using the difference in time between the reinforcement reflection and the ground couple signal to determine propagation distance within the concrete deck.

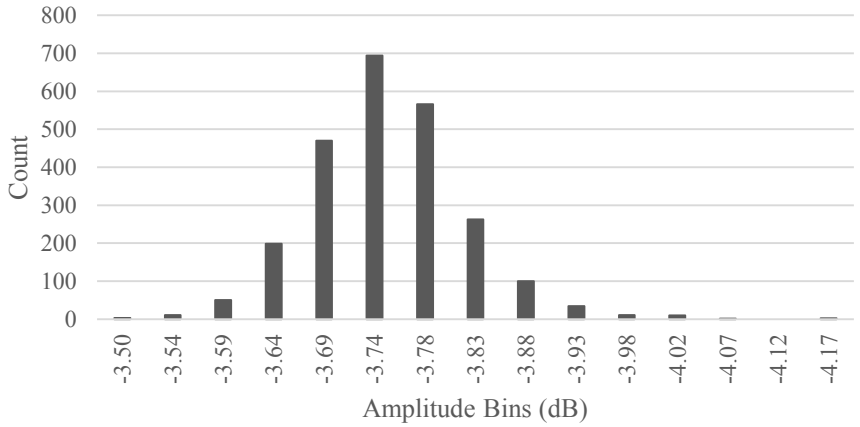

Figure 4.7: Frequency of direct couple amplitudes (antenna in air)

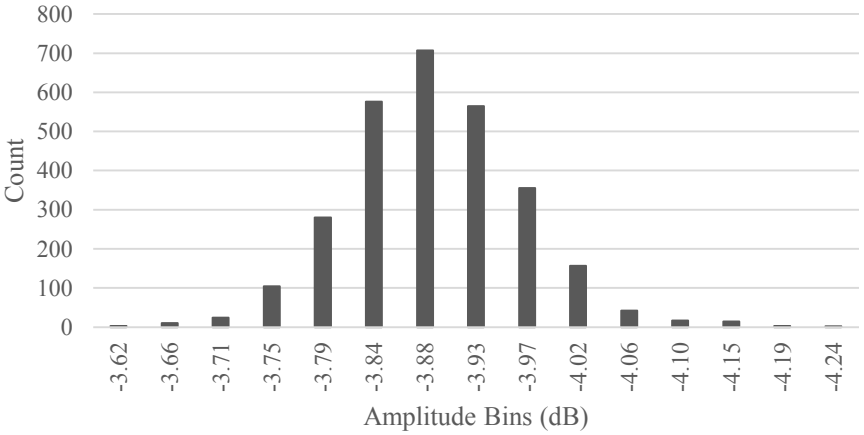

Figure 4.8: Frequency of direct couple amplitudes (antenna on polystyrene)

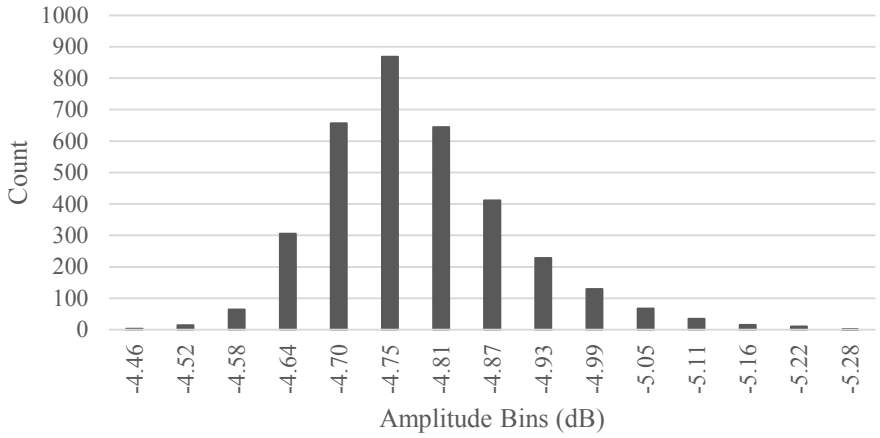

Figure 4.9: Frequency of reflected amplitudes (antenna on polystyrene)

The fact that these signals are varying without passing through any significantly conductive material shows that the output amplitude must naturally vary over time. Since the data tends to a normal distribution, it seems natural to adjust for its effects based on the mean ground couple amplitude of the data. For analysis of bridge decks, the amplitude of each scan is modified before material properties are calculated to account for the variation of the input signal strength. The direct couple amplitude while the antenna is on the concrete surface is used to accomplish this. For each recorded two way travel time, the frequency of returning amplitudes were plotted as in the tests discussed above to evaluate the significance of any power fluctuations and to account for them.

The reflections collected in the field also tended to a normal distribution as seen in the lab testing. In order to analyze the deck as a whole, scans with each two way travel time were individually gained so that the means for each two way travel time coincided with the mean direct couple amplitude of the deck. Each scan was then gained so that each direct couple amplitude coincided with the deck mean. This removes the effect of any power fluctuation before full data analysis. GPR data from the Milford overpass before and after this normalization is shown in Figures 4.10 and 4.11. It can be seen that the normalization process provides data that has a clearer trend, especially after about 1.4 ns in Figure 4.11.

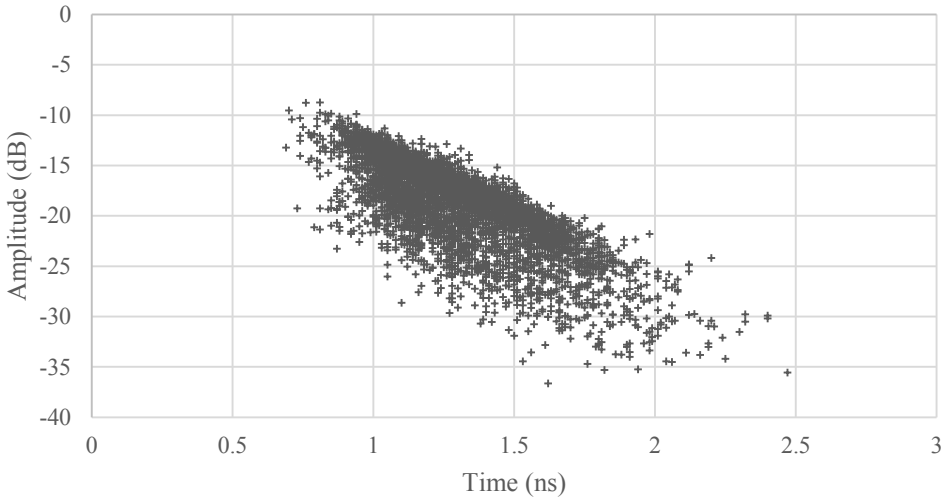

Figure 4.10: Raw reflection amplitudes from Milford Overpass

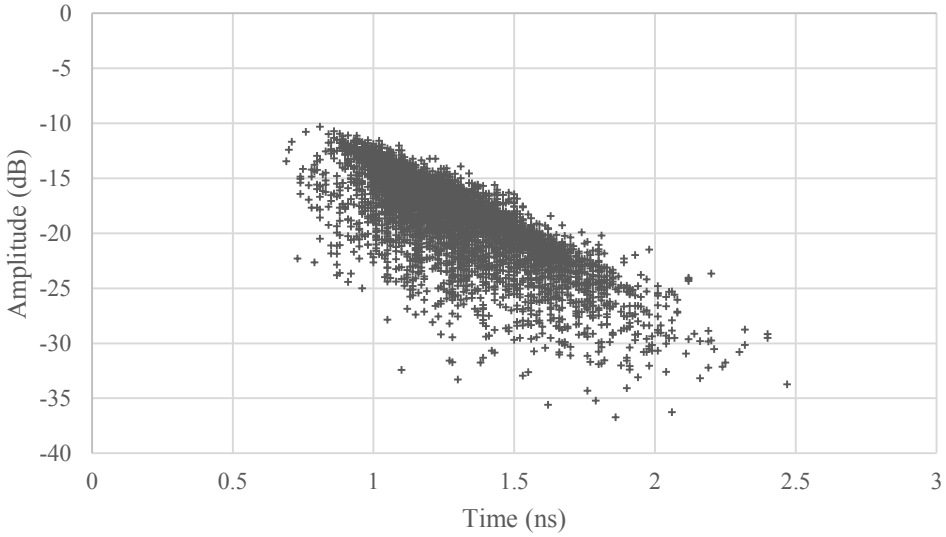

Figure 4.11: Reflection amplitudes after normalization from Milford Overpass

4.4 Deck Modeling

Once the variable initial amplitude had been accounted for, the properties of the concrete in a given deck were modeled. First, representative points were chosen from the total population of radar data. These points were assumed to be representative of constant

deterioration levels throughout the deck. This was done by finding reinforcement reflections that represented the 90th, 60th, and 30th percentile amplitude values of the total deck. These points were then used as a baseline for the model and are found in Figure 4.12. Each percentile corresponds to a different level of chloride induced deterioration. The 90th percentile data for instance would correspond to some of the lowest conductivities and chloride contents while the 30th percentile data would have some of the highest.

If a substantial amount of fluctuation was determined in the 30th percentile data, a higher percentile value would have been used to ensure the constant permittivity assumption was still valid. Substantial fluctuations could be indicative of damage to the point of increased permittivity, which would not be valid with the constant permittivity assumption. Naturally, decks with more data points will have better representative data as these representative points are selected from the entire population of data. With a larger data population, these representative points will follow a smooth curve that is indicative of a constant attenuation coefficient and signal velocity. Decks with fewer points will not have representative points that plot as smoothly. The slight variation shown in the 30th percentile data below would become more pronounced and could be present in all three sets of representative data if few points were available.

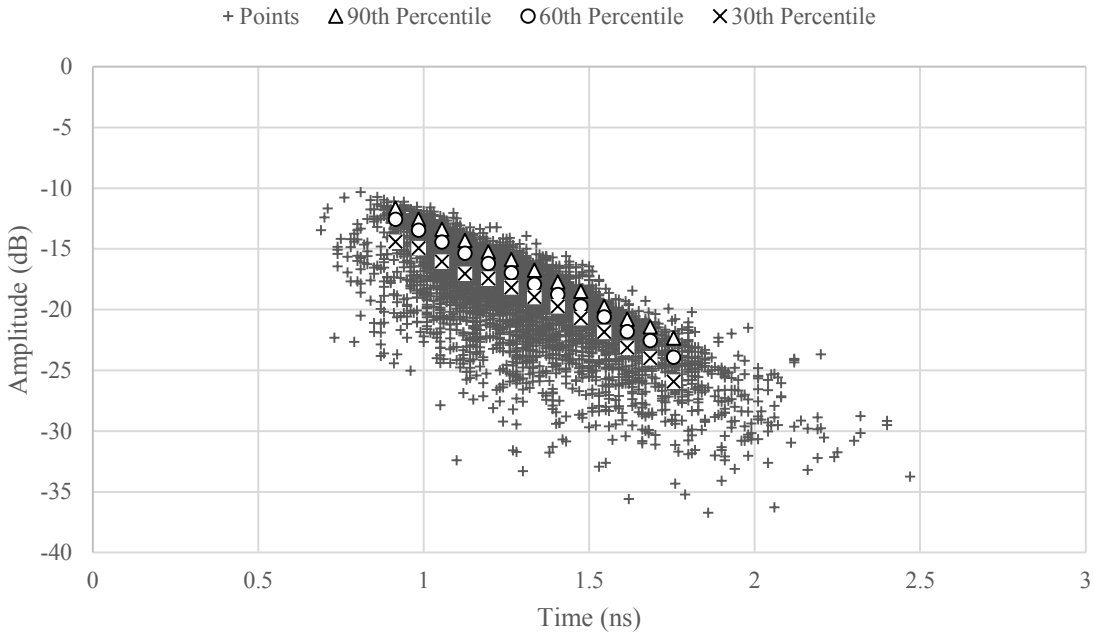

Figure 4.12: Representative data from Milford Overpass

Once these reference points are plotted, a model of spreading and attenuation losses and propagation velocity is fit to the data. Spreading losses in decibels are proportional to $1/d^2$ with d being the total travel distance of the signal. Since this relationship is proportional and not exact, it is beneficial to determine spreading losses relative to a known point. By relating to a known point, any coefficient attached to the distance term is cancelled out when the relative spreading loss is calculated as will be shown in Equation 4.3. The velocity and attenuation equations used in the model are Equations 2.20 and 2.21 respectively. The amplitude as a whole can be calculated as shown in Equation 4.2 in Radan's amplitude units (AU).

$$\mathrm{A}(t) = \mathrm{A}_0 * \frac{1}{\mathrm{vt}} * \exp\{-\alpha \mathrm{vt}\} \qquad \textbf{[4.2]}$$

where:

A_0 – initial amplitude (AU)
A(t) – amplitude at time t (AU)
t – time (s)
v – velocity (m/s)
α – attenuation coefficient (Np/m)

Laboratory testing was conducted to confirm that the spreading losses are proportional to the inverse of the distance squared. During the testing described in Section 4.3, the average amplitude in decibels returned from the steel plate at each polystyrene thickness was recorded for each of the two trials. The average signal from each test was plotted along with a model of $1/d^2$ multiplied by a constant of 0.0054. The constant was determined by minimizing the decibel difference in amplitude between the spreading loss curve and the collected data. The square of the distance was used due to the conversion from amplitude units to decibels because power is proportional to the square of amplitude. The model fit the majority of the points very well as shown in Figure 4.13, confirming the validity of the model. The divergence of the model points from the collected data was at an antenna height of 50 mm and below, becoming very pronounced when the antenna was directly on the steel plate. This is likely due to the complicated signal reflections in the near field of the radar antenna (Daniels 2004).

The assumptions made in radar analysis are based on the far field range of a given antenna. When reflections are extremely close to the antenna transmitter, these assumptions are no longer valid and more complex models must be used. The majority of reflections from concrete decks are deep enough to be outside the near field, so this seldom poses an issue. Surface reflections are inside this zone and therefore become difficult to use for the determination of concrete properties with ground coupled antennas. Although they are in the near field, the normalization described in Section 4.3 simply adjusts the signals so that they are consistent and determines no properties from the surface reflection.

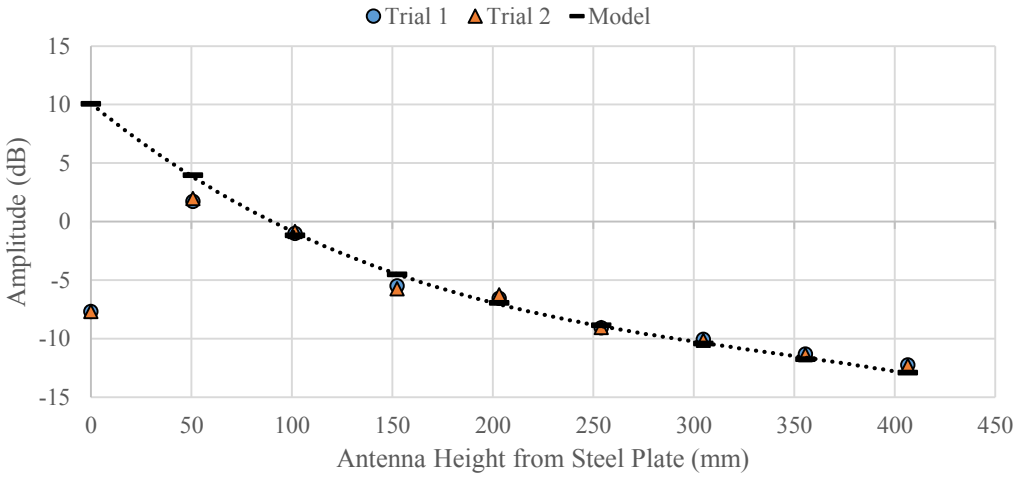

Figure 4.13: Modeled and recorded spreading losses

After representative points are chosen, a reference time with a sufficient amount of data points is chosen from the middle third of the data. This reference time was necessary to be able to determine relative losses from a fixed travel distance. The middle third of the data was used due to the high concentration of data points, giving a more statistically significant value. The 90^{th}, 60^{th}, and 30^{th} percentile amplitude values for this time are determined and used as reference points to calculate relative losses for each percentile level as the concrete cover thickness changes. The signal model is built around each of these three reference points by setting the model equal to the amplitude of the reference point at the reference time, and then calculating the relative change in amplitude and travel time as the cover changes. The model values are then compared to the values of the representative data of the same percentile level.

For a given change in travel distance, the difference in amplitude between the reference point and the point being calculated can be determined based on the attenuation and velocity values determined for the model curve. Initial values of permittivity and conductivity are chosen for the model, then optimized to fit the collected data. One permittivity is used for each deck and a different conductivity value is used for each of the three representative percentile data sets.

The decibel change in amplitude due to spreading is shown in Equation 4.3. Since the velocity is constant for the model curve due to constant permittivity of the deck and constant conductivity of the deterioration level, this change simplifies to Equation 4.4. Amplitude changes due to attenuation with a constant attenuation coefficient for each model curve are calculated as shown in Equation 4.5 which simplifies to Equation 4.6. The total decibel change is calculated by adding the attenuation and spreading effects together. Equations 2.20 and 2.21 can then be incorporated to calculate the total decibel change for a change in travel distance as in Equation 4.7. Since conductivity and permittivity only appear in Equation 4.7 as a ratio, an infinite number of solutions could be determined as long as the ratio of conductivity over permittivity remains constant. A conductivity of 0.1 S/m and a relative permittivity of 7.5 is a much different situation in reality than a conductivity of 0.2 S/m and a relative permittivity of 15. In the second case, much more moisture is present, leading to a lower velocity, while the conductivity value is significantly larger. This could result in false identification of chloride induced damage, or the omission of such damage and would result in incorrect determination of cover thicknesses.

In order to overcome this problem, multiple curves were fit to each deck. Since they all have the same permittivity, the conductivities for each curve can be determined iteratively by relating their amplitude values at given points to each other. The differences between the amplitudes and travel times of the individual model curves should agree with calculated signal losses and velocity changes based on the shift in conductivity from one curve to another.

$$\Delta dB_{Spread} = 10 * \log\left(\left[\frac{B * v_{ref} t_{ref}}{B * v_i t_i}\right]^2\right) \quad \textbf{[4.3]}$$

$$\Delta dB_{Spread} = 20 * \log\left(\frac{t_{ref}}{t_i}\right) \quad \textbf{[4.4]}$$

$$\Delta dB_{Atten} = 10 * \log\left(\left[\frac{\exp\{-\alpha v t_i\}}{\exp\{-\alpha v t_{ref}\}}\right]^2\right) \quad \textbf{[4.5]}$$

$$\Delta dB_{Atten} = 20 * \log(\exp\{-\alpha v(t_i - t_{ref})\}) \quad \textbf{[4.6]}$$

$$\Delta dB = 20 * \log\left(\exp\left\{-\omega(t_i - t_{ref})\sqrt{\frac{\sqrt{1+\left(\frac{\sigma}{\omega\varepsilon}\right)^2}-1}{\sqrt{1+\left(\frac{\sigma}{\omega\varepsilon}\right)^2}+1}}\right\}\frac{t_{ref}}{t_i}\right) \quad \textbf{[4.7]}$$

where:

B – spreading loss coefficient
t_i – two-way travel time of point of interest (s)
t_{ref} – reference time (s)
v_i – velocity at point of interest (m/s)
v_{ref} – velocity at reference time (m/s)
ΔdB_{Atten} – decibel loss due to attenuation (dB)
ΔdB_{Spread} – decibel loss due to spreading (dB)
ε – dielectric permittivity (F/m)
σ – electric conductivity (S/m)

These model curves are calibrated to fit to the reference data by fitting three constraints. First, the absolute difference in amplitude of each point on the model compared to the reference data is minimized and summed for a given curve to ensure each model adequately represents its data. This is similar to a regression fit, but alone is not enough to solve for conductivity and permittivity for a given model curve due to the two properties being present only as a ratio in Equation 4.7. Second, the amplitude and time difference between each of the model curves must fit the conductive model. This means that for a given distance and a given change in conductivity, the travel time and amplitude of the curves

should change a set amount based on Equations 2.20 and 2.21. This is done by using each point of the 60th percentile curve and calculating the travel time and amplitude based on the conductivity values of the 90th and 30th percentile curves at the same travel distance. These predicted values are compared to the actual amplitude data for the 90th and 30th percentile curves and the sum of the decibel differences at each point on each curve is minimized. This is similar to using the changing conductivity curve from Figure 4.4 to see what the amplitude and travel time values should be for the conductivities of the 90th and 30th percentile curves when compared to the 60th percentile curve. These ideal amplitude and travel time values are compared to the actual values of the model curves and summed. This assures that not only are the model curves fitting the reference data, but the conductivities and permittivity calculated for a given deck make sense for the deck as a whole. Finally, each curve is extrapolated back to a two way travel time of zero. Since each of these curves are representative of the same source, they should all have the same amplitude at a travel time of zero. The sum difference between the decibel values of each curve at this zero point is also minimized. The permittivity value for the deck and the conductivity for each curve are found to be the solution set that gives the best optimization over all three of the defined constraints.

Since these model curves are built around specified data points, signal gain in decibels has no effect on the conductive and dielectric properties determined by the model. As long as the same gain is applied to the entire data set, the GPR data as a whole simply moves along the amplitude axis along with the model curves. The only factors that affect the properties of the model curves are the slope and curvature of the reference data. Since this is the case, any internal gains applied by the radar system due to pre-set options will not be a factor in data analysis with this model as long as the same settings are used for the whole deck.

The optimization process to calculate a permittivity and three conductivities for each deck was done using MATLAB software by starting with an initial value for each of the four parameters and determining the combination of values that minimized the three criteria described above. The initial value for each parameter was individually incremented and the minimization was carried out again. This process was repeated for 2750 combinations of initial values to ensure that a global minimum for the system was reached. The MATLAB

program would return conductivity and permittivity values for each of the 2750 iterations along with a value for how well the three constraints were fit. The majority of these iterations failed to come to a credible solution as the solver within MATLAB would often maximize one property and ignore the rest. For each deck, between 10 and 15 credible solutions would be provided from the program. Of these credible solutions, there were between 1 and 5 unique solutions. In each case, a single unique solution stood out as the best one based on the three constraints discussed above, a comparison to the migration velocity used, and a visual comparison of the model curves passing through the reference data. This prevented a solution being chosen that represented some of the data extremely well, but did not represent the rest. The precise velocity used in migration was not used as a constraint due to the invalidated assumptions surrounding the migration process. Once the global minimum for the constraints was found, the calculated parameters were input into the model and conductivities for each individual reinforcing bar were determined.

To calculate the conductivity of the concrete at each scan location, each data point was related to one of the model curves. The curve that best fit its respective reference data was chosen to calculate each individual conductivity value. The model curve used for this process was idealized as a quadratic function using a least squares approach over the range of two way travel times found in GPR data as seen in Figure 4.14. This is done to ease the calculation of points on the model curve so they can be related to the individual reinforcement reflections. The quadratic approximation eliminates the need to calculate individual spreading and attenuation losses for each point on the model curve when determining the conductivities of the remaining reinforcing bars. Since permittivity is assumed constant for the entire deck, each data point must have the same two way travel distance as a point on the model curve, the only difference between the two being a change in conductivity, similar to that shown by the changing conductivity curve in Figure 4.4. Once the conductivity has been determined for each point on the deck, the entire data set is transferred to a surface plot using the software Surfer 10.

Once a conductivity map of the bridge has been created, conductivity thresholds can be put in place to determine problematic areas of the deck. These thresholds can be set to delineate areas of extensive damage having high conductivity or areas that will likely see damage in

the years to come with slightly lower conductivity. In order to confirm that high levels of conductivity map out actual deterioration to a bridge deck, the conductivity map for each deck was compared to half-cell and chain drag survey results and will be discussed in Chapter 5. Finally, determined conductivity levels were compared to chloride contents of cores taken from each structure after the completion of the GPR surveys.

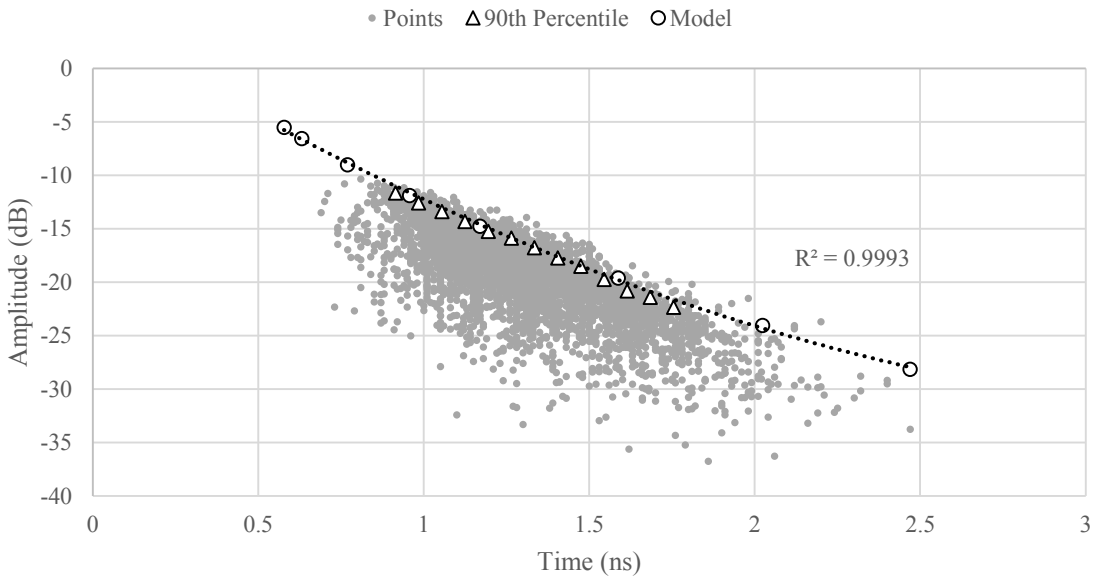

Figure 4.14: Model curve as a quadratic (90th percentile data from Milford Overpass)

4.5 Recommended Combination with Diffusion Models

In order to perform a complete assessment of a bridge's current and future condition, GPR surveys conducted at regular intervals could eventually allow for a complete chloride profile when combined with exposure and diffusion models. Using conductivity levels that have been monitored over time in conjunction with these models could establish chloride profiles relatively accurately, allowing for planned maintenance or preventative measures before the onset of corrosion.

To establish chloride profiles, the changes in conductivity over time at each point of a given bridge deck would have to be compared to previous conductivity results for the same location. Diffusion models could then be used in conjunction with chloride exposure conditions at the surface of the deck to establish a chloride profile. This profile and diffusion model would then be used to predict the movement of chlorides through the concrete deck in the future. Once the diffusive properties and chloride profiles are established, forward models of the movement of the chloride profile over time can be completed to give estimates of the date and extent of repairs that are to be expected based on chloride content around individual reinforcing bars. These models should of course be updated once additional surveys are conducted and a better deterioration projection can be made.

There are two feasible uses for the tracking of chloride profiles through a concrete deck. The first use would be on relatively new bridge decks that would be scanned regularly over their lifetimes. This would allow each new bridge deck to extend its service life through continued monitoring and scheduled maintenance that could be predicted with diffusion models. During the establishment of a baseline chloride profile over the early years of the bridge, it is unlikely that any significant repairs would be needed, so the progress of chlorides could be focused on. The lack of repairs would simplify modeling as any repairs to the deck would have to be taken into account during forward modeling of the condition of the structure as repaired sections will have different concrete that will have significantly different diffusive properties. Also, it could be assumed that a negligible amount of chlorides were pre-existing in the deck, allowing models to assume chlorides were only penetrating from the wearing surface. Since the only chlorides in the deck would be near the surface, the chloride profile could be established fairly quickly.

The second use would be for older bridges that pre-existing chloride profiles. These structures would require regularly scheduled surveys in order to establish a baseline chloride profile. The accuracy and speed of this process could be increased by taking cores from the deck and determining a true chloride profile from them. These cores could be compared to GPR data to establish profiles for the deck as a whole much faster than without cores. With no cores, it could take a fair amount of time to establish a profile with any

accuracy due to the fact that there is an existing chloride profile in the deck in addition to chloride penetrating from the surface. The initial surveys would be able to provide a condition assessment, but would not be able to estimate the true chloride profile without subsequent scans. Once the profile is determined, a final condition assessment and forward model could be established and maintenance schedules could be devised to get the most of the remaining service life. Older bridges that are already significantly deteriorated would of course have any maintenance that was deemed necessary done as it was required during the establishment of the chloride profile. This would make the modeling slightly more difficult as there would effectively be two separate areas of concrete to model. Modeling could be achieved by taking into account different diffusion models for the newer and older concrete in the bridge due to these repairs.

Chapter 5: Results

Five previously scanned bridge decks were made available for this study. Each deck was scanned in the summer of 2005 in preparation for a previous thesis (Redmond 2007). All five bridges were located in Nova Scotia and were at varying stages in their service lives. Field testing of each bridge deck included a GPR survey, chain drag, half-cell, visual inspection, and coring.

Several cores were taken from each bridge studied in order to establish cover depth and to visually identify signs of corrosion and delamination. Delaminations within the cores are noted as either being present or not while evidence of corrosion was noted as not present, low, medium, or high. Low corrosion indicates the beginnings of corrosion product on the surface of reinforcement as seen from the core. Medium corrosion indicates substantial corrosion product on the surface of the bar which was beginning to cause distress to the deck. High corrosion indicates sufficient corrosion on the reinforcement to cause cracking and delamination. Three cores from each deck were also tested for water soluble chloride content in accordance with ASTM C1218 (ASTM 2008a). Seven layers with a thickness of 5-8 mm were ground into a powder by Wilbert Langley Concrete Testing. The powder from each layer was tested for water soluble chloride content by titration at the Dalhousie University Minerals Center and then used to establish a chloride diffusion profile as described in ASTM C1543-02 (ASTM 2002). Water soluble chlorides determined by this testing were compared to conductivities determined from data analysis of GPR data with the conductive model.

5.1 Milford Overpass

Milford overpass is a two lane, three span structure that was constructed in 1969 and is located in West Shubenacadie, near the center of the province. Upon visual inspection, it was seen that extensive asphalt patching was present in varying states of decay with evidence of chloride residue around the edges of the patches. In some areas, these patches had deteriorated sufficiently to expose the reinforcement due to continued corrosion. Joint condition was noted to be poor and the concrete showed very high air content. Ten cores

were taken from the deck, the plan view of which can be seen in Figure 5.1. Inspection results from the cores are listed in Table 5.1 where it can be seen that only one of the cores showed evidence of corrosion or delamination. This is likely due to the extensive asphalt patching over the more deteriorated areas as a core would not be taken through the asphalt patches.

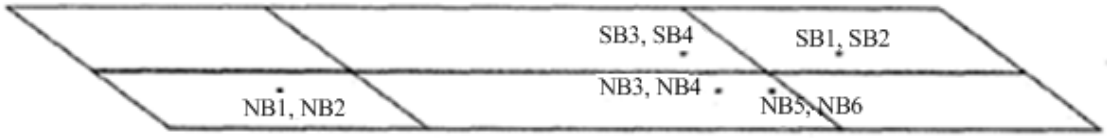

Figure 5.1: Core locations for Milford Overpass (Redmond 2007)

Table 5.1: Core descriptions for Milford Overpass

Core	Depth to Bar (mm)	Corrosion	Delamination	Chloride Profile*
NB 1	56.1	None	None	
NB 2	52.5	None	None	
NB 3	49.8	High	Yes	
NB 4	48.2	None	None	Yes
NB 5	71.5	None	None	
NB 6	70.1	None	None	
SB 1	48.7	None	None	
SB 2	50.3	None	None	Yes
SB 3	53.0	None	None	Yes
SB 4	51.6	None	None	

*Chloride profile measured in accordance to ASTM C1218

Half-cell and chain drag tests were conducted on the bridge deck for comparison to GPR results. The half-cell test identified an active corrosion area covering 37.0% of the deck while the chain drag survey identified 18.0% of the deck as delaminated. It was expected

for the half-cell to delineate a larger area than the chain drag as corrosion activity occurs well before deterioration to the point of delamination. Results from the half-cell and chain drag tests show the area outlined as deteriorated during testing and can be seen in Figures 5.2 and 5.3 respectively.

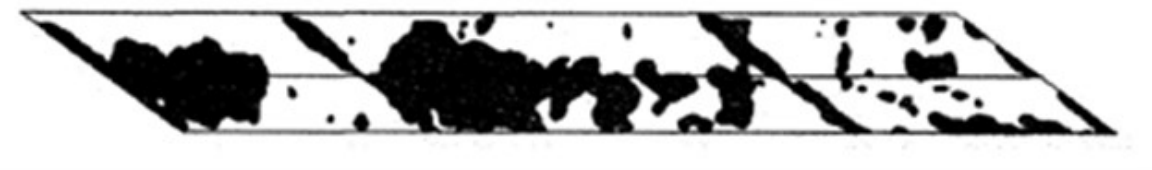

Figure 5.2: Half-cell results for Milford Overpass (Redmond 2007)

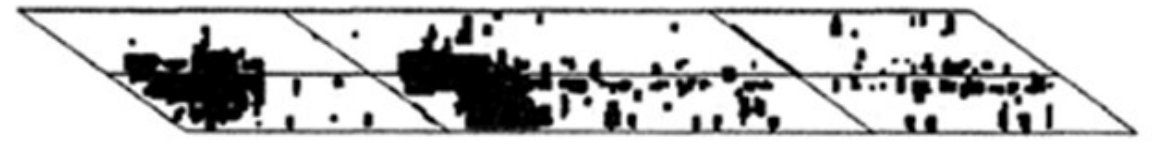

Figure 5.3: Chain drag results for Milford Overpass (Redmond 2007)

Analysis of the GPR data collected in the field was completed and the results were compared to the half-cell and chain drag data. Plots of radar data before and after normalization are shown in Figures 5.4 and 5.5 respectively while model curves that were fit to the data are shown in Figure 5.6. It was determined with this model that the permittivity of the deck was 8.9 F/m while the 90^{th}, 60^{th}, and 30^{th} percentile conductivities were 0.10, 0.11, and 0.13 S/m respectively.

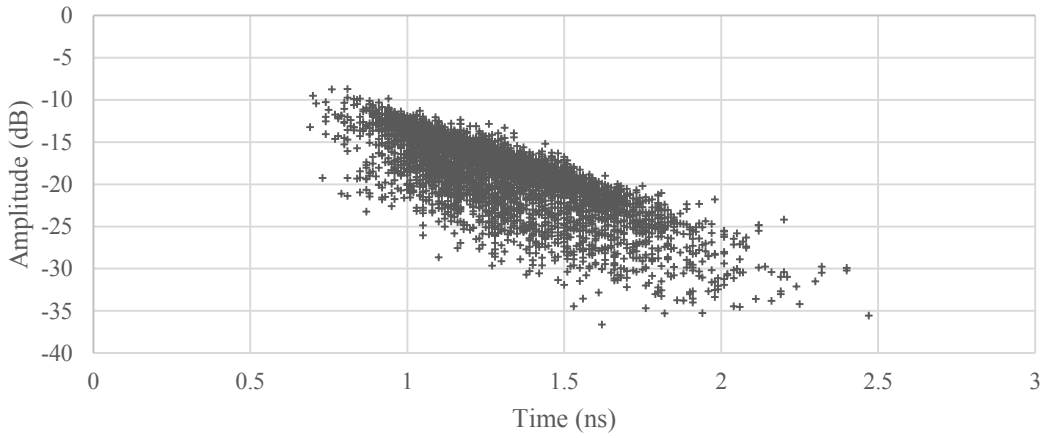

Figure 5.4: GPR data from Milford Overpass before normalization

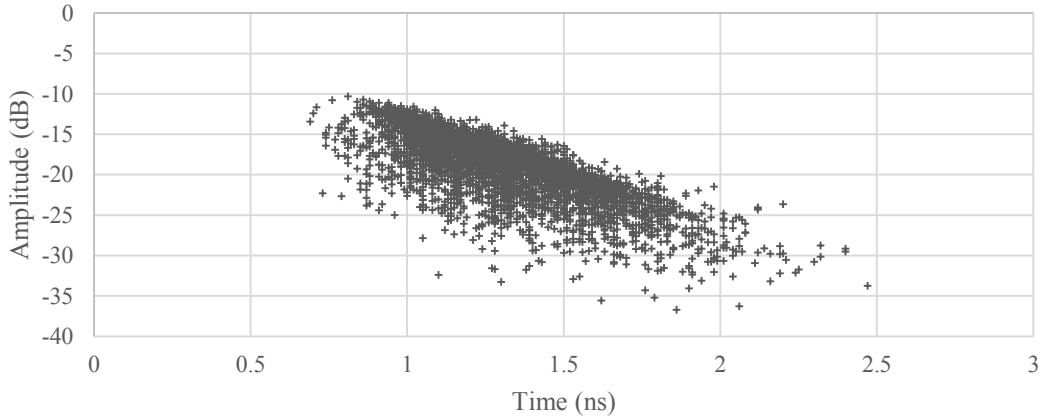

Figure 5.5: GPR data from Milford Overpass after normalization

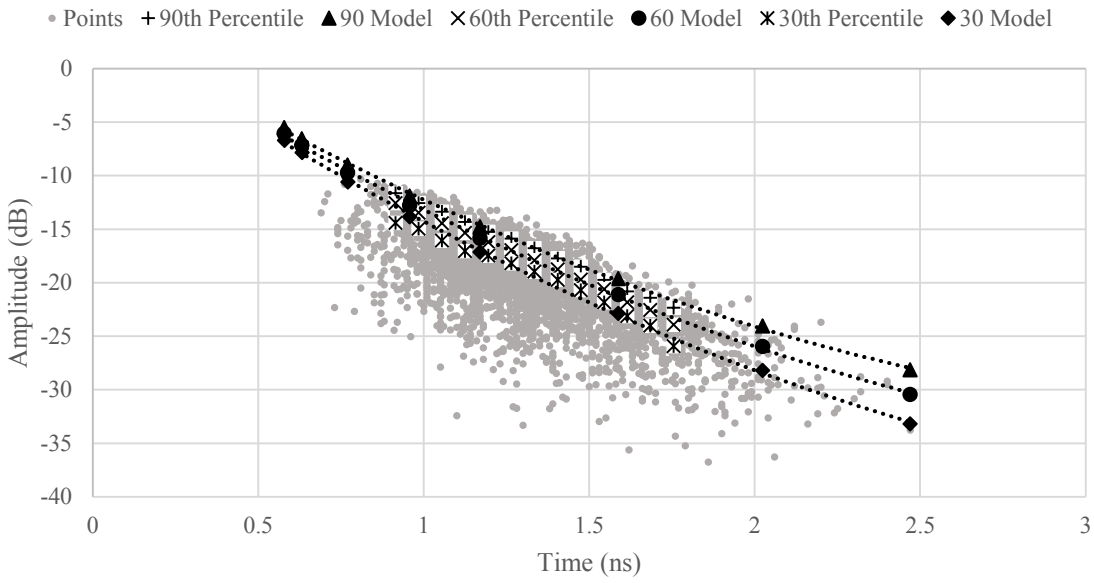

Figure 5.6: Model curves fit to Milford Overpass data

Conductivity values for the deck were plotted as a surface and compared to half-cell and chain drag data. Figure 5.7 shows the conductivity map of the Milford Overpass with the span of the bridge in metres along the horizontal axis and the width of the bridge in metres along the vertical axis. The areas of high conductivity coincided with the large asphalt patches. To compare the conductivity map to both the half-cell and chain drag results, two conductivity levels were chosen that best visually compared to the field test results. The threshold used to compare the conductivity map to the chain drag (0.14S/m) has a higher conductivity than that used to compare to the half-cell (0.11S/m) as the delaminated area identified by the chain drag has more extensive damage and would therefore have a higher chloride content and conductivity than the active corrosion area identified by the half-cell. Plots of each conductivity level compared to its respective test results are shown in Figures 5.8 and 5.9 respectively. A comparison of the areas determined by each of these methods is shown in Table 5.2. It can be seen that the two chosen conductivities both accurately determine the shape and area of deteriorated regions of the deck. The first conductivity overestimates the half-cell area by 2.3% of the deck while the second underestimates the chain drag area by 0.9%. The chain drag delineates some small areas that were not picked

up by the conductivity plot. This is likely due to visual anomalies being outlined during the chain drag testing that were not necessarily delaminated. These anomalies would most likely also be noticed during a GPR survey, so they would not be overlooked. Some small areas of elevated conductivity could be missed by the GPR due to the spacing between consecutive passes of the antenna. This could be avoided by scanning at smaller distance intervals, but would not likely increase accuracy enough to warrant the additional testing. Any areas small enough to be omitted from GPR results would be of negligible concern to deck condition as any severe damage would likely be more widespread.

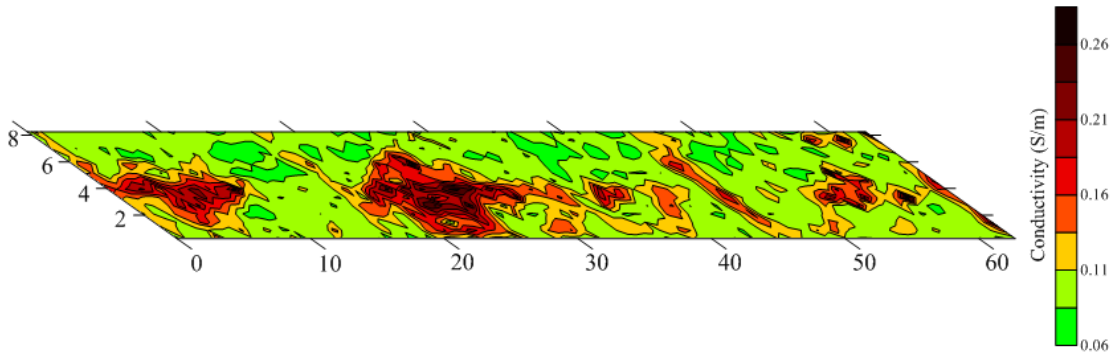

Figure 5.7: Conductivity plot of Milford Overpass

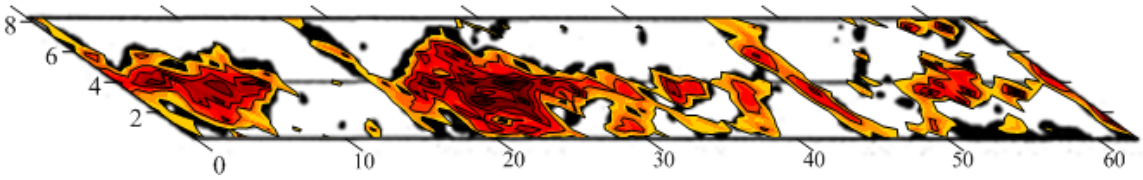

Figure 5.8: Conductivity compared to half-cell data for Milford Overpass

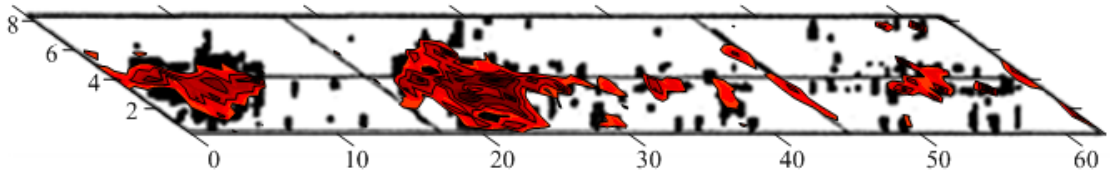

Figure 5.9: Conductivity compared to chain drag data for Milford Overpass

Table 5.2: Comparison of conductivity thresholds and field testing damage estimates – Milford Overpass

	Deck Area (m^2)	Deck Area (%)
Half-Cell	186	37.0
0.11 S/m	197	39.3
Chain Drag	90	18.0
0.14 S/m	86	17.1

5.2 Shubenacadie Overpass

The Shubenacadie Overpass spans about 74 m and has two traffic lanes. Construction of this four span structure located in central Nova Scotia was completed in 1967. Visual inspection of the deck identified significant corrosion induced deterioration (Redmond 2007). It was noted that four substantial delaminations were identified with some asphalt patching over potholes. The surface appeared to have a high air content and the deck was deemed highly deteriorated. Nine cores were taken from the locations noted in Figure 5.10. Core data confirmed the visual identification of delamination and corrosion products as summarized in Table 5.3. Locations with no depth listed correspond to cores that were damaged sufficiently to prevent accurate depth measurement. Cores SB3 and SB4b were identified as having a significant buildup of gel due to alkali aggregate reactivity (AAR). It was unclear how localized the AAR was, but the remainder of the cores showed no indication of the presence of gel. If the AAR was localized only to this area of the deck, it would increase conductivity in that location alone. How much the conductivity would be

raised specifically due to AAR is unknown at this time and its potential effects will be discussed in Section 5.5.

Half-cell and chain drag tests identified 149 m^2 and 64 m^2 of deck area respectively. Figure 5.11 shows the area outlined by the half-cell test while Figure 5.12 shows that outlined by the chain drag. As expected, the two tests outlined similar areas, with the half-cell showing larger areas than the chain drag.

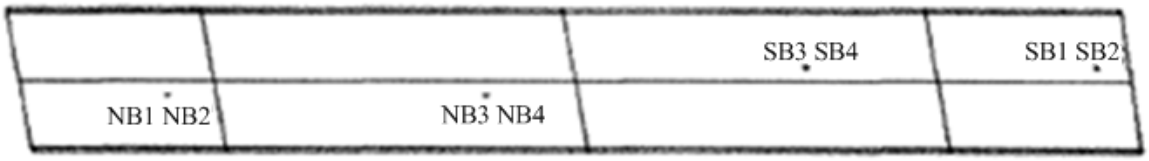

Figure 5.10: Core locations for Shubenacadie Overpass (Redmond 2007)

Table 5.3: Core descriptions for Shubenacadie Overpass

Core	Depth to Bar (mm)	Corrosion	Delamination	Chloride Profile*
NB 1	38.7	None	None	Yes
NB 2	39.5	Medium	Yes	
NB 3	55.1	None	None	
NB 4	52.6	None	None	
SB 1	55.3	None	None	Yes
SB 2	53.1	None	None	
SB 3	-	None	Yes	
SB 4	59.5	High	None	Yes
SB 4b	-	None	None	

*Chloride profile measured in accordance to ASTM C1218

Plots of the GPR data before and after normalization are shown in Figures 5.13 and 5.14 respectively. Model curves were fit to the data and determined a permittivity of 11.1 F/m while the conductivity values were 0.09, 0.11, and 0.13 S/m respectively for the 90^{th}, 60^{th},

and 30th percentile curves as in Figure 5.15. The conductivity map determined for the deck is shown in Figure 5.16. Conductivity levels were compared to the half-cell and chain drag data and a strong correlation between the conductivity and the reference testing was found. A comparison between the first level and the half-cell data can be found in Figure 5.17 while a comparison between the second level and the chain drag data is shown in Figure 5.18.

Figure 5.11: Half-cell results for Shubenacadie Overpass (Redmond 2007)

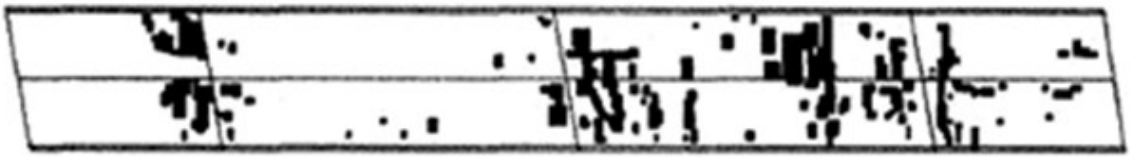

Figure 5.12: Chain drag results for Shubenacadie Overpass (Redmond 2007)

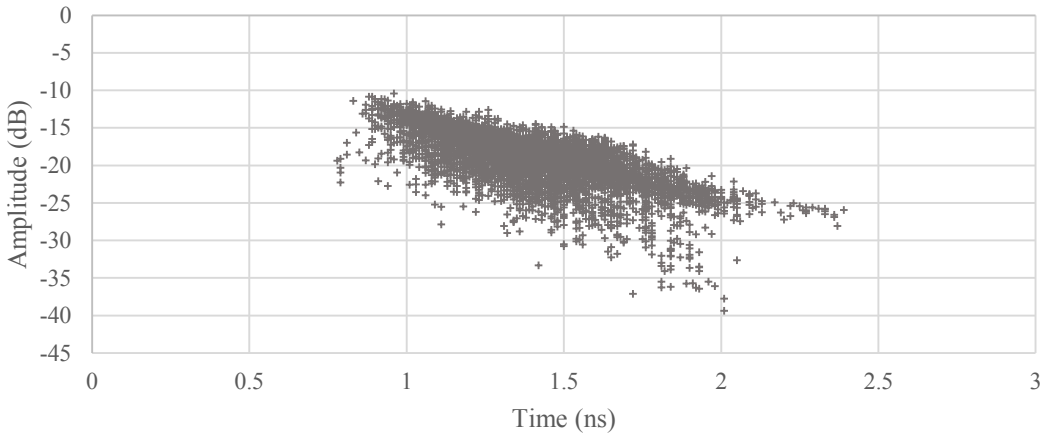

Figure 5.13: GPR data from Shubenacadie Overpass before normalization

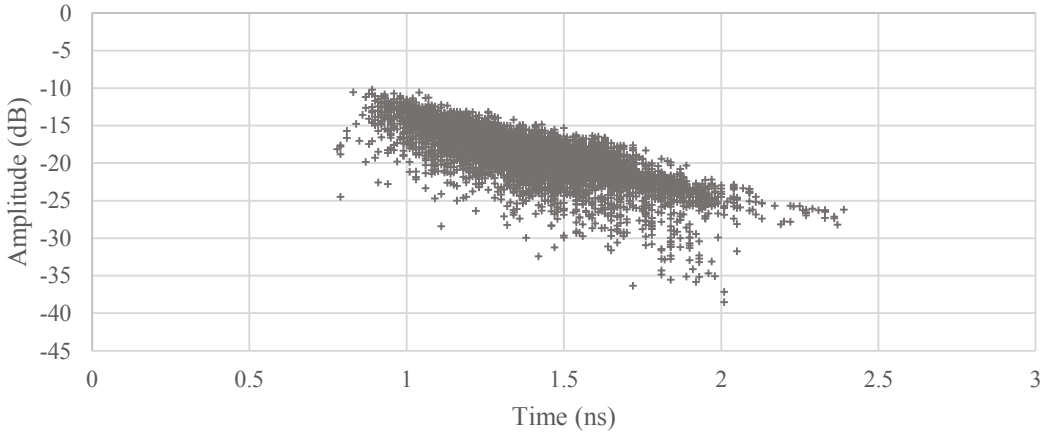

Figure 5.14: GPR data from Shubenacadie Overpass after normalization

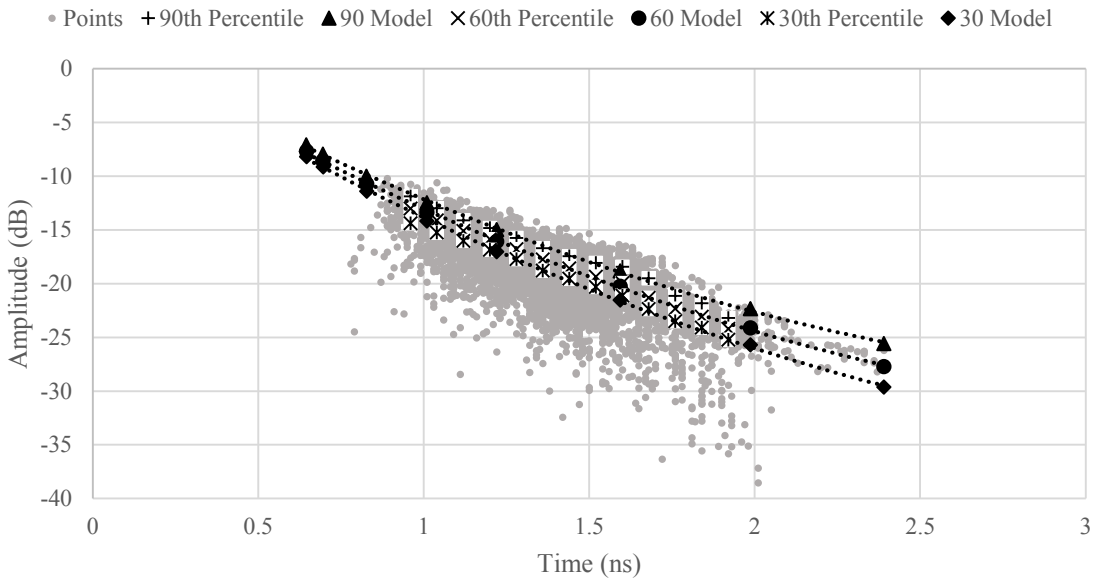

Figure 5.15: Model curves fit to Shubenacadie Overpass data

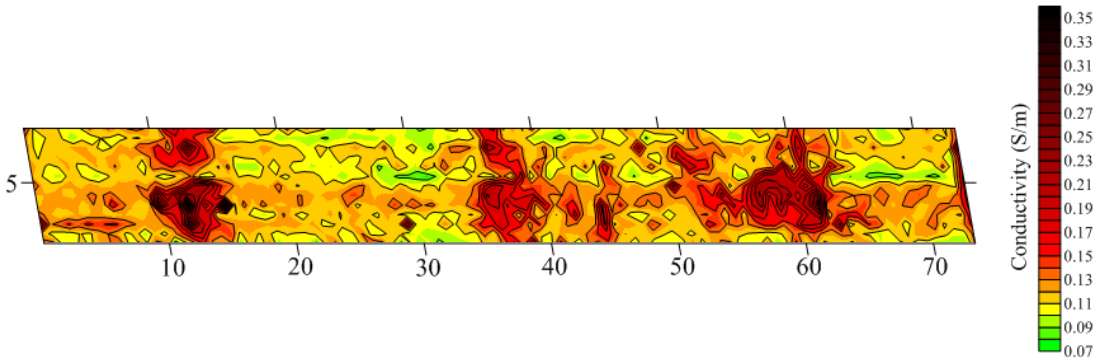

Figure 5.16: Conductivity map of Shubenacadie Overpass

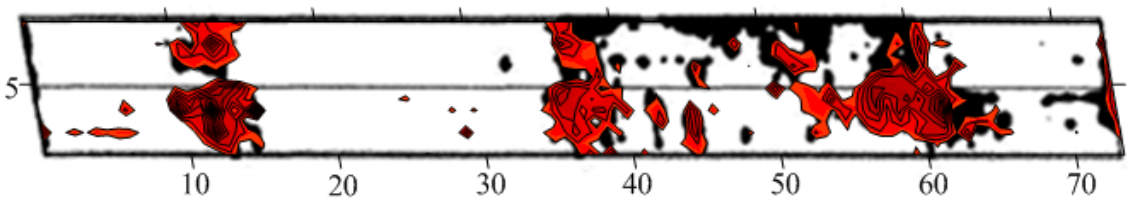

Figure 5.17: Conductivity compared to half-cell data for Shubenacadie Overpass

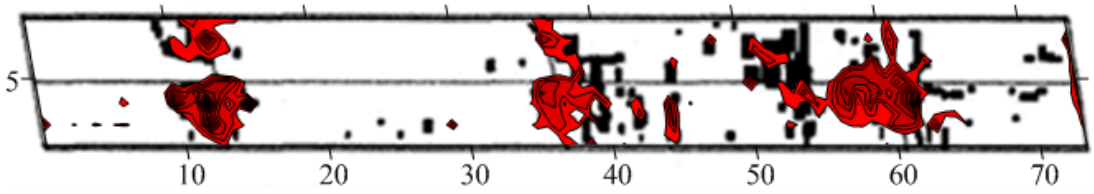

Figure 5.18: Conductivity compared to chain drag data for Shubenacadie Overpass

Both conductivity levels clearly identify much of the same area as reference tests with a small area missed in the conductivity plot compared to the half-cell at the top of Figure 5.17 and some small areas where there are discrepancies. Although the conductivity map did show elevated levels in this region, they were not high enough to meet the level plotted. It is unclear how much of an effect the AAR in the deck had on the GPR data as the extent of the expansive gel is unknown. If it was prevalent enough to significantly increase conductivity, it would only have done so in the affected areas. The most likely areas to have been affected by AAR would be the leftmost and rightmost areas identified by both thresholds in Figure 5.17 and 5.18, although they could simply be evidence of aggressive chloride induced corrosion. These regions have higher conductivity values than the rest of the deck by 0.03-0.10 S/m with the cores with evidence of AAR being in the rightmost area. Areas outlined by each test method and the conductivity map are located in Table 5.4.

Table 5.4: Comparison of GPR and field testing damage estimates – Shubenacadie Overpass

	Deck Area (m^2)	Deck Area (%)
Half-Cell	149	22.6
0.14 S/m	130	19.8
Chain Drag	64	9.7
0.15 S/m	94	14.3

The conductivity plot underestimates the half-cell test by 2.8% of the deck while it overestimates the chain drag area by 4.6%. For the first level, the difference is mostly in

one area of the half-cell, as seen in the top of Figure 5.17. The only other significant area missed was the small band coming from the joint on the right hand side of the figure. Both of these regions showed some elevated conductivities, but missed the plotted conductivity level. Again the conductivity that best compared to the chain drag was higher than that that best compared to the half-cell as would be expected based on the level of deterioration identified by each test.

5.3 Victoria Harbour Overpass

The Victoria Harbour Overpass is a two lane bridge located near Nova Scotia's Western Shore that spans approximately 43 m and was built in 1977. The two lanes scanned with the GPR were done on separate days, neither of which are recorded as having precipitation by Environment Canada (Environment Canada 2014). Visual inspection carried out on the bridge noted some small concrete patching with no significant deterioration around the patches compared to the majority of the deck (Redmond 2007). Some corrosion staining was noted near the joints, but this was deemed to have originated from the joints themselves and not the deck reinforcement. Minor corrosion staining was present in other locations of the deck with some cracking noted.

Seven cores were taken during testing at the locations outlined in Figure 5.19 with visual inspection of these cores described in Table 5.5. Core data showed mixed results as three of the cores showed high levels of corrosion, with two to the point of delamination, while the remainder of the cores showed no sign of corrosion damage. Variations in core condition to this degree make determination of overall deck condition difficult based on core data and visual inspection alone.

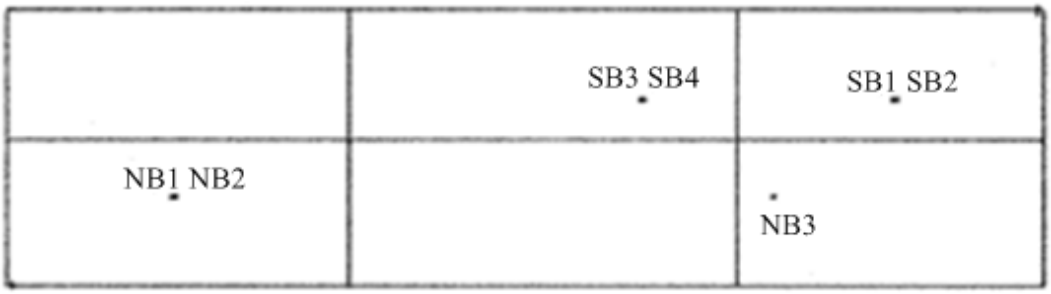

Figure 5.19: Core locations for Victoria Harbour Overpass (Redmond 2007)

Table 5.5: Core descriptions for Victoria Harbour Overpass

Core	Depth to Bar (mm)	Corrosion	Delamination	Chloride Profile*
NB 1	39.4	None	None	
NB 2	37.2	High	None	Yes
NB 3	61.2	None	None	Yes
SB 1	56.4	High	Yes	
SB 2	-	High	Yes	
SB 3	-	None	None	
SB 4	47.0	None	None	Yes

*Chloride profile measured in accordance to ASTM C1218

Half-cell testing on the deck identified 16 m^2 in total having a potential drop of -0.35 V or more as shown in Figure 5.20. The chain drag survey delineated 5 m^2 of delamination and agreed with the half-cell results for the location of corrosion damage. A plot of the chain drag results can be found in Figure 5.21.

GPR data for this bridge had some inconsistencies between the two lanes tested. Data collected in the northbound direction showed on average ground couple amplitudes 1.4 dB larger and rebar reflection amplitudes 3.8 dB larger than in the southbound direction. Also, the two way travel times for ground couple reflections were on average 0.18 ns lower for northbound scans than for southbound scans. These inconsistencies are likely due to the

testing being conducted on two separate days. It is not entirely clear however why exactly this error occurred, but there was clearly a difference in results from one day to the next.

One possible explanation is that some settings on the unit were inadvertently changed between tests. All visible settings documented in the data files seemed to be identical so this is unlikely to be the cause. Since no precipitation was recorded in the area and no moisture was evident on the deck surface (Redmond 2007), it is unlikely that moisture on the deck caused the error. The final explanation could be that the antenna did not warm up properly on one of the testing days. It is unlikely that this was the result of operator error as the data recorder clearly shows the antenna functioning during any warm up period and it would be noticed if it was not actively warming up. Instead, there could have been an error in the device itself that prevented it from warming up properly.

Whatever the cause, inconsistencies such as this can be a major pitfall for GPR surveys. It was found however that after normalization of the surface reflections, the difference in amplitudes between the two lanes had been substantially reduced. After normalization, the ground couple amplitudes were, by definition, the same on both lanes and the rebar reflection amplitudes for the northbound lane were only 2.4 dB higher on average than the southbound lane. The problem had not been entirely resolved, but the conductivity results were a much better fit to the reference tests than they would have been without normalization. Plots of rebar reflection amplitude before and after normalization are shown in Figures 5.22 and 5.23 respectively while Figure 5.24 shows the GPR data plot from before normalization and Figure 5.25 shows the GPR data after.

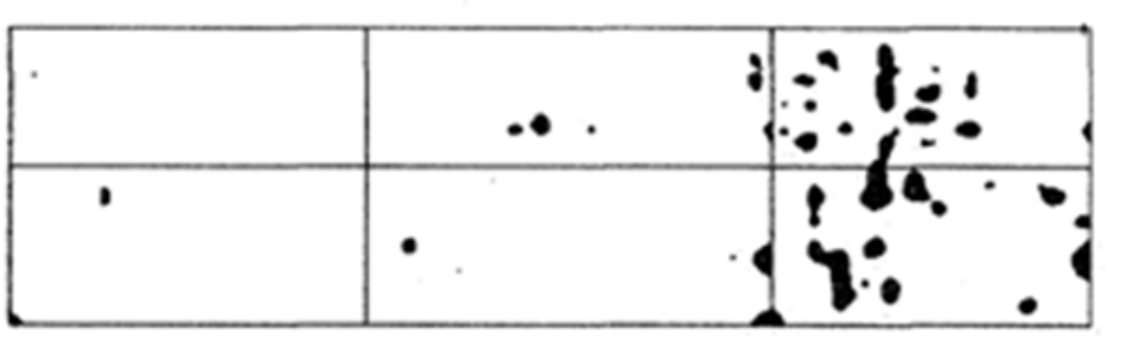

Figure 5.20: Half-cell results for Victoria Harbour Overpass (Redmond 2007)

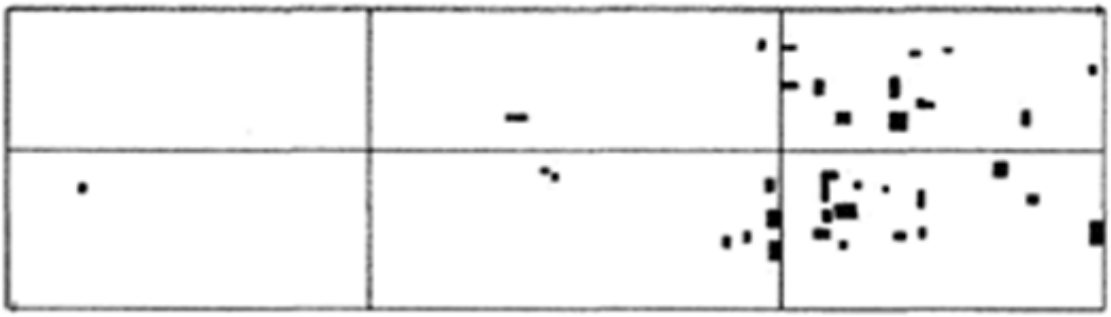

Figure 5.21: Chain drag results for Victoria Harbour Overpass (Redmond 2007)

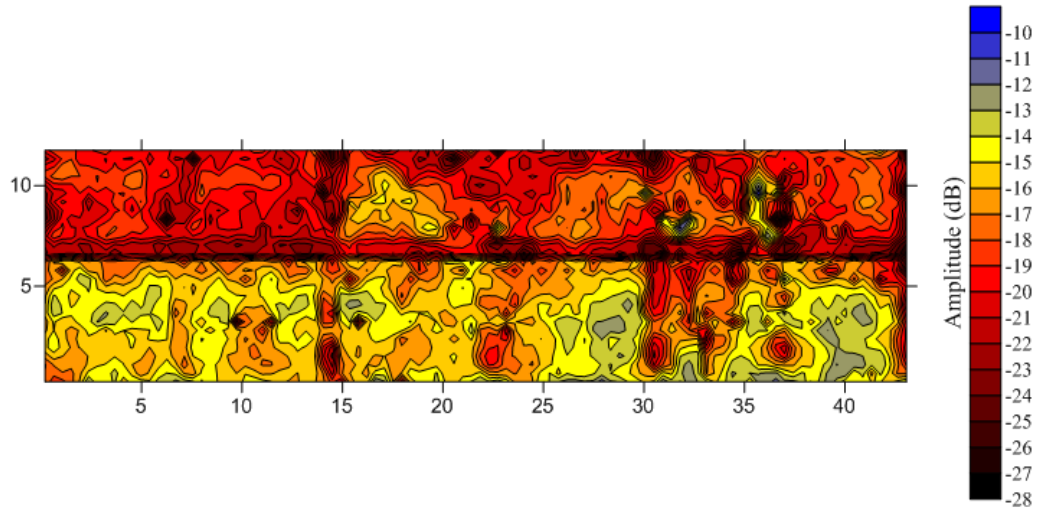

Figure 5.22: Victoria Harbour Overpass reinforcement reflection amplitudes before normalization

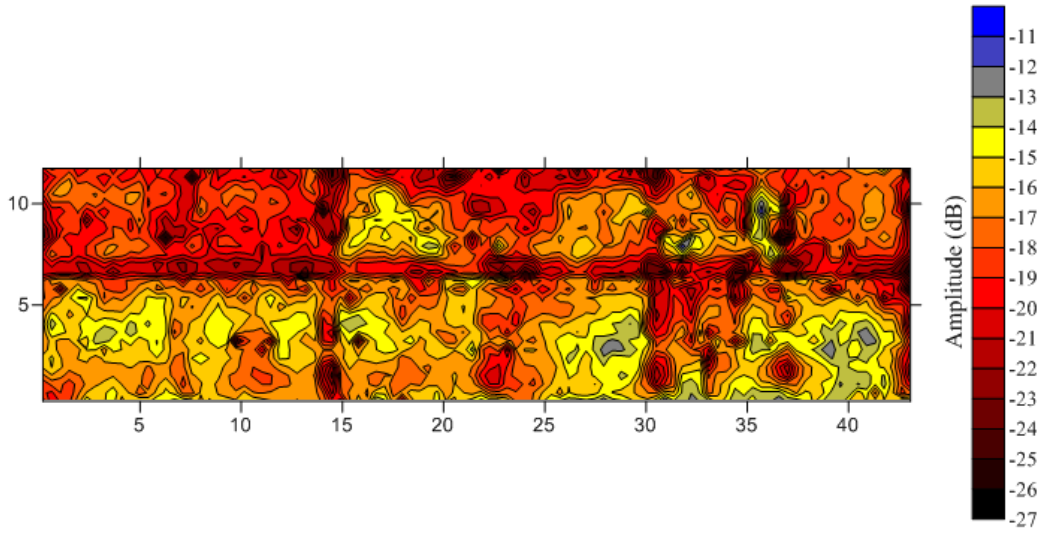

Figure 5.23: Victoria Harbour Overpass reinforcement reflection amplitudes after normalization

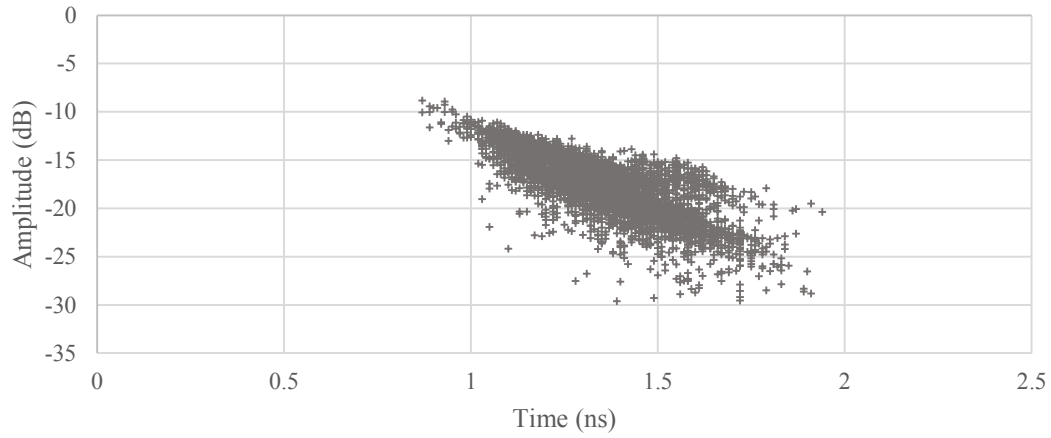

Figure 5.24: GPR data from Victoria Harbour Overpass before normalization

The model curves that were fit to the data are located in Figure 5.26. It was determined that Victoria Harbour Overpass had a permittivity of 7.7 F/m and 90th, 60th, and 30th percentile conductivities of 0.09, 0.11, and 0.12 S/m respectively. The resulting conductivity map is shown in Figure 5.27. Conductivities were compared to both the half-cell plot (0.13S/m) in Figure 5.28 and the chain drag plot (0.14S/m) in Figure 5.29.

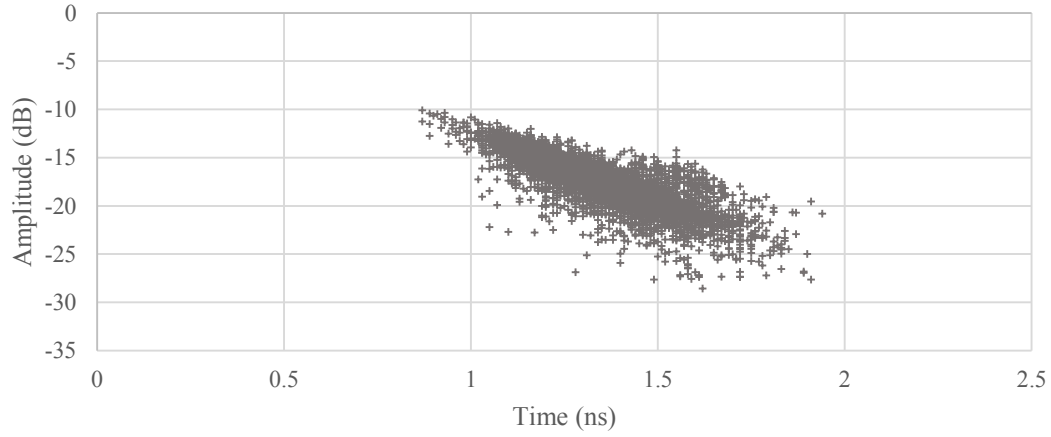

Figure 5.25: GPR data from Victoria Harbour Overpass after normalization

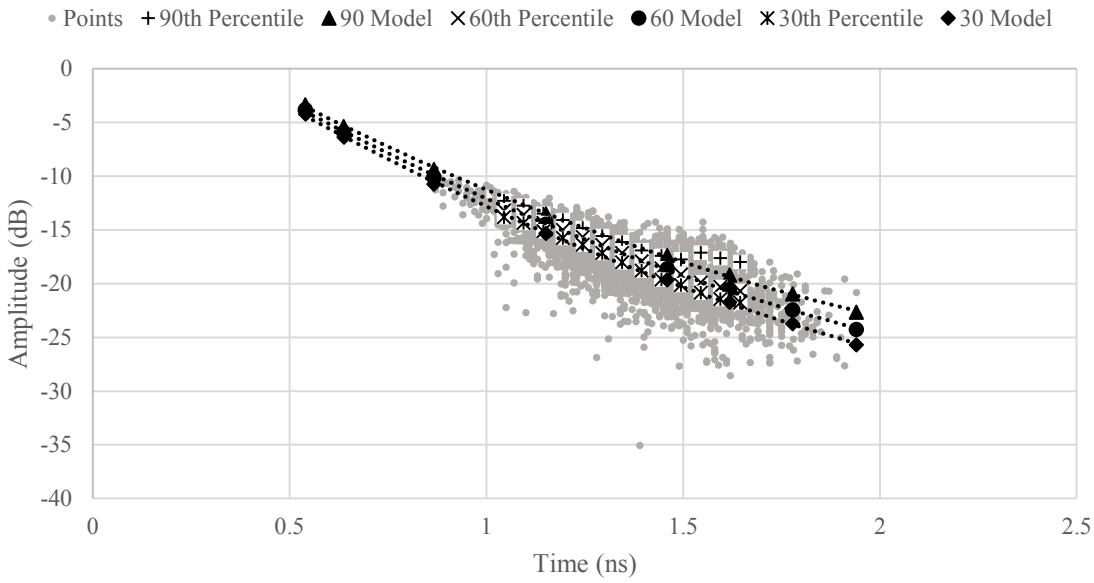

Figure 5.26: Model curves fit to Victoria Harbour Overpass data

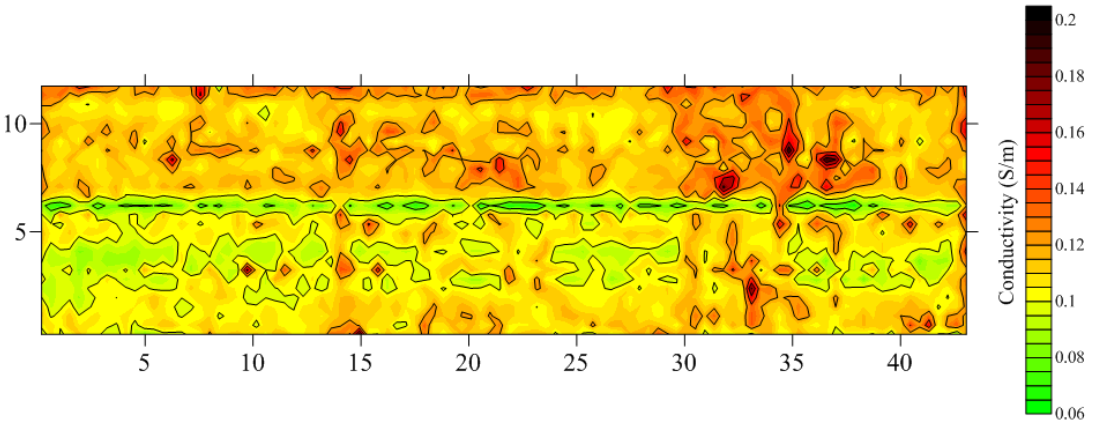

Figure 5.27: Conductivity map of Victoria Harbour Overpass

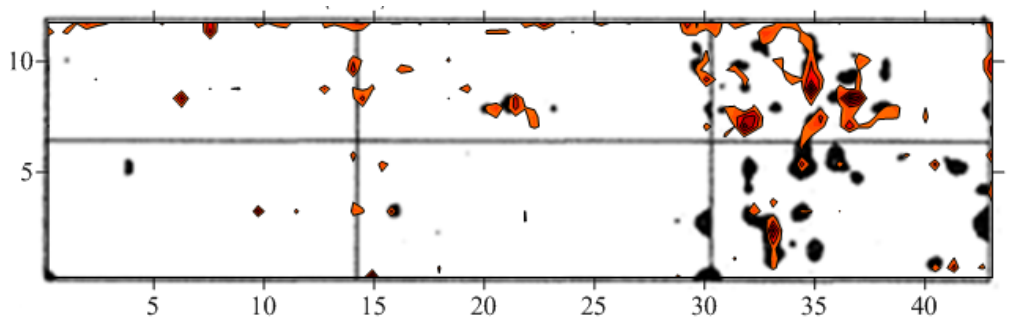

Figure 5.28: Conductivity compared to half-cell data for Victoria Harbour Overpass

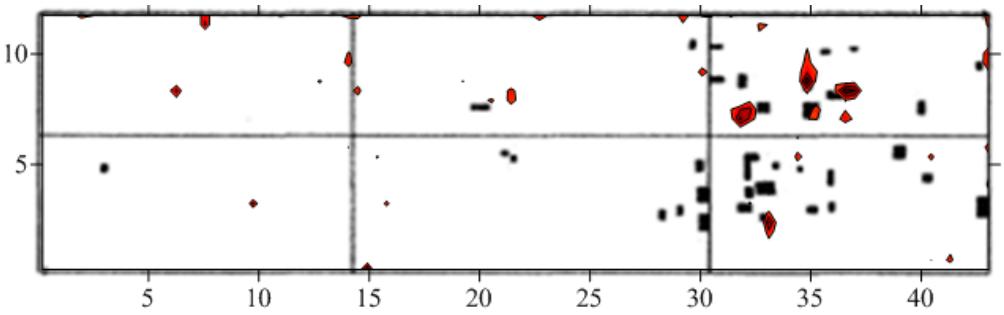

Figure 5.29: Conductivity compared to chain drag data for Victoria Harbour Overpass

Both conductivity levels identified much of the area that was picked out in the half-cell and chain drag tests. Clearly, the conductivities in the southbound lane (top of Figures 5.28 and 5.29) have a better correlation to both testing methods than in the northbound lane. Even though the cause of the amplitude difference from lane to lane is unknown, it is safe to assume that it is effectively a gain difference between the two days of testing. To combat this effect, the returned amplitudes in the northbound lane were gained to have the same average reinforcement reflection amplitude as the southbound lane in an attempt to equalize the gain across the structure as a whole. Normalization was then carried out on both lanes individually in order to keep the average reinforcement reflection amplitude consistent throughout the deck. A gain of -2.375 dB was applied to the northbound lane to level out the amplitudes across the deck. Model curves were again fit to the data as seen in Figure 5.30 and conductivities were determined for each point in the deck. The updated properties were a permittivity of 10.8 F/m and conductivities of 0.10, 0.12, and 0.13 S/m for the 90th,

60th, and 30th percentile data respectively. The updated conductivity map is shown in Figure 5.31. This new map was compared to half-cell and chain drag plots in Figures 5.32 and 5.33 respectively.

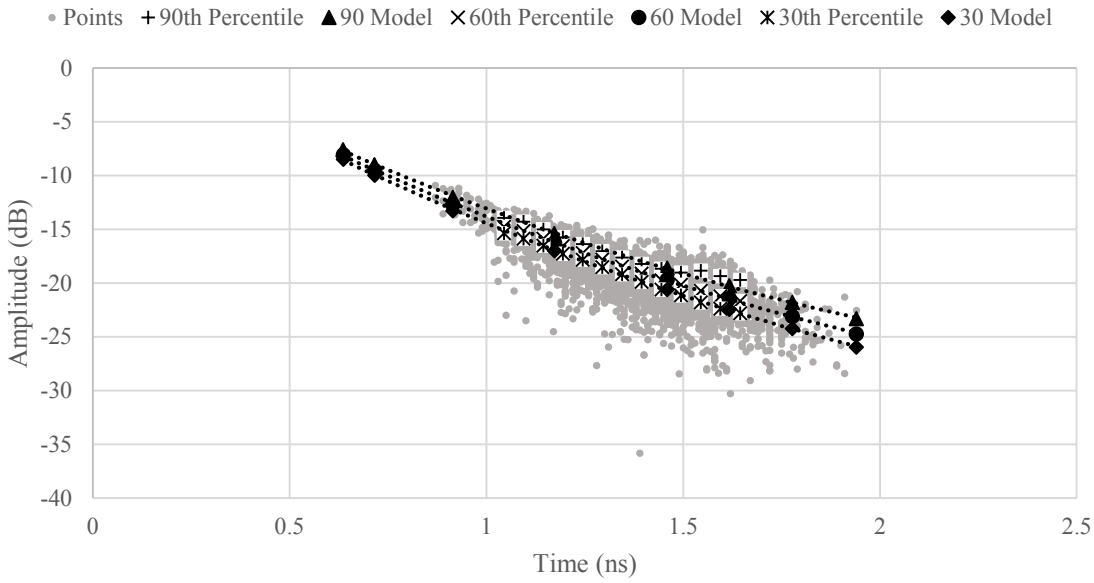

Figure 5.30: Model curves fit to updated Victoria Harbour Overpass data

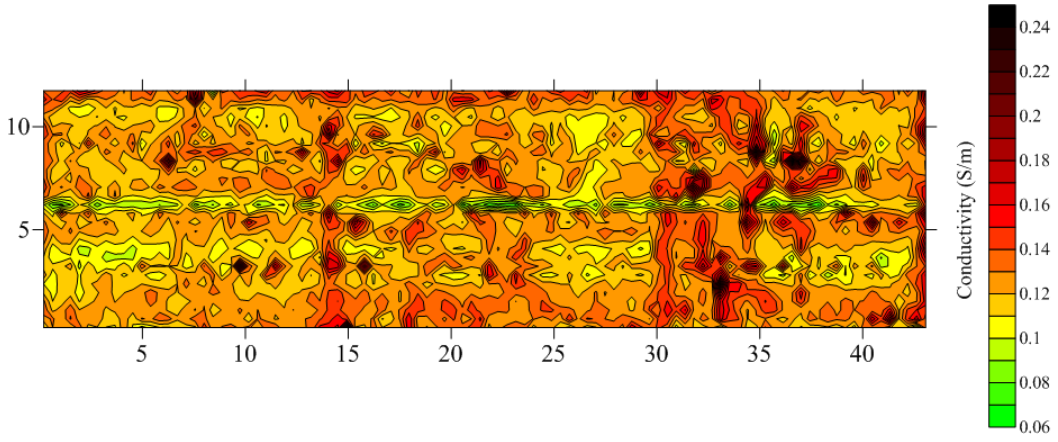

Figure 5.31: Updated conductivity map of Victoria Harbour Overpass

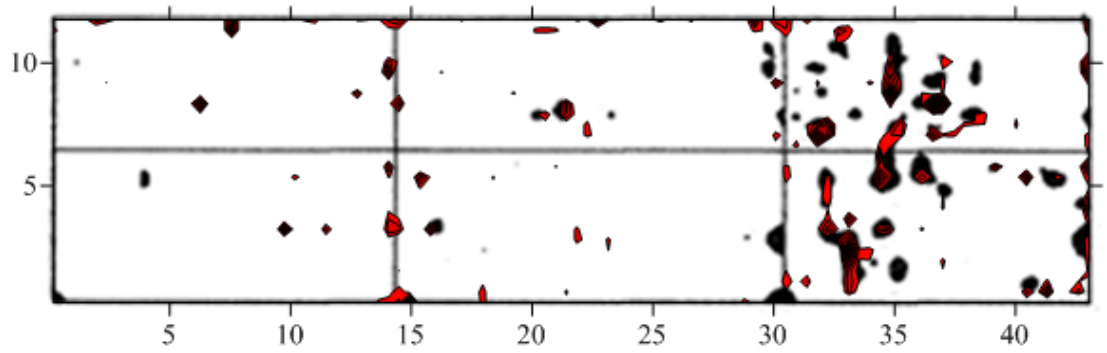

Figure 5.32: Updated conductivity compared to half-cell data from Victoria Harbour Overpass

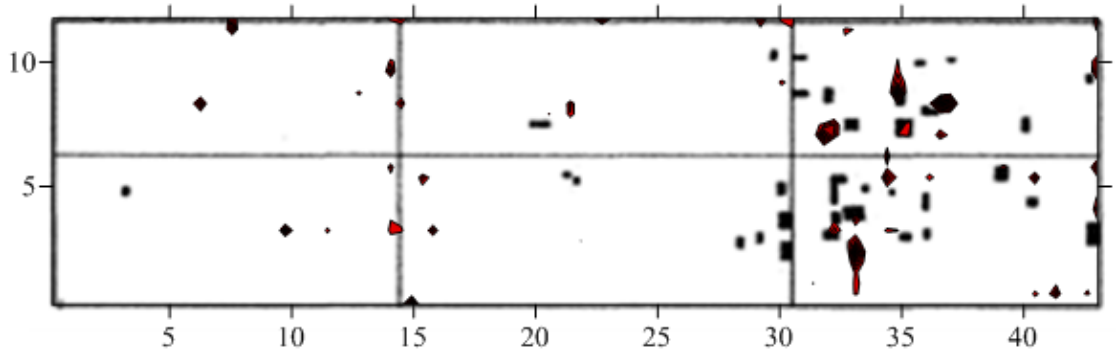

Figure 5.33: Updated conductivity compared to chain drag data from Victoria Harbour Overpass

Clearly the new threshold conductivity levels compare much better with the half-cell and chain drag data than the previous processing. The newly determined material properties differ considerably from those initially determined, but are a better representation of the true properties of the deck as the gain on each of the lanes has been equalized. This shows the importance of using the same gain for an entire bridge deck as it can substantially affect results. A summary of the areas determined with the conductivity plot compared to field testing data for each of the two processing techniques is shown in Table 5.6. The updated processing matches the half-cell area better and while the chain drag threshold is slightly further from the reference value than the original technique it only overestimates by 0.4% of the deck. Although the first technique shows a better chain drag area, the physical

locations mapped by the updated method are more accurate. This result shows that this troubling inconsistency with GPR data can be overcome with careful processing of the data to ensure equal gain is applied to all points on a given deck. Had the southbound scans been gained to equal the northbound scans, the results would have been exactly the same due to the method of building model curves from representative points.

The problem of gain differences across a deck can arise when data is not collected all at the same time. Gain differences should be looked for whenever data is collected on multiple occasions for the same data set. In this case, the difference from one day to the next was clearly visible due to the significant change in reinforcement reflection amplitude between lanes and the fact that the two lanes seemed to have similar states of deterioration.

Table 5.6: Comparison of two GPR data processing techniques and field test results for Victoria Harbour Overpass

		Deck Area (m^2)	Deck Area (%)
Original Processing	Half-Cell	16	3.2
	0.13 S/m	20	4.0
	Chain Drag	5	1.0
	0.14 S/m	6	1.1
After Gain Adjustment	Half-Cell	16	3.2
	0.15 S/m	18	3.7
	Chain Drag	5	1.0
	0.16 S/m	7	1.4

5.4 West River Overpass

The West River Overpass is located near the Northern Shore of Nova Scotia, spans about 71 m, and consists of two traffic lanes. The bridge was constructed in 1997 using high performance concrete (HPC) and has no interior joints along its span. Only one lane was tested for this study as the lane was closed and no traffic control was required. The lane

closure was due to an exterior girder being struck by a passing vehicle resulting in closure for repairs. Visual inspection identified no evidence of corrosion damage on the structure as would be expected at such a young age. The surface was noted as being grooved to increase vehicle traction and some cracking, with no indication of corrosion, was noted above one of the piers. This cracking appeared to be due to the natural stresses in the deck over time since the area over the pier would experience a negative moment due to the continuous deck. Eight cores were taken from the deck as seen in Figure 5.34. Two of the cores broke during extraction. Core depths were measured from the top of the grooved surface and none of the cores showed any sign of corrosion or delamination. Core depths are listed in Table 5.7. Neither the half-cell nor chain drag tests identified any damage to the young deck, as would be expected.

This bridge was of special interest to this investigation as previous research has shown that GPR has had inconsistencies when assessing the condition of bridges that have low levels of deterioration (Barnes and Trottier 2004). Overcoming these inconsistencies with the conductive model would prove GPR based condition assessment to be much more robust than in the past. It would be necessary for the conductive model to be accurate for young decks if frequent inspections were to be utilised to track chloride ingress over time.

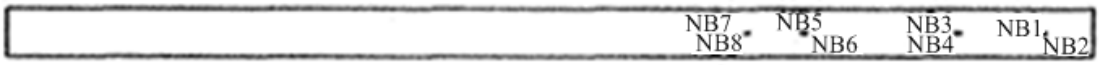

Figure 5.34: Core locations for West River Overpass (Redmond 2007)

Since only one narrowed lane was tested, this bridge had significantly fewer GPR data points than the rest of the decks studied. This affects both the normalization of the data and the determination of reference points for the model to be fit to. Naturally, ranking data to certain percentiles and manipulating normally distributed data about their means is increasingly accurate as more data is collected. This is generally not a problem for bridge decks, however the tested area of this bridge was 142 m^2 (45%) smaller than the next smallest deck examined. There was enough data present to process in the same fashion as the other decks, although the amount of data had to be considered to some degree during

modeling. Radar data before normalization is shown in Figure 5.35 while the data after normalization is in Figure 5.36. The representative data did not follow as smooth a curve as in many of the other bridge decks studied simply due to the lack of data points. Instead of the absolute sum difference of the model and each reference point, each of the model curves were fit through the center of their respective reference data as shown in Figure 5.37.

Table 5.7: Core descriptions for West River Overpass

Core	Depth to Bar (mm)	Chloride Profile*
NB 1	57.4	Yes
NB 2	55.3	Yes
NB 3	74.5	
NB 4	-	
NB 5	-	
NB 6	73.8	
NB 7	69.0	Yes
NB 8	63.2	

*Chloride profile measured in accordance to ASTM C1218

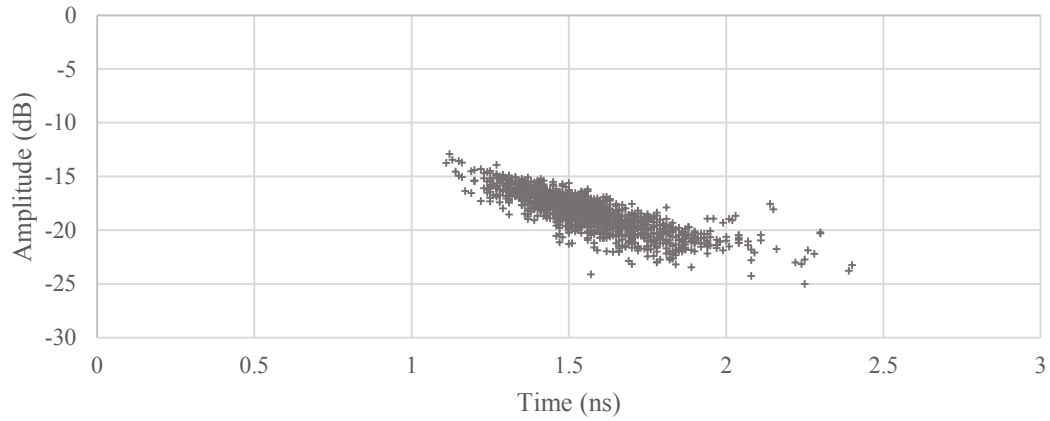

Figure 5.35: GPR data from West River Overpass before normalization

The model curves that fit this data determined the permittivity of the concrete deck to be 9.3 F/m while the 90th, 60th, and 30th percentile conductivities were 0.04, 0.05, and 0.06 S/m respectively. Conductivities determined by the model came to the same conclusion as the half-cell and chain drag tests that there was no significant damage to the bridge deck. The determined conductivity map is shown in Figure 5.38.

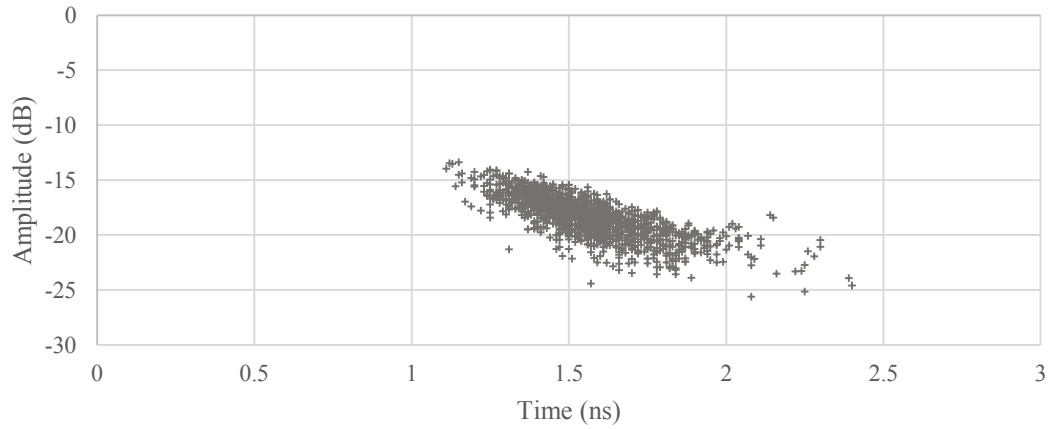

Figure 5.36: GPR data from West River Overpass after normalization

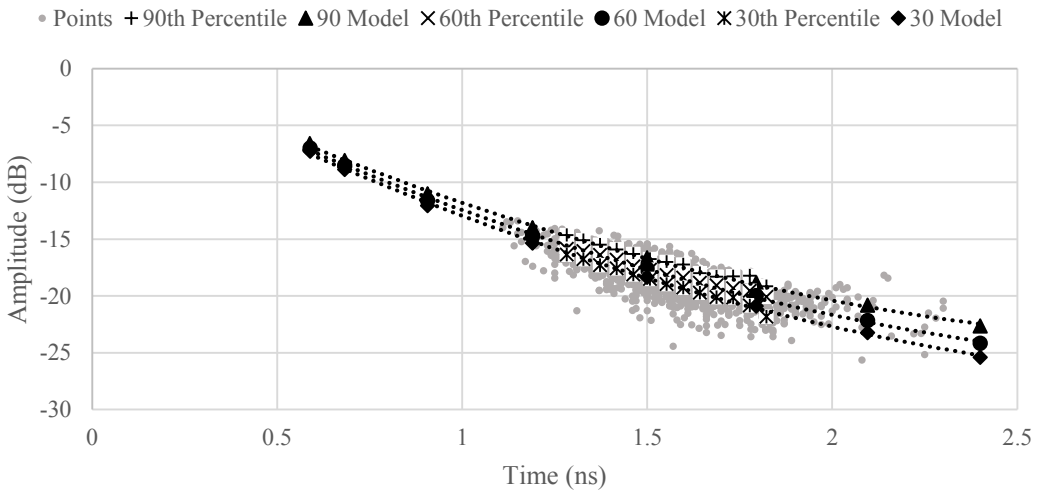

Figure 5.37: Model curves fit to West River Overpass data

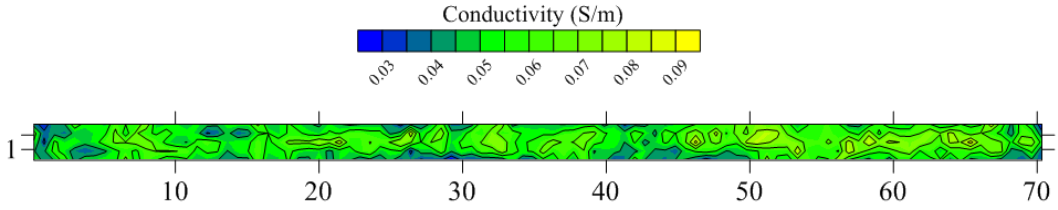

Figure 5.38: Conductivity map for West River Overpass

5.5 Sambro Harbour Overpass

Sambro Harbour Overpass is a two lane, three span structure located on the Eastern Shore of Nova Scotia that was built in 1978. Only the outbound lane from Halifax was scanned with GPR and compared to the reference testing methods. Visual inspection did not reveal any signs of corrosion activity, but did identify extensive shrinkage cracking and a different surface condition on the third span. Six cores were taken from the deck, four of which were taken from the third span where most of the deck distress was evident. Cores taken from the deck were located as shown in Figure 5.39 with the third span being on the far right of the figure. Condition of each core was as described in Table 5.8. Cores with no depth listed were damaged significantly enough during extraction to not be measured accurately. A

significant amount of white residue was found on each of the cores that were removed from the deck. White residue like this is often evidence of alkali aggregate reactivity (AAR) in concrete structures (Fournier and Bérubé 2000).

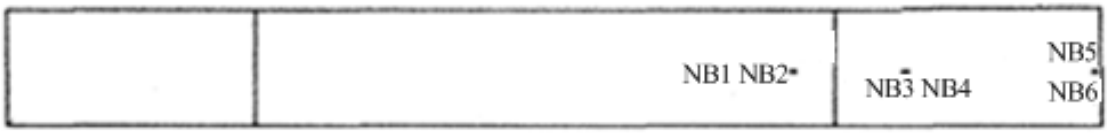

Figure 5.39: Core locations for Sambro Harbour Overpass (Redmond 2007)

Table 5.8: Core descriptions for Sambro Harbour Overpass

Core	Depth to Bar (mm)	Corrosion	Delamination	Chloride Profile*
NB 1	94.4	None	None	Yes
NB 2	97.9	None	None	
NB 3	72.7	Low	None	Yes
NB 4	-	None	None	
NB 5	74.8	Low	None	Yes
NB 6	-	None	None	

*Chloride profile measured in accordance to ASTM C1218

Alkali aggregate reactions are the result of poorly crystallized aggregate, often silica, used in construction. The aggregate reacts with alkali hydroxides in concrete during hydration and forms a gel that expands when it reacts with water. This gel is surrounding the aggregate so as the gel expands, it causes significant stresses at the interface between the aggregate and cement which can result in extensive cracking. During the reaction, the silica particles become charged and create an electrical double layer with neighboring alkali particles (Pignatelli et al. 2013). Particles that have formed this double layer create an electrostatic force against each other, adding to the stress induced on the concrete deck by the AAR gel.

The presence of AAR has been shown to increase the conductivity of concrete, which would contribute to attenuation and alter the velocity of an electromagnetic signal passing through affected regions (Shi 2004). Over time the alkalis further go into solution and increase the conductivity even more, which would be evident in an investigation of the conductive properties of a given concrete deck as it ages (Grattan-Bellew 1994). Since the conductivity due to chloride content is the focus of this study, the effect of AAR on conductivity should not be neglected as it will have a significant effect on results from the conductive model and would alter determined chloride contents. Although it is not the focus of this study, AAR in bridge decks should still be monitored and dealt with when assessing the condition of a deck due to the potential damage it could cause. Increased conductivity due to AAR should not be ignored in the conductive model due to the fact that higher levels still indicate potential damage to areas of the deck that should be rehabilitated or replaced.

Half-cell and chain drag tests showed 1% and 4.6% deterioration of the deck respectively. This is not common as the half-cell would normally show more area than the chain drag due to the progression of corrosion. Furthermore, the half-cell and chain drag plots do not occupy significant portions of the same areas even though there was some evidence of corrosion on the cores taken from the deck. The half-cell test only showed active corrosion at the joints while the chain drag was primarily in the third span where the shrinkage cracking was located. The half-cell and chain drag plots are shown in Figures 5.40 and 5.41 respectively.

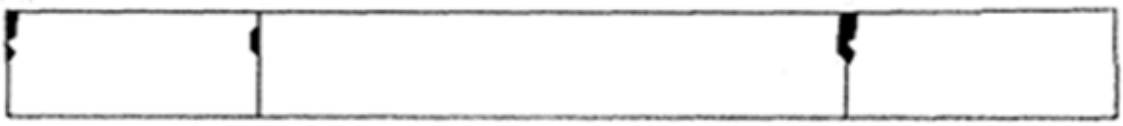

Figure 5.40: Half-cell results for Sambro Harbour Overpass (Redmond 2007)

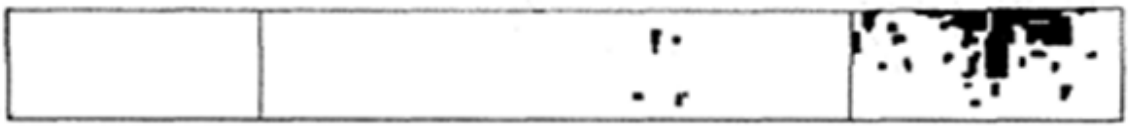

Figure 5.41: Chain drag results for Sambro Harbour Overpass (Redmond 2007)

Plots of the radar data before and after the normalization are in Figures 5.42 and 5.43 respectively. During modeling of the GPR data, it was determined that the permittivity of the deck was 7.2 F/m while the 90th, 60th, and 30th percentile conductivities were 0.12, 0.13, and 0.14 S/m. Figure 5.44 shows these representative curves fit to the GPR data.

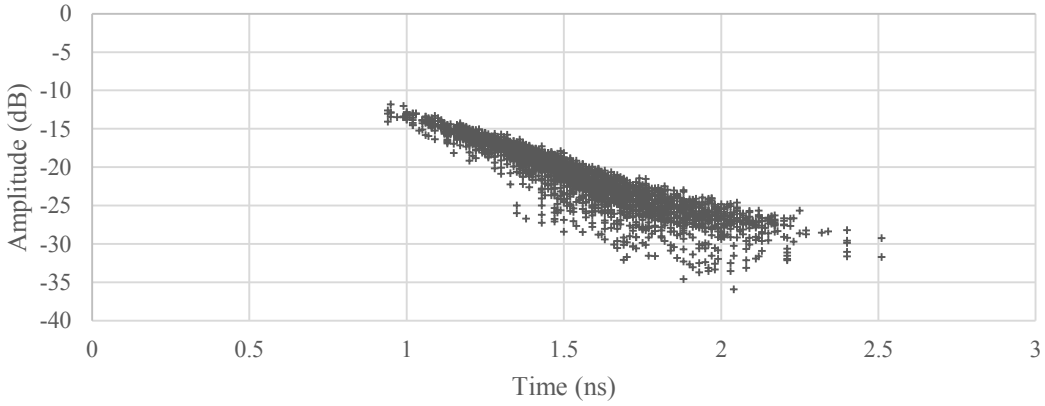

Figure 5.42: GPR data from Sambro Harbour Overpass before normalization

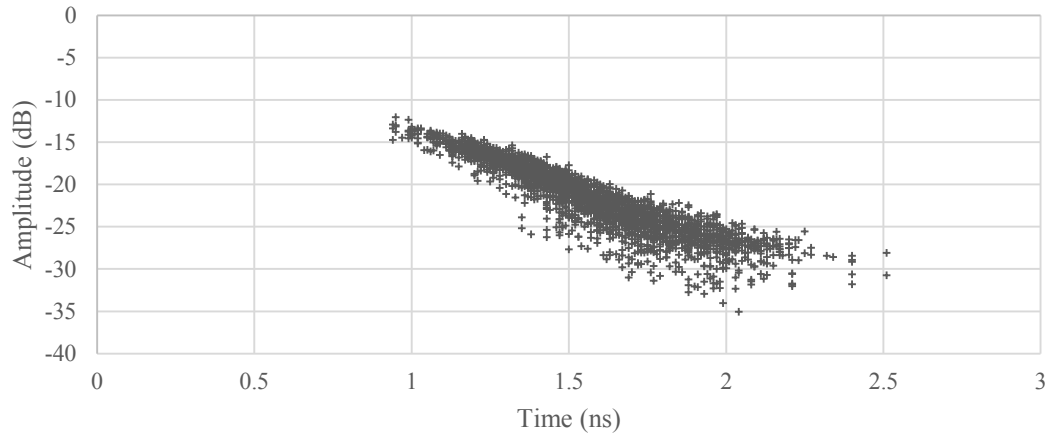

Figure 5.43: GPR data from Sambro Harbour Overpass after normalization

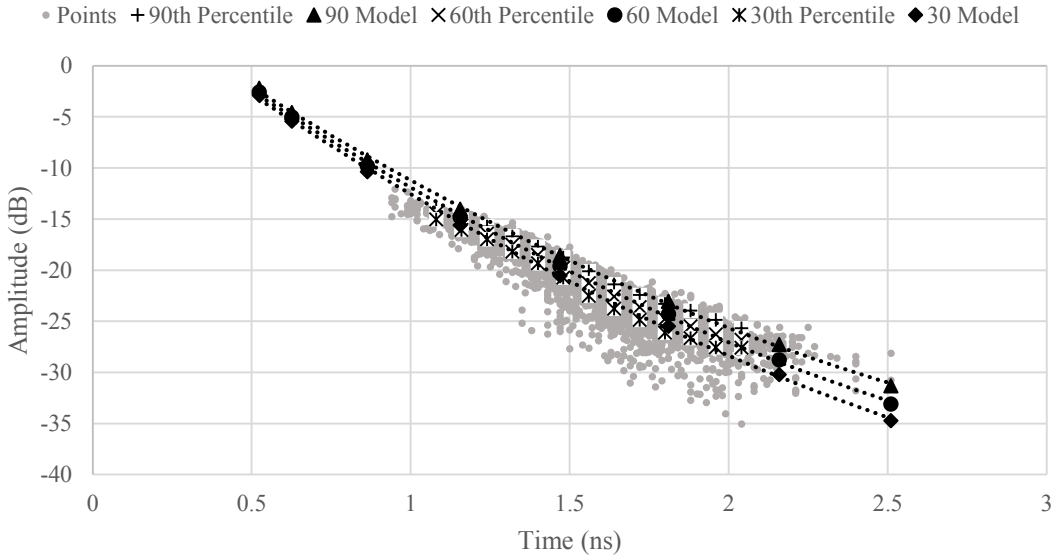

Figure 5.44: Model curves to fit Sambro Harbour Overpass data

Due to the small area outlined by the half-cell test and its lack of correlation with the chain drag and core results, GPR results were only compared to the chain drag test. This decision was made under the assumption that there was something wrong with the half-cell results. Another explanation could be that there was little corrosion present and AAR was the cause of the cracking and delamination. There were however chloride contents in the cores

examined between 3.22 and 5.77 kg/m^3 as outlined in section 5.6 and some evidence of corrosion on the extracted cores was present. The conductivity level used to compare the radar data to the chain drag plot showed good correlation between the two so whatever the cause of damage, the conductive model of collected GPR data identified the most severely deteriorated areas. The conductivity map is shown in Figure 5.45 and the plot of the conductivity compared to the chain drag is shown in Figure 5.46. A comparison of the areas identified as damaged by the GPR data and the reference tests is shown in Table 5.9. It should be noted however that much of the highest conductivities found were around the joints. This could indicate elevated chlorides in addition to the increased conductivity from AAR or it could mean higher AAR levels due to excess moisture ingress at the joints.

The conductivity level chosen showed 4.9% more of the deck than the chain drag testing outlined. All of the regions picked up by the chain drag were located by the GPR data however, with the area of the regions being slightly larger than those indicated by chain drag. The radar data also indicated that the concrete near the joints was in need of attention as was identfied by the half-cell testing. This is shown in Figure 5.45 at 13.5m and 44m along the deck. Even though the validity of the half-cell showing next to no corrosion activity in the deck is questionable, the fact that the only areas identified were at the joints cannot be ignored. If the half-cell worked properly, this would mean there was significant corrosion activity at the joints and if the half-cell was reading lower magnitude values than it should have, it would mean substantial corrosion activity at the joints while some activity may be present in other locations. Either way, the radar did pick up some level of deterioration at these locations.

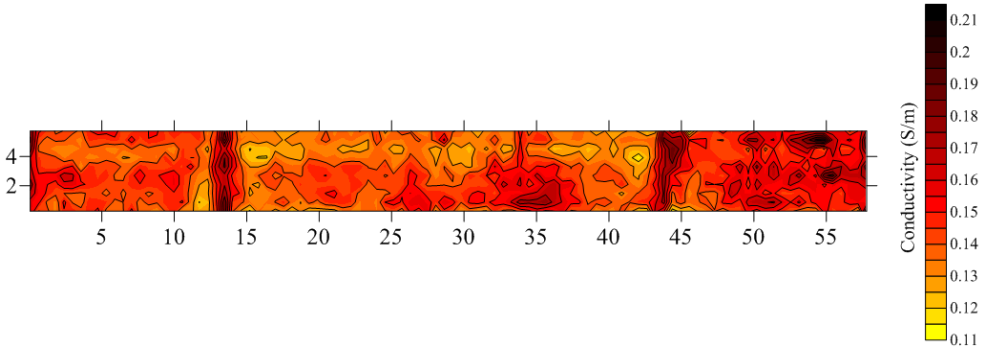

Figure 5.45: Conductivity map of Sambro Harbour Overpass

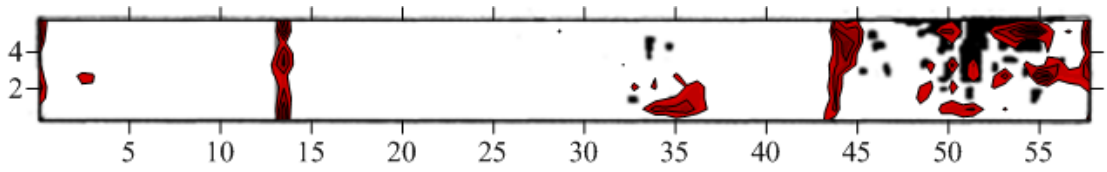

Figure 5.46: Conductivity compared to chain drag data for Sambro Harbour Overpass

Table 5.9: Comparison of GPR and field testing damage estimates – Sambro Harbour

	Deck Area (m^2)	Deck Area (%)
Half-Cell	3	1.0
Chain Drag	15	4.6
0.16 S/m	30	9.5

5.6 Comparison to Chloride Profiles

Three cores from each of the bridges were ground layer by layer and tested for water soluble chlorides to determine a chloride profile. Each of the chloride profiles were compared to the calculated conductivity at the nearest reinforcing bar to the core location. Chloride testing was only done to 7 layers of each core, covering approximately 30 mm (Redmond 2007). In order to compare conductivities to the true chloride content throughout the full depth of each core, diffusion models (Redmond 2007) were used to supplement the

data. The models were determined by fitting a diffusion coefficient to the chloride profile determined from the core data. Although the diffusion model was determined using an error function approach instead of the finite difference method, the values were assumed to be accurate enough to compare with the calculated conductivities. Both the measured and calculated chloride data are shown in Tables 5.10 through 5.14. The profile was averaged over the depth of each core for comparison with conductivity to estimate the average effect on each GPR scan. Since the West River Overpass was constructed from HPC which naturally has a lower diffusion coefficient, it was expected that there would be a much higher concentration at the surface than in the rest of the deck, especially at this young age as can be seen in the provided data.

Table 5.10: Chloride profiles from Milford Overpass

NB 4		SB 2		SB 3	
Depth (mm)	Cl (kg/m^3)	Depth (mm)	Cl (kg/m^3)	Depth (mm)	Cl (kg/m^3)
5	12.75	5	11.21	6.5	6.58
9	13.60	9	9.53	10.5	7.49
13	12.03	13	9.89	14.5	5.61
17	10.81	17	8.97	18.5	5.54
21	9.53	21	6.94	22.5	3.36
25	11.74	25	6.75	26.5	2.94
28.5	7.83	28.5	6.24	30.5	2.58
33.7	7.04*	30.2	5.67*	31.8	2.46*
38.6	6.12*	35.2	4.78*	37.1	1.81*
43.3	5.27*	40.2	3.99*	42.4	1.30*
48.2	4.50*	45.3	3.28*	47.7	0.90*
-	-	50.3	2.67*	53.0	0.61*
Average	9.03	Average	6.56	Average	3.41

*Points extrapolated with diffusion curve

Table 5.11: Chloride profiles from Sambro Harbour Overpass

NB 1		NB 3		NB 5	
Depth (mm)	Cl (kg/m^3)	Depth (mm)	Cl (kg/m^3)	Depth (mm)	Cl (kg/m^3)
5	7.85	5	4.26	6.5	10.51
9	9.13	9	6.85	10.5	9.43
13	8.44	13	7.92	14.5	10.85
17	6.93	17	7.68	18.5	9.47
21	6.75	21	7.68	22.5	10.11
25	6.41	25	7.46	26.5	8.90
28.5	5.36	28.5	6.86	30.5	7.56
29.8	5.24*	36.4	5.83*	37.4	5.89*
39.8	3.80*	43.6	5.07*	44.9	4.48*
49.7	2.63*	50.9	4.37*	52.4	3.32*
59.6	1.75*	58.2	3.73*	59.8	2.40*
69.6	1.11*	65.4	3.15*	67.3	1.69*
79.5	0.67*	72.7	2.64*	74.8	1.15*
89.5	0.39*	-	-	-	-
99.4	0.21*	-	-	-	-
Average	3.22	Average	5.22	Average	5.77

*Points extrapolated with diffusion curve

Table 5.12: Chloride profiles from Shubenacadie Overpass

NB 1		SB 1		SB 4	
Depth (mm)	Cl (kg/m^3)	Depth (mm)	Cl (kg/m^3)	Depth (mm)	Cl (kg/m^3)
5	9.39	6.5	13.12	6.5	10.83
9	10.37	10.5	11.20	10.5	9.97
13	9.15	14.5	10.61	14.5	11.31
17	7.86	18.5	11.49	18.5	9.72
21	6.91	22.5	9.69	22.5	9.92
25	5.82	26.5	8.60	26.5	8.74
28.5	4.45	30.5	8.19	30.5	10.86
31.0	4.18*	33.2	7.93*	35.7	8.54*
34.8	3.40*	38.7	7.08*	41.7	8.08*
38.7	2.73*	44.2	6.27*	47.6	7.63*
-	-	49.8	5.52*	53.6	7.19*
-	-	55.3	4.83*	59.5	6.76*
Average	6.64	Average	8.62	Average	8.93

*Points extrapolated with diffusion curve

Table 5.13: Chloride profiles from Victoria Harbour Overpass

NB 2		NB 3		SB 4	
Depth (mm)	Cl (kg/m^3)	Depth (mm)	Cl (kg/m^3)	Depth (mm)	Cl (kg/m^3)
5	11.07	6.5	13.87	6.5	11.66
9	10.77	10.5	13.53	10.5	11.30
13	14.70	14.5	11.44	14.5	10.25
17	13.93	18.5	11.87	18.5	11.52
21	12.77	22.5	11.33	22.5	10.08
25	11.14	26.5	11.23	26.5	10.20
28.5	10.67	30.5	8.70	30.5	6.00
33.5	10.02*	36.7	8.65*	32.9	7.87*
37.2	9.38*	42.8	7.72*	37.6	7.14*
-	-	49.0	6.84*	42.3	6.46*
-	-	55.1	6.03*	47.0	5.80*
-	-	61.2	5.27*	-	-
Average	11.58	Average	9.39	Average	9.04

*Points extrapolated with diffusion curve

Table 5.14: Chloride profiles from West River Overpass

NB 1		NB 2		NB 7	
Depth (mm)	Cl (kg/m^3)	Depth (mm)	Cl (kg/m^3)	Depth (mm)	Cl (kg/m^3)
5	16.23	5	12.31	6.5	8.67
9	7.69	9	8.54	10.5	3.66
13	2.75	13	12.66	14.5	1.16
17	0.66	17	2.77	18.5	0.97
21	0.71	21	1.68	22.5	0.34
25	0.47	25	0.91	26.5	0.23
28.5	0.49	28.5	0.52	30.5	0.21
34.4	0*	33.2	0.13*	34.5	0*
40.2	0*	38.7	0.03*	41.4	0*
45.9	0*	44.2	0.01*	48.3	0*
51.7	0*	49.8	0*	55.2	0*
57.4	0*	55.3	0*	62.1	0*
-	-	-	-	69.0	0*
Average	2.30	Average	3.08	Average	1.20

*Points extrapolated with diffusion curve

The average chloride content for each core was plotted against the conductivities calculated by the conductive model at the corresponding locations on each deck. Due to the degree of

AAR present in the Sambro Harbour Overpass cores, its chloride values were plotted separately since it would likely have elevated conductivity as discussed in Section 5.5. The plot of the average chloride contents from Tables 5.10 through 5.14 versus the calculated conductivities can be found in Figure 5.47 where it can be seen that conductivity appears to increase linearly with chloride content.

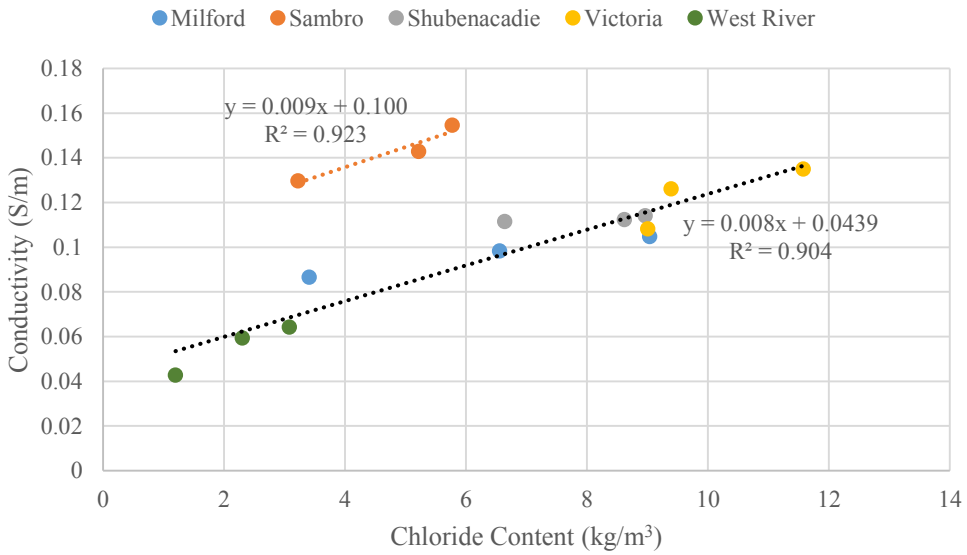

Figure 5.47: Chloride contents of cores compared to calculated conductivities

As expected, Sambro Harbour displayed higher conductivity levels than the other bridges in the study due to the presence of AAR. Both the Sambro Harbour Overpass and the other four bridges studied displayed a good linear fit with fairly similar slopes as shown in Table 5.15. It is possible that chloride content increases conductivity linearly as described by the slope while any additional increases in conductivity due to the mix design or AAR cause the line to move along the conductivity axis. This would mean that conductivity profiles such as the ones determined in this study could be used to estimate the average chloride content throughout any given bridge deck if the conductivity of the chloride free deck was known. This could be accomplished with Equation 5.1 which determines chloride content (C) in kg/m^3 from the conductivity and the initial conductivity of the concrete which

represents the intercept with the conductivity axis (σ_0). This equation also removes the effects of AAR or any other external factors (σ_E).

Table 5.15: Relationship between conductivity and chloride

Deck(s)	R^2	Slope	Intercept
Sambro	0.92	0.0090	0.10
Remaining	0.90	0.0080	0.044

$$C = \frac{\sigma - \sigma_0 - \sigma_E}{0.008} \quad \textbf{[5.1]}$$

The slope of 0.008 was chosen for Equation 5.1 as it was taken from the line with more points in Figure 5.47 and therefore more statistical significance. This equation allows the direct calculation of chloride content from conductivities determined with GPR. In order to increase the accuracy of this method, further research should be conducted to confirm the slope of the conductivity/chloride relationship as well as the conductivity increase due to AAR or other external factors. By determining chloride content, direct estimations of both degree of corrosion and time to corrosion can be made by applying traditional chloride thresholds. Having this capability would dramatically improve condition assessment and could lead to effective predictions of time to corrosion by combining with diffusion models and exposure conditions.

Chapter 6: Discussion

A conductive approach to modeling electromagnetic wave propagation through concrete has been applied to GPR data in an attempt to determine dielectric and conductive properties of bridge decks. This was done with the objective of determining the chloride content of bare concrete bridge decks with GPR to improve the condition assessment process and to increase the amount of information gained. This model accounted for spreading losses and power fluctuations within the GPR system to isolate signal attenuation and determine the conductive properties of the bridge deck. One permittivity was determined for each deck and the conductivity of the concrete above each reinforcing bar was determined based on representative data from the population of each deck. Determined conductivities showed strong correlation with reference half-cell and chain drag testing with higher conductivities relating to the higher degree of damage detected by the chain drag. These higher conductivities correspond to higher levels of chloride and a more severe state of corrosion expected in delaminated concrete. This agreement reinforces the notion that GPR is a robust tool for condition assessment of concrete bridge decks. The versatility of this method has been shown as it accurately determined locations of deterioration for bridge decks of varying ages as well as with the presence of AAR and with an HPC deck.

Normalization was carried out on the data due to the inherent variations in signal strength that are present in GPR antennas due to fluctuating power sources. Removing this variability makes GPR analysis more robust due to the individual adjustments made to each scan. This allows the precise detection of smaller changes in signal strength due to the properties of the concrete being scanned, which yields more accurate results than previously attained. With this method of processing and modeling GPR data, radar could be incorporated into more bridge management systems to reduce life cycle cost while increasing the service lives of bridge decks.

Normalization of the GPR data before modeling proved to be an effective method of reducing some of the variability that has plagued GPR surveys in the past; the Victoria Harbour Overpass being the most definitive example of this. Traditional GPR processing and analysis would have shown one side of the deck in impeccable condition while the other side would be identified as severely deteriorated. By applying gain to equalize the

amplitude on both lanes of the deck after normalizing the lanes individually, the amplitude differential was substantially reduced and a more accurate conductivity map was determined.

Conductivities determined through the modeling of concrete as a conductive medium have shown a strong linear relationship with the chlorides measured from cores taken from each of the 5 bridge decks in this study. Four of the decks fit the same trend line, while the one deck with substantial AAR was plotted separately due to increased conductivity from the AAR itself. It was suggested that plots of chloride and conductivity could be a series of parallel lines with different y-intercepts due to a baseline conductivity value for the deck as a whole and an equation was produced which describes the relationship between conductivity and chloride. The correlation found can be used to determine chloride levels for the remainder of each bridge deck. By calculating chloride contents, it is possible to apply traditional chloride thresholds to delineate deteriorated areas of a surveyed bridge deck.

Conducting these surveys frequently over a number of years for a given bridge deck would show a change in chloride content over time, aiding the establishment of a chloride profile for the deck. Monitoring chlorides over time would also allow diffusion coefficients to be determined for a given bridge deck, aiding the creation of forward condition models. Once both a diffusion coefficient or range of coefficients and the chloride profiles have been determined, diffusion models could be coupled with the chloride data to predict time until a threshold chloride content has been reached. This would allow predictions to be made of the time to onset of corrosion.

Establishment of chloride profiles and the determination of the diffusive properties of a network of bridge decks would prove invaluable to management agencies. The ability to monitor chlorides and predict the onset of corrosion in a deck allows repair decisions to be made on a case by case basis while remaining aware of the costs associated with the entire network of bridges. Estimating the time to corrosion would allow agencies to provide realistic estimates of the schedule and extent of repairs and would greatly increase the accuracy of estimated budgets due to maintenance. This inspection program would also

allow material and labour resources to be allocated efficiently so that all the bridge decks in a network could be maintained at the lowest possible cost while extending service lives.

6.1 Conclusion

The conductive model of electromagnetic propagation proved to be effective in assessing the condition of unpaved reinforced concrete bridge decks. During the course of this investigation, several conclusions were made based on the comparisons of calculated conductivities to reference nondestructive testing methods and chloride contents of surveyed bridges measured from extracted cores. The conclusions of this study using a conductive model of GPR signals through concrete are as follows:

- Conductive model was successfully developed to isolate effects of attenuation.
- Conductivities were extremely well correlated to regions of each bridge deck deemed deteriorated by half-cell and chain drag reference tests.
- Strong linear relationship shown between chloride contents from each examined bridge deck and conductivities calculated with model.
- Traditional chloride thresholds for corrosion initiation can be applied to conductive results by calculating chloride levels from conductivities.

6.2 Recommendations

Future research into GPR inspection should focus on accounting for asphalt on paved concrete bridge decks. It would be necessary to determine if asphalt should be modeled as a conductive or non-conductive medium and then to determine concrete condition without having to remove the asphalt. Most of the current inspection techniques available require the removal of asphalt before testing the deck which is only an option when the asphalt is in need of replacement due to the associated costs. Eliminating this need would dramatically reduce testing costs and would allow routine inspections to be much more frequent and thorough, leading to a higher degree of accuracy in condition assessment and more efficient repairs.

Research should also be done to further examine the conductive effects of AAR as well as those of mix designs and any other factors that would significantly affect the conductivity. Accounting for these effects would provide a baseline conductivity that would allow chloride content to be calculated accurately. In the case of AAR, this method could eventually be used to determine how severe the AAR is in a deck in conjunction with the amount of chlorides in the deck. The effects of the mix design on conductivity would be of use to establish that same y-intercept for a chloride/conductivity plot, especially for young decks that would have few other factors affecting conductivity.

Further examination of bare concrete decks with GPR should be turned to a layered approach that could eventually determine the chloride content with depth in a single deck inspection. This would have to done by splitting the deck into discrete strips and using the entire hyperbolic reflection from each reinforcing bar to determine the conductivity of each strip based on changes in attenuation as the antenna approached the reinforcing bar. The possibility of combining this process with the migration of these hyperbolas should also be examined to limit calculation time and increase accuracy. By determining chloride profiles with each survey, diffusion models could be fit to the deck much faster and be updated regularly to reflect the true changes in the deck over time.

Migration itself should also be examined as the conductive media approach invalidates many of the assumptions made during the migration process. Signal losses should be accounted for when migrating GPR signals so that better velocity estimates and average amplitudes could be determined. Doing this could further increase the accuracy of GPR analysis, especially if the change in attenuation with depth could be determined during the migration process by proper modeling as a conductive medium.

References

Ahmad, S. (2003). Reinforcement corrosion in concrete structures, its monitoring and service life prediction—a review. *Cement and Concrete Composites*, *25*(4), 459-471.

Alongi, A. V., Cantor, T. R., Kneeter, C. P., & Alongi Jr, A. (1982). Concrete evaluation by radar theoretical analysis. Transportation Research Record, (853).

Alonso, C., Andrade, C., & González, J. A. (1988). Relation between resistivity and corrosion rate of reinforcements in carbonated mortar made with several cement types. Cement and concrete research, 18(5), 687-698.

Ansuini, F. J., & Dimond, J. R. (1994). Factors affecting the accuracy of reference electrodes. *Materials performance*, *33*(11), 14-17.

ASTM C1218/C1218M-99. (2008a). Standard Test Method for Water-Soluble Chloride in Mortar and Concrete. West Conshohocken, PA: American Society for Testing and Materials.

ASTM C1543. (2002). Standard Test Method for Determining the Penetration of Chloride Ion into Concrete by Ponding. West Conshohocken, PA: American Society for Testing and Materials.

ASTM C876-09. (2009). Standard Test Method for Half-Cell Potentials of Uncoated Reinforcing Steel in Concrete. West Conshohocken, PA: American Society for Testing and Materials.

ASTM D4580 (2012). Standard Practice for Measuring Delaminations in Concrete Bridge Decks by Sounding. West Conshohocken, PA: American Society for Testing and Materials.

ASTM D6087 (2008b). Standard Test Method for Evaluating Asphalt-Covered Concrete Bridge Decks Using Ground Penetrating Radar. West Conshohocken, PA: American Society for Testing and Materials.

Bank of Canada. (2014). *Historical Data.* Retrieved from http://www.bankofcanada.ca/rates/indicators/capacity-and-inflation-pressures/inflation/historical-data

Barnes, C. L., & Trottier, J. F. (2004). Effectiveness of ground penetrating radar in predicting deck repair quantities. Journal of infrastructure systems, 10(2), 69-76.

Barnes, C. L., Trottier, J. F., & Forgeron, D. (2008). Improved concrete bridge deck evaluation using GPR by accounting for signal depth–amplitude effects. *NDT & E International*, *41*(6), 427-433.

Belli, K., Rappaport, C. M., Zhan, H., & Wadia-Fascetti, S. (2009). Effectiveness of 2-D and 2.5-D FDTD ground-penetrating radar modeling for bridge-deck deterioration evaluated by 3-d FDTD. Geoscience and Remote Sensing, IEEE Transactions on, 47(11), 3656-3663.

Berke, N.S. (2006). Corrosion of Reinforcing Steel, in J.F. Lamond and J.H. Pielert (eds), *Significance of Tests and Properties of Concrete and Concrete Making Materials*, STP 169D, West Conshohocken: ASTM International.

Bertolini, L., Elsener, B., Pedeferri, P. Polder, R. (2004). *Corrosion of Steel in Concrete: Prevention, Diagnosis, Repair.* Weinheim: Wiley-VCH, Germany.

Broomfield, J. P. (2006). Corrosion of steel in concrete: understanding, investigation and repair. CRC Press.

Cardimona, S., Willeford, B., Wenzlick, J., & Anderson, N. (2000). Investigation of bridge decks utilizing ground penetrating radar. In *International conference on the application of geophysical technologies to planning, design, construction and maintenance of transportation facilities. St. Louis/USA*.

Cantor, T. R., & Kneeter, C. P. (1978). Radar and acoustic emission applied to study of bridge decks, suspension cables, and masonry tunnel. Transportation Research Record, (676).

Cantor, T. R., & Kneeter, C. P. (1982). Radar as applied to evaluation of bridge decks. Transportation Research Record, (853).

Carter, C. R., Chung, T., Holt, F. B., & Manning, D. G. (1986). An automated signal processing system for the signature analysis of radar waveforms from bridge decks. Electrical Engineering Journal, Canadian, 11(3), 128-137.

Clemeña, G. G. (1983). Nondestructive inspection of overlaid bridge decks with ground-penetrating radar. Transportation Research Record, (899).

Clemeña, G. G. (2003). Short-pulse radar methods, in the 'CRC Handbook on Nondestructive Testing of Concrete', Malhotra and Carino/Editors. CRC Press, 2003.

Cowell Jr, J. W. (1988). The effects of inadequate component inspection on facility repair projects. Massachusetts Institute of Technology, Cambridge Dept. of Civil Engineering.

Crank, J. (1975). The Mathematics of Diffusion: 2d Ed. Clarendon Press.

Daniels, D. J. (Ed.). (2004). *Ground penetrating radar 2nd edition*. Institute of Electrical Engineers, London, United Kingdom.

El-Enein, S. A., Kotkata, M. F., Hanna, G. B., Saad, M., & El Razek, M. M. (1995). Electrical conductivity of concrete containing silica fume. Cement and concrete research, 25(8), 1615-1620.

Elsener, B., & Bohni, H. (1990). Potential mapping and corrosion of steel in concrete. Corrosion rates of steel in concrete, ASTM STP, 1065, 143-156.

Environment Canada (2014). *Daily Data Report for July 2005: Berwick, Nova Scotia*. Retrieved from http://climate.weather.gc.ca/climateData/dailydata_e.html?timeframe=2&Prov=NS&StationID=7105&dlyRange=1994-06-01|2012-09-30&Year=2005&Month=7&Day=01

Federal Highway Administration. (1995). Bridge inspector's training manual/90. US Department of Transportation, Federal Highway Administration, McLean, VA.

Federal Highway Administration. (2014). *Deficient Bridges by State and Highway System.* Retrieved from http://www.fhwa.dot.gov/bridge/deficient.cfm

Federal Highway Administration. (2013a). *Estimated 2012 Costs to Replace or Rehabilitate Structurally Deficient Bridges.* Retrieved from http://www.fhwa.dot.gov/bridge/nbi/sd2012.cfm

Federal Highway Administration. (2013b). *Deck Structure Type.* Retrieved from http://www.fhwa.dot.gov/bridge/nbi/deck.cfm

Federal Highway Administration. (2013c). *Highway Bridge by Wearing Surface.* Retrieved from http://www.fhwa.dot.gov/bridge/wearing.cfm

Fitch, M. G., Weyers, R. E., & Johnson, S. D. (1995). Determination of end of functional service life for concrete bridge decks. *Transportation research record*, 60-66.

Fournier, B., & Bérubé, M. A. (2000). Alkali-aggregate reaction in concrete: a review of basic concepts and engineering implications. Canadian Journal of Civil Engineering, 27(2), 167-191.

Frederiksen, J. M. (2009). On the need for more precise threshold values for chloride initiated corrosion. Materials and corrosion, 60(8), 597-601.

Gagnon, M., Gaudreault, V., & Overton, D. (2008). *Age of public infrastructure: A provincial perspective*. Statistics Canada.

Glass, G. K., & Buenfeld, N. R. (1997). The presentation of the chloride threshold level for corrosion of steel in concrete. *Corrosion Science*, *39*(5), 1001-1013.

Glass, G. K., Page, C. L., & Short, N. R. (1991). Factors affecting the corrosion rate of steel in carbonated mortars. Corrosion Science, 32(12), 1283-1294.

Gucunski, N., Feldmann, R., Romero, F., Kruschwitz, S., Abu-Hawash, A., & Dunn, A. (2009). Multimodal condition assessment of bridge decks by NDE and its validation. In *Proc. 2009 Mid-Continent Transportation Research Symp. Ames, Iowa, 18p* (Vol. 261, No. 5).

Hansson, C. M., Poursaee, A., & Laurent, A. (2006). Macrocell and microcell corrosion of steel in ordinary Portland cement and high performance concretes. *Cement and Concrete Research*, *36*(11), 2098-2102.

Hearn, N, Hooton, R. D., and Nokken, M. R. (2006). Pore Structure, Permeability, and Penetration Resistance Characteristics of Concrete, in J.F. Lamond and J.H. Pielert (eds), *Significance of Tests and Properties of Concrete and Concrete Making Materials*, STP 169D, West Conshohocken: ASTM International.

Hugenschmidt, J., & Loser, R. (2008). Detection of chlorides and moisture in concrete structures with ground penetrating radar. *Materials and Structures*, *41*(4), 785-792.

Huisman, J. A., Hubbard, S. S., Redman, J. D., & Annan, A. P. (2003). Measuring soil water content with ground penetrating radar. Vadose zone journal, 2(4), 476-491.

Jol, H. M. (Ed.). (2009). *Ground penetrating radar theory and applications*. Access Online via Elsevier.

Kalogeropoulos, A. (2012). *Non-Destructive Determination of Chloride and Water Content in Concrete Using Ground Penetrating Radar* (Doctoral dissertation, École Polytechnique Fédérale De Lausanne).

Kim, W., Ismail, A., Anderson, N. L., Atekwana, E. A., & Buccellato, A. (2003). Non-destructive testing (NDT) for corrosion in bridge decks using GPR. In The 3rd International Conference on Applied Geophysics. Orlando, Florida, USA.

Lambot, S., Slob, E. C., van den Bosch, I., Stockbroeckx, B., & Vanclooster, M. (2004). Modeling of ground-penetrating radar for accurate characterization of subsurface electric properties. Geoscience and Remote Sensing, IEEE Transactions on, 42(11), 2555-2568.

Leucci, G., di Chimica, O., Negri, S., di Chimica, O., Carrozzo, M. T., & di Chimica, O. (2003). Ground Penetrating Radar (GPR): an application for evaluating the state of maintenance of the building coating. Annals of Geophysics.

Leucci, G. (2008). Ground penetrating radar: the electromagnetic signal attenuation and maximum penetration depth. *Scholarly research exchange*, *2008*.

Manning, D. G., & Holt, F. B. (1983). Detecting deterioration in asphalt-covered bridge decks. Transportation Research Record, (899).

Martın-Pérez, B., Zibara, H., Hooton, R. D., & Thomas, M. D. A. (2000). A study of the effect of chloride binding on service life predictions. Cement and Concrete Research, 30(8), 1215-1223.

Maser, K. R. (1989). New technology for bridge deck assessment, Phase I report. Rep. No. FHWA-NETC-89, 1.

Maser, K. R. (1990). New technology for bridge deck assessment. New England Transportation Consortium Phase II Final Report, Center for Transportation Studies, MIT.

Montemor, M. F., Simoes, A. M. P., & Ferreira, M. G. S. (2003). Chloride-induced corrosion on reinforcing steel: from the fundamentals to the monitoring techniques. *Cement and Concrete Composites*, *25*(4), 491-502.

Moore, M., Phares, B. M., Graybeal, B., Rolander, D., & Washer, G. (2001). *Reliability of visual inspection for highway bridges, volume I: Final report* (No. FHWA-RD-01-020).

Pignatelli, R., Comi, C., & Monteiro, P. J. (2013). A coupled mechanical and chemical damage model for concrete affected by alkali–silica reaction. Cement and Concrete Research, 53, 196-210.

Poulsen, E., & Mejlbro, L. (2006). Diffusion of chlorides in concrete. Modern concrete technology, vol. 14.

Poursaee, A., & Hansson, C. M. (2009). Potential pitfalls in assessing chloride-induced corrosion of steel in concrete. *Cement and Concrete Research*, *39*(5), 391-400.

Redmond, E. (2007). The use of ground penetrating radar to determine corrosion risk potential for steel reinforced exposed concrete bridge decks. In *Masters Abstracts International* (Vol. 46, No. 03).

Reppert, P. M., Morgan, F. D., & Toksöz, M. N. (2000). Dielectric constant determination using ground-penetrating radar reflection coefficients. Journal of Applied Geophysics, 43(2), 189-197.

Roberge, P. (2008). *Corrosion Engineering: Principles and Practice*. McGraw Hill Professional.

Sbartaï, Z. M., Laurens, S., Balayssac, J. P., Arliguie, G., & Ballivy, G. (2006). Ability of the direct wave of radar ground-coupled antenna for NDT of concrete structures. NDT & E International, 39(5), 400-407.

Shaari, A., Millard, S. G., & Bungey, J. H. (2004). Modelling the propagation of a radar signal through concrete as a low-pass filter. NDT & E International, 37(3), 237-242.

Song, H. W., Shim, H. B., Petcherdchoo, A., & Park, S. K. (2009). Service life prediction of repaired concrete structures under chloride environment using finite difference method. *Cement and concrete composites*, *31*(2), 120-127.

Thomas, M. D., & Bamforth, P. B. (1999). Modelling chloride diffusion in concrete: effect of fly ash and slag. *Cement and Concrete Research*, *29*(4), 487-495.

Travassos, L., Ida, N., Vollaire, C., & Nicolas, A. (2007). Solution of Maxwell's equations for the simulation and optimization of the radar assessment of concrete structures. Research in Nondestructive Evaluation, 18(3), 151-161.

Williamson, G. S., Weyers, R. E., Brown, M. C., & Sprinkel, M. M. (2007).*Bridge Deck Service Life Prediction and Costs* (No. VTRC 08-CR4).

Yilmaz, Ö. (2001). Seismic Data Analysis; Processing, Inversion, and Interpretation of Seismic Data, Vol I and II. Society of Exploration Geophysicists (Vol. 1). 0